Ana Beatriz Brito de Oliveira

Licenciatura em Bioquímica

A novel approach for chip-based digital LAMP towards the quantification of prostate cancer biomarkers

Dissertação para obtenção do Grau de Mestre em Biotecnologia

Orientador: Pedro Viana Baptista, Professor catedrático, Departamento de Ciências da Vida, FCT-NOVA

Júri:

Presidente: Professora Susana Barreiros

Arguente: Professora Rita Branquinho

FACULDADE DE CIÊNCIAS E TECNOLOGIA
UNIVERSIDADE NOVA DE LISBOA

Setembro, 2019

A novel approach for chip-based digital LAMP towards the quantification of prostate cancer biomarkers

ACKNOWLEDGEMENTS

It is often though that scientific research it is a lonely work, however I cannot realize how this path could be more the exact opposite. As a matter of fact, there are a lot of people who deserve my most sincere appreciation and to whom I would like to thank.

First, I would like to express my very great appreciation to Prof. Pedro Baptista, whose door was always open whenever I reached into a trouble or doubt. Thank you for all the patience to my almost bipolar hype/ hopelessness mood swings. You consistently allowed this thesis to be my own but steered me into the right direction whenever you thought I needed it, despite my stubbornness and obsession not always allowing me to realize it immediately. Most importantly, thank you for always make me feel appreciated and welcomed in the family of the Nanomedicine group.

I would also like to offer my special thanks to Dr. Bruno Veigas for all the work, help, enthusiasm and friendship demonstrated, without you it wouldn't be the same. Thank you for giving me room to grow and learn and more importantly for teaching me what it means to be a researcher.

To Daniela "Consuela" Ferreira, I hope someday I can find the words to express my endless gratitude for all the companionship, support and joy you presented me every day. Thank you for allowing me to stay until late hours into the laboratory and for stood by my side through the endless DNA extractions, real-time and electrophoresis experiments.

To Inês "Jeová" Martins, I would like to thank you for your friendship and kindness. For the laughs, conversations and morning coffees, which helped me pass through the lower moments.

I would like to acknowledge all my friends for all the support and patience, thank you to Beatriz Penha, Beatriz Oliveira, Maria Inês, Bernardo Brito, Filipa Amendoeira, Daniel Landum, Catarina Pires and João Costa.

I must express my very profound gratitude to my parents and sister for providing me with unfailing support and continuous encouragement throughout my years of study and through the process of researching and writing this thesis. This accomplishment would not have been possible without them. Thank you.

I would also like to offer my special thanks to all my colleges, researchers and staff who at some point helped me and directly or indirectly contributed to this work. Without their participation and input, this thesis could not have been successfully conducted.

ABSTRACT

Nucleic acids amplification-based methods can profit from the features offered by Lab-on-a-chip technologies, in particular those that aimed for molecular diagnosis purposes. Currently, isothermal amplification approaches, more precisely Loop-mediated isothermal amplification (LAMP), have become promising alternatives to the current gold standard technology (PCR). Regardless the amplification mechanism, accurate target quantification is still challenging. To this end, the development of digital amplification methods has helped to circumvent this limitation.

This thesis focused on the development of a chip-based digital LAMP system towards the quantification of prostate cancer biomarkers. For this, LAMP was integrated with droplet-based digital amplification concept. LAMP positive amplification was achieved after 60 minutes, leading to a 2-fold increase in fluorescence when compared to the negative amplification controls, in a vortex-based droplet generation approach. However, aspects inherent to this method prevented a quantitative assessment of LAMP amplification. In order to overcome these limitations, a novel microfluidics chip-based device was developed and implemented towards digital LAMP (dLAMP) quantification of *c-Myc* gene. The T-junction type droplet generator chip achieved droplets of 1.5 nL with a coefficient of variation bellow 3%, in line with the standard for this technique. This system showed a sharp response to template concentration, observable by the raise in the fraction of positive droplets. Additionally, the target quantification proven to be precise (R^2 =0.99) for 4 orders of magnitude of copies/µL (5 copies/µL - $5x10^5$ copies/µL) after Poisson's modulation.

Aiming for the implementation of this chip-based dLAMP system into the detections of prostate cancer-associated biomarkers, amplification reactions of *Second Chromosome Locus Associated with Prostate-1 (SChLAP1)* and *Prostate cancer antigen 3 (PCA3)* genes were developed and further optimized for real-time fluorescence monitoring. As a result, it was possible to develop a quantitative method for cDNA amplification, that presented higher amplification efficiencies and a reduction on the overall reaction time, when compared to the gold standard real time quantitative PCR (RT-qPCR). Furthermore, the proposed strategy is compatible with the integration into the chip-based microfluidics device, hence easily extended to the monitorization of gene expression levels.

Keywords: Lab-on-a-chip; Microfluidics device; isothermal DNA amplification; digital LAMP; *c-Myc*; prostate cancer; *SChLAP1*; *PCA3*.

RESUMO

Os métodos baseados em amplificação de ácidos nucleicos podem beneficiar dos recursos oferecidos pelas tecnologias *Lab-on-a-chip,* em particular aquelas que visam fins de diagnóstico molecular. Atualmente, as abordagens de amplificação isotérmica, mais precisamente o LAMP, tornaram-se alternativas promissoras à atual tecnologia *standard* (PCR). Independentemente do mecanismo de amplificação, a quantificação precisa do alvo ainda é um desafio. Para este fim, o desenvolvimento de métodos de amplificação digital ajudou a contornar esta limitação.

Esta tese teve como foco o desenvolvimento de um sistema de LAMP digital baseado em chip para a quantificação de biomarcadores de cancro da próstata. Para isto, o LAMP foi integrado com o conceito de amplificação digital baseada em gotas. A amplificação positiva do LAMP foi alcançada após 60 minutos, levando a um aumento de 2 vezes na fluorescência quando comparado com os controlos de amplificação negativos, numa abordagem de formação de gotas baseada em vórtex. No entanto, aspetos inerentes a este método impediram uma avaliação quantitativa da amplificação de LAMP. De modo a superar estas limitações, um novo dispositivo baseado em chip de microfluídica foi desenvolvido e implementado para quantificação de dLAMP do gene *c-Myc*. O chip para produção de gotas com uma geometria *T-junction* alcançou gotas de 1,5 nL com um coeficiente de variação abaixo de 3%, em conformidade com o padrão para esta técnica. Este sistema mostrou uma resposta nítida à concentração do alvo, observável pelo aumento na fração de gotas positivas. Além disso, a quantificação do alvo provou ser precisa (R^2 = 0,99) para 4 ordens de magnitude de cópias/µL (5 cópias/µL - $5x10^5$ cópias/µL) após a modulação de Poisson.

Com o objetivo de implementar este sistema dLAMP baseado em chip nas deteções de biomarcadores associados ao cancro da próstata, as reações de amplificação dos genes *SChLAP1* e *PCA3* foram desenvolvidas e otimizadas para a monitorização em tempo real da fluorescência. Como resultado, foi possível desenvolver um método quantitativo para amplificação de cDNA, que apresentou maior eficiência de amplificação e redução no tempo de reação geral, quando comparado com o método *standard* RT-qPCR. Além disso, a estratégia proposta é compatível com a integração no dispositivo de microfluídica, sendo facilmente estendida à monitoração dos níveis de expressão génica.

Palavras-chave: *Lab-on-a-chip*; Dispositivo de microfluídica; isotérmico; Amplificação de DNA; LAMP digital; *c-Myc*; cancro da próstata; *SChLAP1*; *PCA3*.

LIST OF ABBREVIATIONS AND SYMBOLS

5-TAMRA – 5-Carboxytetramethylrhodamine

ADT – androgen-depravation therapy

bp – base pairs

C – concentration in copies per µL

cDNA – complementary DNA

CV – coefficient of variation

CPD – copies per droplet

dLAMP – digital LAMP

ddLAMP – droplet digital LAMP

DRE - digital rectal exam

ds – double stranded

ELISA – Enzyme-linked immunosorbent assay

EDTA – Ethylenediaminetetraacetic acid

E_{pos} – Fraction of positive droplets

E_{pos}^{C} – Poisson corrected fraction of positive droplets

GMV – grey mean value

HDA – Helicase dependent amplification

IPA – Isopropyl Alcohol

IA – isothermal amplification

kb – kilobase

LOC – Lab-on-a-chip

lncRNA – long non-coding RNA

LAMP – Loop-mediated isothermal amplification

MAPKs – Mitogen-activated protein kinases

MTBC – *Mycobacterium tuberculosis* complex

N – Total number of droplets

NCBI – National Center of Biotechnology Information

NTC – Non-template control

NCDs - Noncommunicable diseases

NASBA – Nucleic acid sequence-based amplification

NAATs – Nucleic acids amplification technologies

N_{pos} – Number of positive droplets

ORFs – open reading frames

PoC – Point-of-care

PCR – Polymerase chain reaction

PS – Polystyrene

PCa – Prostate cancer

PCA3 – Prostate cancer antigen 3

PCATs – Prostate Cancer Associated Transcripts

Pr (0) – Poisson probability of a droplet contain zero target molecules

PSA – prostate-specific antigen

Qc – Flow rate of continuous phase

Qd – Flow rate of dispersed phase

RT-LAMP – Real-time LAMP

RT-PCR – Real-time PCR

RT-qPCR –real time quantitative PCR

RPA – Recombinase polymerase amplification

rt – Reverse transcription

RCA – Rolling circle amplification

SChLAP1 – Second Chromosome Locus Associated with Prostate-1

SNP – Single nucleotide polymorphisms

ss – Single stranded

SDS – Sodium Dodecyl Sulfate

SDA – Strand displacement amplification

$\mathbf{T_T}$ – Threshold time

TMA – Transcription-mediated amplification

TRIS – Tris(hydroxymethyl)aminomethane

µF – Microfluidics

$\mathbf{V_{droplet}}$ – Droplet volume

WHO – World Health Organization

TABLE OF CONTENTS

LIST OF FIGURES

LIST OF TABLES

1. INTRODUCTION

Noncommunicable diseases (NCDs) are the major cause of mortality worldwide (World Health Organization, 2019). Among the most relevant NCDs, cancer is one of the leading causes of death in the developed world and, thus, with severe impact on life expectancy in most of the countries. In fact, the World Health Organization (WHO) estimates that cancer is the first or second cause of death before the age of 70 years in 91 out of 172 countries (Bray *et al*., 2018). The global raise on both cancer mortality and prevalence are a reflex of the ongoing aging and growth of the population, as well as the changes in the distribution and prevalence of the main risk factors associated with the development of cancer, most of them linked to the socioeconomic development (Omran, 2005).

Despite all the knowledge gathered about cancer mechanisms, the clinical management is still anchored on morphological and histopathological methods to diagnosis and estimate prognosis, which could lead to overdiagnosis, overtreatment or late detection of cancer (Ilic *et al.,* 2018; Kumar-Sinha and Chinnaiyan, 2018). Besides, most of these methods undergo limitations like the lack of immediate and on-demand clinical use, due to their high cost, slow analysis and patient's discomfort (Grosso *et al.,* 2010; Rusling et al., 2010). Additionally, treatment modalities often rely on surgery to remove tumors and chemo and/or radiation therapy (Hanahan and Weinberg, 2011). These treatments could have late or long-term effects, such as radiation-induced cancers and cardiovascular diseases for radiotherapy, premature or accelerated aging, telomere shortening, increased levels of cytokines and decreases in the maximum oxygen consumption for chemotherapy (Shapiro, 2018). These practices have revealed themselves as inadequate and outdated, so an urge for the development of accurate cancer diagnostics and better therapeutics has arisen in the last decades. The ideal risk-preventive test should integrate the effects of both genetic and nongenetic factors and aim to an approach that relies on easy obtention of biological samples and technical reproducibility (Widschwendter *et al*., 2018).

More recently, breakthroughs in molecular characterization of aberrant genes, signaling pathways, cell-surface markers and hormonal or endocrine mediators associated with cancer have been incorporated into new diagnostic and treatment modalities allowing an earlier detection and a more efficient monitoring and staging of cancer, which improve the efficiency of therapeutics outcomes and welfare of patients (Dalton, 2006; Kumar-Sinha and Chinnaiyan, 2018). However, there is still a pressing demand to develop point-of-care (PoC) platforms for cancer diagnostics, that combine the specificity and accuracy with portability, user friendly and cost-effectively features, for use in

routine screening and resource-poor settings (Sandbhor Gaikwad and Banerjee, 2018; Vashist *et al*., 2015).

1.1 Molecular diagnosis

1.1.1 Current approaches of molecular diagnosis based on nucleic acids amplification

Amplification-based methods of nucleic acids are regarded as essential tools in life science research, among them are clinical medicine, diagnosis of genetic conditions, gene expressions analysis, detection and monitorization of infectious diseases. The value of these methods relies on their sensitivity and specificity for specific targets (Aoi, Hosogai and Tsuneda, 2006). The most widely used method to amplify nucleic acids is the polymerase chain reaction (PCR), where a sample is heated through two or three cycles of temperature, usually between 50 ºC and 95 ºC (Mullis *et al*., 1987). Additionally, real time quantitative PCR (RT-qPCR) technology has become the "gold standard" tool in molecular diagnosis, especially on the clinical oncology and gene expression context (Klein, 2002). However, the wide use of RT-qPCR has disclosed some critical points and limitations. Among them are the need for a precise temperature control, which is a restraining step, preventing the use of PCR in applications with narrow resources (Hsieh *et al*., 2012).

1.1.2 New approaches that aim to outmatch PCR limitations

In order to overcome the temperature issues of PCR, isothermal amplification methods have been developed. These techniques eliminate the need for complicated temperature control, while lowering energy consumption, making them suitable methods for point-of-care diagnosis and home-medicine applications (Gansen *et al.*, 2012). Additionally, these cost-effective techniques allow to drastically reduce the amplification time and simplify detection when compared to PCR (Li and Macdonald, 2015). The aim of these techniques is to achieve robust nucleic acids amplification at constant temperature. To achieve this, particular reaction conditions, primers and enzymes more complex than those used in PCR are usually required. These techniques include nucleic acid sequence-based amplification (NASBA), transcription-mediated amplification (TMA), strand displacement amplification (SDA), rolling circle amplification (RCA), helicase dependent amplification (HDA), recombinase polymerase amplification (RPA) and loop-mediated isothermal amplification (LAMP). A comparation between the different isothermal amplification methods is provided in Annex section, **Table A1**.

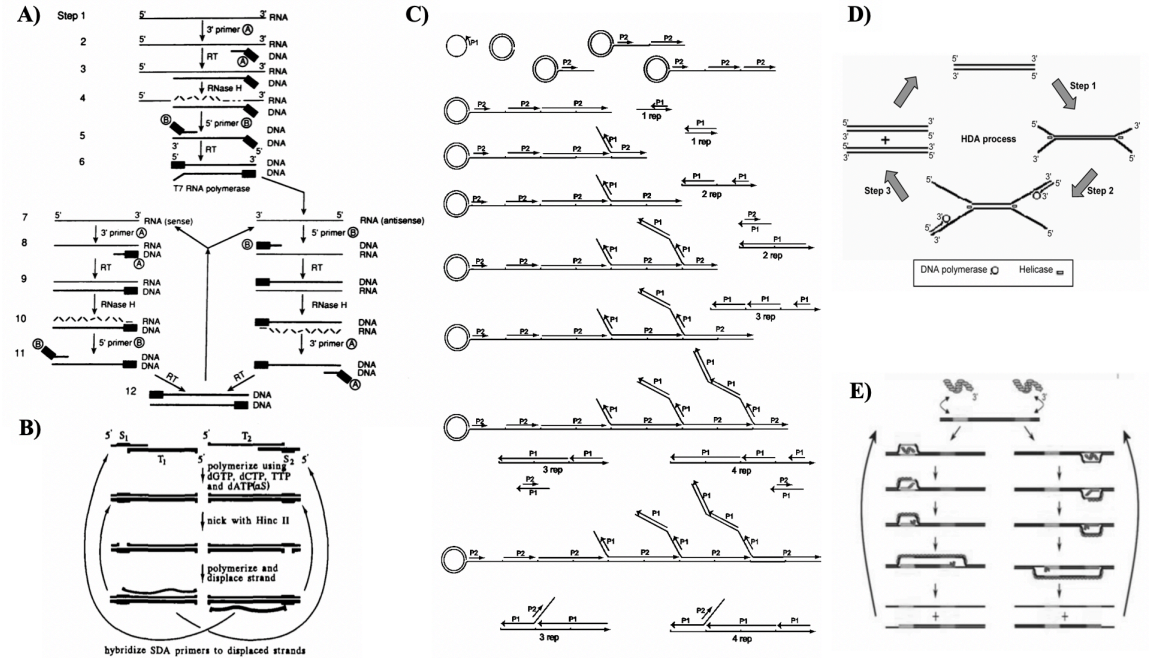

Figure 1. Isothermal amplification mechanisms. **(A)** Schematic representation of NASBA. Initially, the forward primer hybridizes to the target RNA molecule, leading to the formation of complementary DNA (cDNA) intermediate by reverse transcriptase and RNase H activity. Secondly, the reverse primer hybridizes in the cDNA intermediate forming a double stranded (ds) cDNA intermediate with a promoter region, which is recognized by T7 DNA-dependent RNA polymerase to produce more initial RNA template targets by transcription of the cDNA intermediate. The newly formed antisense RNA targets and cDNA serve as templates for the continuous cycling of reverse transcription (rt) and transcription reactions, resulting on the exponential accumulation of antisense RNA molecules complementary to the initial RNA target. **B)** Schematic representation of SDA. The SDA mechanism starts with heat denaturation in the presence of two primers. After this step, primers hybridize forming two primer-template duplexes with 5' overhangs, each containing one restriction site for the endonuclease (NEase) to cleave. Following, DNA polymerase extends the 3' ends of the duplexes to produce dsDNA with complete recognition sites, that will be cleaved after by NEase. These nicks create new 3' ends that promote new extension reaction with the displacement of the downstream fragment by DNA polymerase. The cycles of these sequenced events of cleavage and polymerization/displacement continuously produce a ssDNA molecule complementary to each of the primer-template duplexes, resulting in exponential accumulation of target sequences. **C)** Schematic representation of RCA of a circularized probe using two primers. The first primer (P1) initiates an RCA reaction, and the reverse primer (P2) binds to each tandem repeat generated by the rolling circle. Multiple priming events are initiated by P2 as the original RCA strand elongates. As these priming events elongate and generate displaced DNA strands, new priming sites for the first primer (P1) are generated. To follow the sequence of strand displacement events, note that as the reverse primer P2 binds to the fifth repeat, the primer at the third repeat begins to displace a branch; subsequently, as P2 binds to the seventh repeat, the elongating strand at the fifth repeat begins to displace a branch, and so forth. By the time a reverse primer binds to the tenth repeat, the DNA product already contains three growing branches. New primer extension events initiated in released DNA molecules also generate branches, as shown at the bottom of the figure. As the displaced DNA becomes completely double-stranded, it accumulates in fragments of unit length containing one, two, three or four repeats (shown as: 1 rep, 2 rep, 3 rep, 4 rep). Thus, in the presence of a circular template, the two primers generate a self-propagating, ever-increasing pattern of alternating strand-displacement, branching and DNA fragment release events, which we call hyperbranching. **D)** Schematic representation of HDA. Step1, the helicase unwinds template DNA duplexes. Step 2, specific primers hybridize to ssDNA template molecules. Step 3. DNA polymerase

extends the primers. One duplex is replicated into two duplexes. The newly formed dsDNA molecules are separated by helicase and the chain reaction repeats itself, so that exponential amplification can occur at a single temperature**. E)** Schematic representation of RPA. The recombinase-primer filaments scan the dsDNA target molecule for the homologous site. Recombinase catalyzes the primer hybridization with the homologous template sequence. Strand exchange is promoted by recombinase in the cognate sites. The resulting structures are stabilized by ssDNA-binding proteins to prevent primers displacement by branch migration. DNA polymerase recognize the 3' end of the primer and starts primer extension reaction. The binding/extension events of two opposing primers generate one complete copy amplicon together with the original template.

1.1.3 Nucleic Acid Sequence-based Amplification (NASBA)

NASBA was developed in 1991 to specifically amplify single stranded RNA (ssRNA) in a similar process to the Transcription Mediated Amplification (TMA) (Compton, 1991). The working model (see **Figure 1A**) mimics the retroviral RNA replication and requires three different enzymes: reverse transcriptase, RNase H and DNA-dependent RNA polymerase, whereas TMA uses a unique reverse transcriptase with intrinsic RNase activity. The amplification efficiency of NASBA is commonly between 10^6 to 10^9-fold in 1.5 to 2 hours at 41ºC (Zhao *et al*., 2015). Besides the single working temperature, the simple and rapid detection without the need of denaturation step are additional advantages. Many approaches for the detection have been assessed to detect NASBA amplicons, such as gel electrophoresis (Burchill *et al*., 2002), real-time fluorescence (Abd El Galil *et al*., 2005), electrochemiluminescence (van Gemen *et al*., 1994) and colorimetric assays (Gill *et al*., 2006).

Even though NASBA was developed to RNA amplification, it has also been widely used to probe long RNAs, mostly due to the high sensitivity conferred by exponential signal gain (Lo and Baeumner, 2007). Moreover, some NASBA-based commercial kits have been used for the identification of pathogens in clinical diagnosis (Ginocchio *et al*., 2003). For example, gold nanoprobe-NASBA system based on 16S identification was proposed as a simple and rapid detection method aiming for the differentiation of major salmonellosis-causing agents (Mollasalehi and Yazdanparast, 2013).

1.1.4 Strand displacement amplification (SDA)

In 1992, Walker proposed an amplification system based on the cleavage by restriction enzymes (typically HincII) and subsequent polymerization/displacement by an exonuclease deficient (exo$^-$) DNA polymerase (commonly, klenow DNA polymerase I from *E. coli*), removing the requirement for reverse transcription (rt) and transcription reactions like in NASBA (see **Figure 1B**) (Ridley *et al*., 1991). The exponential accumulation of dsDNA amplicons from genomic DNA, previously heat denatured,

enables an amplification efficiency of nearly 10^7-fold in 2 hours at 37ºC (Walker *et al*., 1992).

The SDA assay has been employed as a detection method for DNA methylation, which is closely associated with various diseases. Zhu *et al*. demonstrated the detection of DNA methylation with a two-stage isothermal amplification method and a short linear probe (Zhu, Yang and Zhang, 2013). Additionally, an ultrasensitive biosensor for methyltransferase activity was assessed with an integrated-molecular-beacon based in SDA strategy (Cui *et al*., 2019).

1.1.5 Rolling Cycle Amplification (RCA)

Rolling cycle amplification is a method proposed in 1995 for *in vitro* amplification of circular template molecules, that is adapted from *in vivo* rolling cycle DNA replication mechanism (see **Figure 1C**) (Fire and Xu, 1995). The original strategy for RCA amplification involved several cycles of enzymatic synthesis, in which ϕ29 DNA polymerase extends a hybrid of primer-circular template by continuously rolling around the circular DNA probe of several dozen nucleotides, in order to generate numerous copies of its sequence (Cho *et al*., 2005; Demidov, 2002). Further developments, led to multiply primed rolling cycle amplification, which uses distinctive proprieties of ϕ29 DNA polymerase and random primers. This technique has an amplification efficiency of 10^4-fold for 1.5 hour at 37 ºC and allows the amplification of circular DNA directly from cells or phages (Dean, 2001).

RCA is extensively used for diagnostic proposes, for direct or indirect detection of RNA/DNA molecules, proteins and other biomarkers. Recently, RCA-based assays have gained attention of research centers and diagnostics-oriented biotech enterprises for proposes such as gene tests and immunoassays, single-cell analysis systems, single nucleotide polymorphisms (SNP) scoring, sequencing template preparation and gene expression studies (Demidov, 2002).

1.1.6 Helicase Dependent Amplification (HDA)

Helicase dependent amplification is based in the unwinding activity of helicase (Vincent, Xu and Kong, 2004). In this process helicase activity is used instead of heat, to separate the two strands of the template molecule, generating single strand templates (see **Figure 1D**) (An *et al*., 2005). In fact, HDA overcomes the incapability of PCR and other isothermal methods on amplifying long DNA targets, *i.e*. kilobase (kb) long regions, which have great interest in many researches and diagnostic applications (Zhao *et al*., 2015).

Mechanistically, HDA comprises three steps (template separation, primer hybridization and primer extension), similar to PCR. However, the template separation is performed by helicase rather than by heat denaturation, within the PCR cycles. So, HDA reaction allows exponential replication of the dsDNA targets at a single temperature, totally eliminating the need for thermocycling equipment (Eisenstein, 2005). HDA amplicons can be detected by gel electrophoresis, real-time monitoring, and enzyme-linked immunosorbent assay (ELISA) (Gill *et al*., 2007). Over 10^6-fold amplification can be achieved. In its original version, HDA reaction occurred at 37ºC, due to thermal instability of *E. coli* UvrD helicase (An *et al.,* 2005). Developments of thermostable proteins enabled faster reaction at higher temperatures (60-65ºC) and increased the sensibility and specificity for pathogens and SNPs detection (Chen *et al*., 2015). Commercial HDA kits can be purchased to BioHelix Corporation.

1.1.7 Recombinase Polymerase Amplification (RPA)

Recombinase polymerase amplification exploits the recombinase activity to separate the dsDNA target molecules rather than temperature cycling (see **Figure 1E**), similar to HDA mechanism (Piepenburg *et al*., 2006). The exponential amplification allows the accumulation of target molecules in 40 minutes at low temperature (37-42ºC). Additionally, the detection limit is low as 1 single target copy. In addition to the common detection methods used for the other isothermal techniques, a unique FRET-based fluorescent probe and a lateral flow strip sensing system were also employed to RPA, in order to decrease the background signal and allow an instrument-free detection, respectively (Zhao *et al*., 2015).

RPA have been applied to the detection of viruses and pathogens, in fact there are commercial RPA kits to this end (TwistDx, Cambridge, UK). Additionally, RPA strategy was also employed on integrated microfluidic platforms for the detection of pathogenic DNA or RNA molecules (Shen *et al*., 2011).

1.1.8 Loop Mediated Isothermal Amplification (LAMP)

Loop-mediated isothermal amplification is a simple, rapid and cost-effective technique when compared with PCR, NASBA and SDA. Among the advantages of LAMP are the ability to carry the amplification of its target in the presence of nontarget DNA, the high sensitivity and specificity of the amplification, the isothermal working temperature (60-65 ºC) without thermocycling and the requirement for less than one hour. LAMP was originally developed by Notomi *et al.* who proposed a system that requires a total of four or six primers, termed outer, inner and loop primers, a polymerase with strand

displacement activity, that produces a great number of amplified products (>10^9) (Notomi, 2000). The final products generated by LAMP are under the form of stem-loop DNA with several inverted repeats of the target DNA, unlike the linear DNA products which are generated by PCR. In **Table 1** can be found a comparative table between LAMP and PCR techniques.

LAMP technique (see **Figure 2**) comprises three steps: 1) Starting material producing step, 2) Cycling amplification step and 3) Elongation and recycling step. The working principle behind this amplification technique can be explained considering one strand of the target DNA sequence, which contains three sites of recognition in the 5' end designated as B3, B2 and B1 and other three sites in the 3' end designated as F3c, F2c and F1c. The outer primers are designed aiming the hybridization in 5' end of each strand of the target DNA. So, the outer primer F3 has the sequence complementary to F3c, whereas the outer primer B3 has the same sequence of B3 site in the target DNA. The inner primers are called Forward Inner Primer (FIP) and Backward Inner Primer (BIP). These primers contain two joint sequences, each one corresponding to sense and antisense sequences of the target DNA, the first sequence is necessary for the priming in the first stage of the amplification and the second one is needed for the later stages. These means that FIP comprises a sequence equal to F1c on the target DNA, an optional TTTT spacer and a sequence F2, which is complementary to F2c. BIP, by its turn, comprises the sequence B1c which is complementary to B1, an optional TTTT spacer and a sequence equal to B2 on the target DNA.

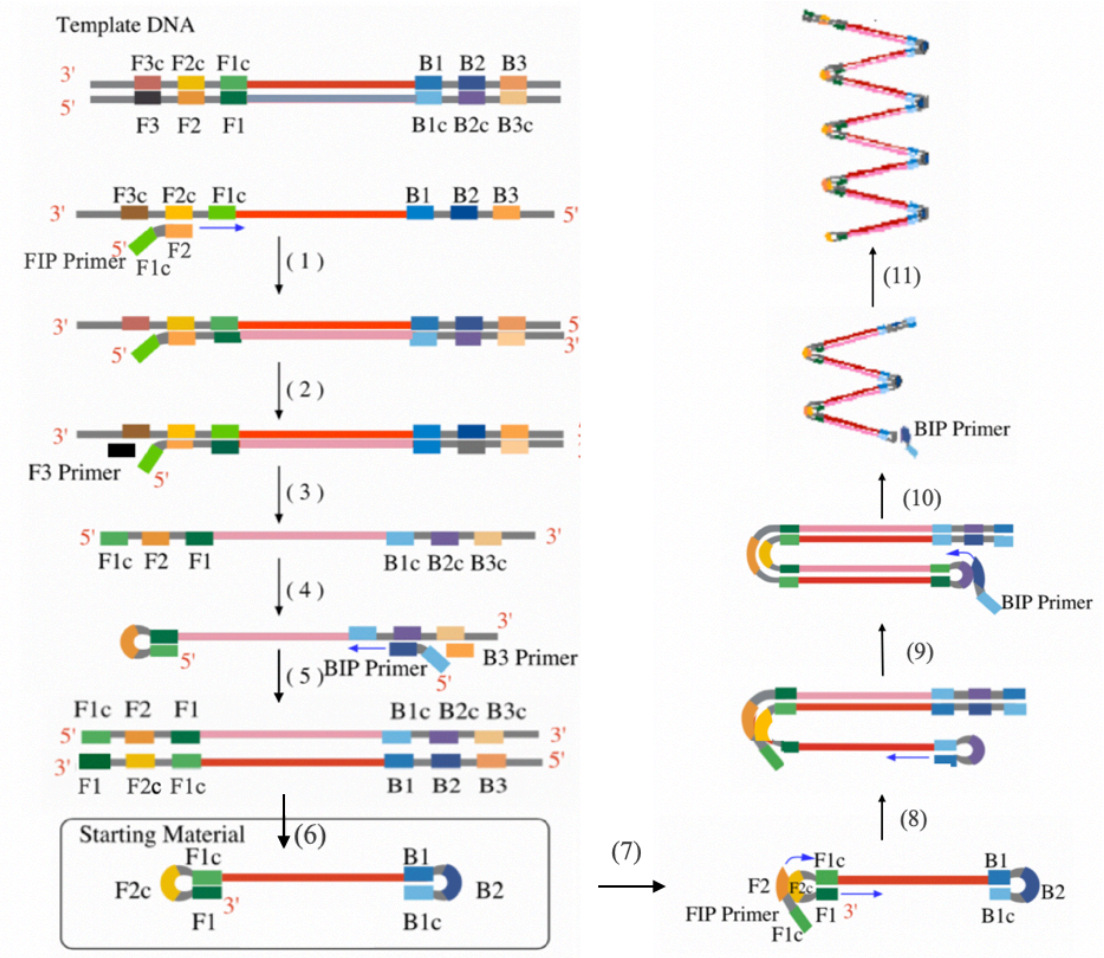

Figure 2. Schematic representation of LAMP reaction. Steps (1) to (6) correspond to the first stage of LAMP – starting material producing stage. Steps (7) to (10) correspond to the second stage – Cycling amplification. Step (11) represent the third and final step of LAMP – Elongation and rolling cycle step. Adapted from reference (Notomi, 2000).

Following sample denaturation, the reaction begins with the hybridization of FIP, which is in a higher concentration then F3, in F2c site of the target DNA, leading to the synthesis of the complementary strand following 3' to 5' direction. Then, the F3 primer hybridizes in the F3c region of the target DNA, causing the displacement of the newly synthetized strand. Due to this displacement, the F1c part of FIP, which is complementary to the F1 site of the new strand can form a loop structure. Then, this primarily strand serves as template for a similar process to occur with BIP as initiator of DNA synthesis and B3 primer causing the strand displacement, culminating in the formation of a dumb-bell structure DNA. At this point the first step of LAMP reaction is completed.

The second stage of LAMP initiates with the elongation of the 3' end of the dumb-bell structure, which is quickly converted to a stem-loop, once the 3' end is recognized as a primer by the DNA polymerase, a phenomenon known as self-priming. The amplification proceeds through successive hybridization of FIP and BIP to their

complementary regions followed by elongation and recycling steps (stage 3), culminating in the formation of the final products that comprises a mixture of stem-loop DNAs and concatenated DNA strings with several loops, formatted by alternative annealing of inverted repeats of the target sequence and other secondary products.

Table 1.1. Comparation of main properties of LAMP and PCR amplification methods

Property	**LAMP**	**PCR**
Sensitivity	High	Low
Reaction time	Usually 1 hour	2 to 3 hours
Amplification factor	10^9 - fold in 1 hour	2^{30} - fold in 2 to 3 hours
Working temperature	Isothermal (60 ºC to 65ºC)	3 different cycling temperatures: 95ºC, 50ºC – 65ºC and 72ºC
Number of enzymes required	1 (Bst polymerase)	1 (Taq polymerase)
Denaturation step	No	Yes
Denaturation agent	Enzyme with strand displacement activity	Heat
Number of primers required	4 - 6	2
Primer design	Complex	Simple
Templates	DNA and RNA	DNA and RNA
Resulting amplicon	Concatenated DNA	Double-stranded DNA
By-products	Many	Few (mostly primer dimers)
Tolerance to unwanted biological elements	High	Low
Influence of non-target DNA	Low	High
Product detection method	Gel electrophoresis, real time, turbidity	Gel electrophoresis, real time, ELISA
Multiplex amplification	Yes	Yes

Since LAMP assay was introduced by Notomi, it has undergone numerous improvements for a broader range of applications, including the detection of human respiratory pathogens, such as *Mycobacterium tuberculosis* (Bentaleb *et al.,* 2016) and *Streptococcus pneumoniae* (Winstel, Xia and Peschel, 2014). Furthermore, LAMP assay was also successfully applied to the diagnosis of pathogens related with foodborne diseases, like *Salmonella typhi* (Fan *et al.,* 2015) and to the detection of a wide range of virus, including adenovirus (Ziros *et al*., 2015) and hepatoviruses, like hepatitis B (Wang *et al*., 2016). In summary, LAMP simplicity, quickness and adaptability to field circumstances denote its prominence as an ideal diagnostic technique, as it fulfills all the criteria proposed by the WHO, on having the ideal molecular diagnostics characteristics (Wong *et al*., 2018).

1.2 Lab-on-a-chip

Lab-on-a-chip (LOC) approaches are considered the next generation of sensing technology and have already showed to be advantageous when compared to the traditional techniques (Zhang *et al*., 2019). In addition to non-conventional methods to nucleic acids amplification, LOC systems have also been under strong development and implementation over the last decade (Ríos, Zougagh and Avila, 2012). This approach brings numerous benefits, mostly due to the scale effect, such as the physical phenomena that appears with it, the portability, low consumption of energy and reagents, low risk of contamination, reduction on the time of the assays and increased sensibility (Francesko, Cardoso and Lanceros-Méndez, 2019).

The increasing demand for faster and accurate detection tools against diseases and pathogens, in the fields of medicine and food safety, directed the focus towards molecular diagnostics for PoC applications. PoC is an approach that involves analyzing the sample in the site where it is collected, thereby reducing the time required for diagnosis and preventing sample transfer to offsite testing laboratories (Ravi *et al*., 2019). Moreover, PoC devices usually do not require professional personal, integrates detection devices and reduces the costs (Yin *et al.,* 2019). The development of PoC devices is related with improvements in microfluidics, which is a key feature of LOC technologies (Francesko, Cardoso and Lanceros-Méndez, 2019). During the last years, the impact of microfluidic technology in the diagnostics field has increased dramatically. In fact, the value of microfluidic devices has been noticeable by outstanding companies such as Merck, Abbott, Roche Diagnostics, Ibidi and Cepheid, which provide microfluidics devices (Ruzycka *et al*., 2019). Additionally, companies specialized in nanotechnology and microfluidic have been emerging, such as Darwin microfluidics, Micronit, uFluidix and Elvesys. The increasing demand for the development of microfluidics devices and

strategies is also reflected in the growing number of papers concerning engineering of new microdevices and their applications (**Figure 3**) (Ruzycka *et al*., 2019).

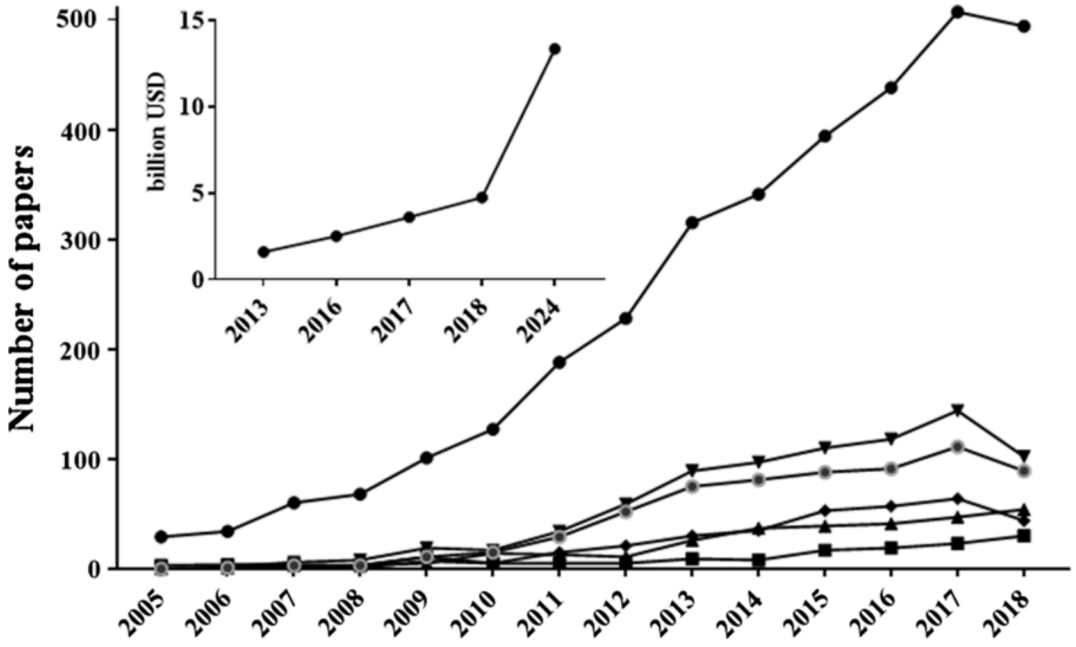

Figure 3. Increased publication trend on microfluidics used in cancer studies in the years 2005–2018. Data were collected based on PUBMED and NCBI databases. The insert presents the estimated and expected worth of the microfluidic market in billion USD based on PR Newswire, Grand View Research, Markets and Markets and Mordor Intelligence estimations. Legend: (–•–) microfluidic and cancer. (–▲–) microfluidic and lung cancer. (–■–) microfluidic chips and cancer. (–◉–) microfluidic and CTC. (–◆–) microfluidic chip and metastasis. (–▼–) microfluidic and metastasis. Reprinted from Ruzycka *et al*., 2019.

Microfluidics is generally described as the precise control and manipulation of small volumes and fluids at microliter scale (10^{-9} to 10^{-18} liters), through the exploit of small size channels and laminar flow of fluids inside them, due to extremely low Reynolds number. These basic properties give rise to advantages that highlighted its potential on applications for biology, diagnostics and chemical synthesis fields, both in academia and industry. Microfluidics offer advantages such as the use of small volumes of samples and reagents, carry out separation and detection with high resolution and sensibility, cost-effectiveness and allow for devices with a small footprint. Since the introduction of microfluidics methods, PCR was the most exploited nucleic acid amplification technique (Kopp, 1998) either on its conventional (Zhang *et al*., 2006), quantitative (Ahrberg, Manz and Chung, 2016) or digital forms (Sreejith *et al*., 2018).

Currently, this is still the most exploited microfluidic-based amplification system. Commercial ddPCR devices such as QX100/QX200 Droplet Digital™ PCR (Bio-Rad, California), RainDrop plus™ system (RainDance™ technologies, Massachusetts) and Crystal Digital PCR™ (Stilla Technologies, Paris) are already under current use. However, the use of PCR amplification demands for a precise temperature control resulting on the increase of challenges and cost of PoC system's design and operation. Conversely, isothermal amplification (IA) techniques became promising alternatives to PCR (Giuffrida and Spoto, 2017) hence the requirement of a single working temperature simplifies the system design, which is a valuable feature, especially for PoC applications (Craw and Balachandran, 2012).

In fact, LAMP is the most commonly used isothermal method, as it provides an outstanding specificity when compared with other isothermal amplification architectures (Notomi, 2000). The potential of LAMP-on-a-chip technology relies on the simplicity of system requirements, easy integration with sample preparation steps, multiple detection methods and tolerance to biological components present in clinical samples, which endorses the use of LAMP-on-a-chip method. Presently, microfluidics, paper-based and digital variants of LAMP-on-a-chip have been trending (see Annex, **Table A2**) (Zhang *et al.*, 2019). Examples of these systems can be found in scientific literature, such as a centrifugal microfluidic system integrated with LAMP method to endpoint detection of foodborne pathogens (Sayad *et al*., 2018). More importantly, LAMP-on-a-chip systems are starting to become available in commercial applications, such as Illumigene® developed by Meridian Bioscience Inc (Cincinnati, OH) as a molecular diagnostic tool for Malaria parasites (Lucchi *et al*., 2016) and LoopAmp® developed by Eiken Chemical Co., Ltd. (Tokyo, Japan) as a qualitative *in vitro* diagnostic test for the detection of *Mycobacterium tuberculosis* complex (MTBC) (Kolluri, Klapperich and Cabodi, 2018).

1.2.1 Association of Digital Amplification-based methods with Lab-on-a-chip technology

Amplification-based methods can benefit from the features that arise from LOC technologies, in particular those that aimed on detection or quantification of DNA/RNA molecules, such as molecular detection, characterization and profiling of diseases. Regardless of the amplification method, accurately quantify the copy number of the target sequence is of the utmost importance. Since, for most cases, RT-qPCR do not provide a precise measurement of the initial template concentrations, digital or limiting dilution DNA amplification methods have been developed, in order to circumvent this limitation (Sanders *et al*., 2011).

Digital amplification-based methods are centered on Poison statistics, presuming that the total sample volume can be diluted and divided into numerous small compartments, such that on average, each compartment contain less than one template molecule. Carrying out the DNA amplification, the number of initial template molecules in the sample is estimated to be equal to the number of compartments that displays amplification. In order to increase the dynamic range, there has to be a higher number of droplets (Gansen *et al*., 2012).

Based on the compartmentalization method, digital LAMP (dLAMP) systems can be assembled into two categories: well-plate-based systems, which use a chip with microchambers, and droplet-based systems, where the reaction mixture is divided, via microfluidics compartmentalization, into droplets suspended in oil (Zhang *et al*., 2019) (see **Figure 4)**. Despite the compartmentalization method, the miniaturization of the reaction offers benefits such as the reduction on the sample and reagents volumes, lowers the risk of contamination and reduces the reaction time, which are particularly advantageous for LAMP reactions (Zhang and Ozdemir, 2009). Various digital amplification systems that aimed on the formation of these microreactors have been developed to performed both PCR and LAMP reactions. Among them is the first chip-based dLAMP system that was composed by 5,000 micro-chambers fabricated in PDMS (Gansen *et al*., 2012). The sample and oil were sequentially loaded into the chamber by air pressure, and the temperature needed to the LAMP reaction was obtained through placing the chip into a water reservoir at approximately 65ºC. Few years later, the introduction of the first self-priming system chip-based dLAMP (Zhu *et al*., 2012) caused an architecture improvement by the removing the external pumping or valves. For this, air was fully removed from the chip, which allows the loading of the sample and oil to occur only due to the pressure differences between the external and internal chip environments. In 2015, a droplet-based dLAMP system was proposed in which droplets were generated by a T-junction type microfluidic channels (μF), then the droplets were moved to a heated incubation chamber for DNA amplification (Rane et al., 2015).

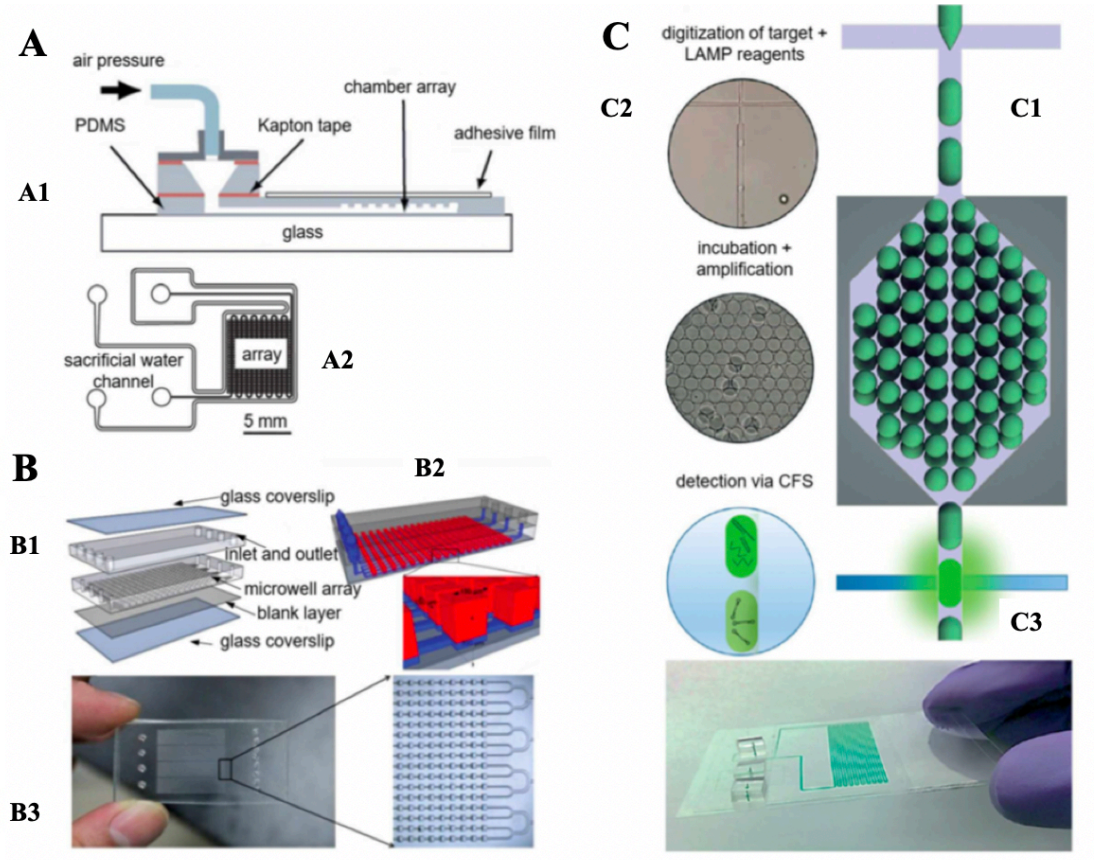

Figure 4. Lab-on-a-chip devices for Digital LAMP. A) Design of the digital LAMP self-digitization chip. **(A1)** Schematic diagram showing the individual components of a fully assembled chip. The microfluidic array was embedded in a thin piece of PDMS, which was covered by a sealant film on top and a PDMS coated cover slip on the bottom. Air pressure was delivered via a removable adapter, which was connected to an external pressure source. **(A2)** Layout of the microfluidic network. A dense array of rectangular side chambers was connected to a thin main channel. The whole array was surrounded by a separate water reservoir to saturate the PDMS during incubation at 65 °C. **B)** Design and mechanism of the self-priming digital LAMP. **(B1)** Schematic diagram of the microfluidic chip, showing the layers of the device structure. **(B2)** Schematic of the whole microchip that contains four separate panels, each of which has an individual inlet and outlet. The blue lines are the flow channel. The red spots stand for the microwells. Each microwell was partitioned by oil. **(B3)** Photograph of the prototype device. The device is composed of three layers of silicone rubber (PDMS), a blank layer and a flow layer containing hundreds of microwells, bonding on a glass coverslip (0.17 mm). The size of the chip is 50 mm 6 24 mm 6 4 mm. **C)** Droplet microfluidic device for continuous flow digital LAMP analysis. **(C1)** Schematic diagram of digital LAMP analysis that are conducted on the droplet microfluidic device. **(C2)** Images of the droplet generation and incubation region on actual microfluidic device are shown in the top two circles. **(C3)** Image of an actual thin microfluidic device. Adapted from Zhang *et al*., 2019.

Results from the dLAMP devices are usually analyzed using either flow cytometry or digital imaging processing, since the detection methods rely on fluorescent DNA intercalating dyes and calcein dye-based indicators (Zhang, Lowe and Gooding, 2014). Currently, conventional detection methods rely on naked eye monitoring to detect

precipitates (Mori and Notomi, 2009), DNA-binding dyes (Hong *et al*., 2011) and colorimetric indicators (Yuan *et al.,* 2018). However, real-time optical monitoring also exists, such as turbidity measurement (Shan *et al*., 2012) and fluorescence with a suitable dye (Yi *et al*., 2014). For endpoint and off-chip detection, gel electrophoresis is the most commonly adopted method (Le *et al*., 2012). Additionally, electrochemical methods are also used for real-time or end-point monitoring (Ahmad *et al*., 2011). Furthermore, antibody-based methods (Lee, Chen and Peng, 2009), nano-Au probes (Suebsing *et al*., 2013), field effect transistors (Veigas *et al*., 2014), bioluminescence (Kiddle *et al.,* 2012) and surface plasmon resonance (Chuang *et al*., 2012) are also being tested. Nevertheless, nonconventional detection methods still required further improvements, in order to outmatch the current demand for chemical preparation or additional instruments to obtain the results (Zhang *et al*., 2019).

In summary, LAMP presents itself as an ideal method for diagnosis in a routine PoC setting, since LAMP assay offers advantages when compared to PCR, such as the requirement of simpler heating systems, higher sensibility and easier detection methods (like naked eye observation). These features are particularly valuable for PoC applications and suitable with dLAMP implementation, which has been conquered a great value as a diagnosis tool of virus, bacteria and allergens in food. Nevertheless, there is still ongoing improvements that need to be addressed, like the miniaturization of the detection modules in order to be integrated on PoC devices. Additionally, there is still room to expand the application of LAMP assays to earlier detection of genetic disorders.

1.3 Prostate Cancer as a model

This work was focused on the development of a digital diagnostics platform for prostate cancer. Still, the concept herein proposed may easily be extended to any other DNA/RNA that constitute a relevant biomarker for any other pathology of interest.

1.3.1 Epidemiology

Prostate cancer (PCa) is the most commonly diagnosed type of cancer in men and the fifth cancer-related death worldwide, accounting for approximately 1.3 million incidences and 359,000 deaths in 2018 (Bray *et al*., 2018). PCa is noticeable for its heterogeneity and variation across the globe. In fact, there is a 40-fold variation in age-adjusted incidence of PCa between American native men (highest incidence rate) and Asian men living in their native countries (lowest incidence rate) (Helming *et al*., 2014). Additionally, the highest mortality rate due to prostate cancer is in Sub-Saharan Africa

and Caribbean regions, controversially the highest incidence rate is found in Australia/New Zeeland, Western and Middle Europe and United States (see **Figure 5**). However, it should be taken in account that this difference can be endorsed by disparities in healthcare that arises from the limited access to effective treatment, diagnostic intensity and the practice of prostate-specific antigen (PSA) screening (Pernar *et al.*, 2018)

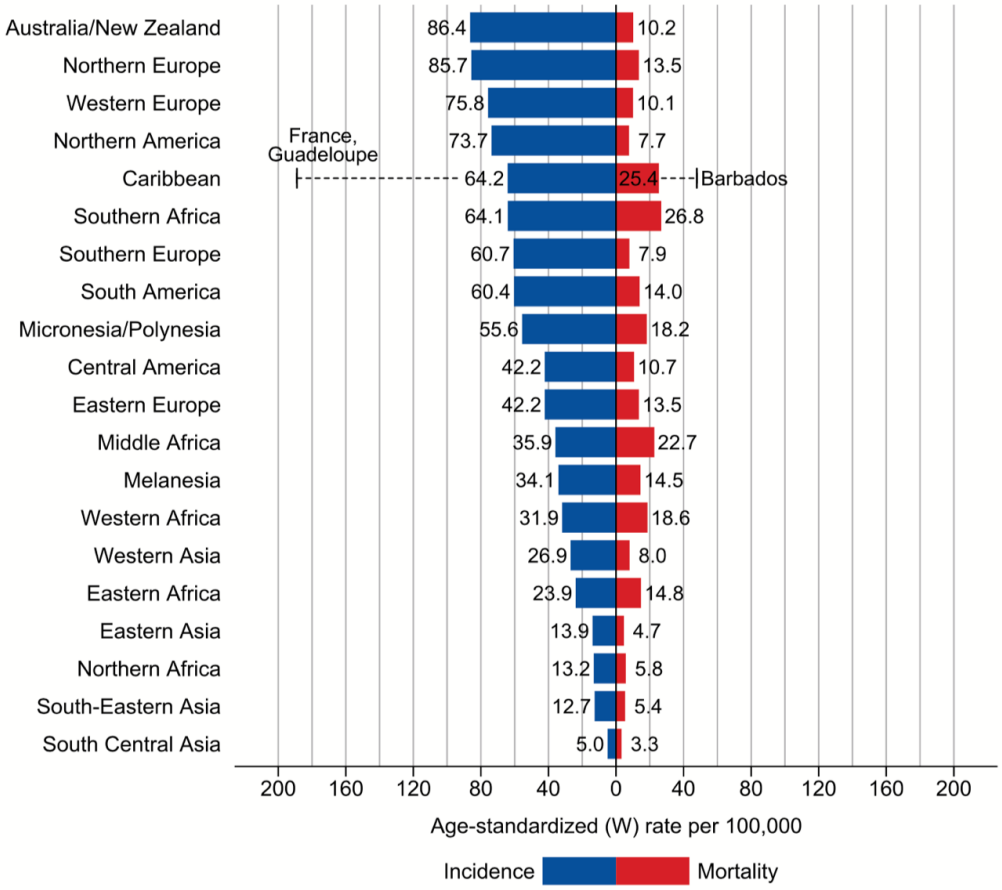

Figure 5. Bar Chart of Region-Specific Incidence and Mortality with Age-Standardized Rates for Cancers of the Prostate in 2018. Rates are shown in descending order of the world (W) age-standardized rate, and the highest national age-standardized rates for incidence and mortality are superimposed. Source: GLOBOCAN 2018.

Recently, an increase in diagnosis of PCa in countries that have adopted PSA screening as routine is leading to *overdiagnosis* (diagnosis of a "disease" that would not cause symptoms or lead to mortality in absence of screening) (Etzioni, 2002). This is being observed in countries like China and Brazil, leading to a raise in incidence rates of PCa in the last few years (Zhou *et al.*, 2015). Even though death rates have been decreasing in North America, Oceania and Northern and Western Europe, mostly due to

the earlier diagnostic and improvement of treatment, there are countries were the rates are rising including those in Central /South America and Central /Eastern Europe (Center *et al.,* 2012). This increase may reflect a change to risk factors and underlying incidence trends that could be related with a more westernized lifestyle. These data suggest that environmental and/or life factors may influence this disease (Coburn *et al*., 2017).

1.3.2 Screening

During the last 30 years, lab diagnostics of PCa relied on the measurement of serum prostate-specific antigen and the results of a digital rectal exam (DRE). However, these revealed to be inadequate for detection of clinically specific PCa (Raja and Russell George, 2019). Currently, the combination of PSA test with physical examination and an overall clinical assessment is needed since PSA is not a specific indicator of PCa. This because factors like urinary tract infection, benign prostatic hypertrophy, prostate surgery and biopsies can also led to a rise in the PSA levels (Roobol and Carlsson, 2013). Furthermore, the cutoffs for PSA screening are not accurate in predicting prostate cancer, with roughly 15% of men with normal levels of PSA having PCa and around 75% of men with high PSA levels without any sign of malignancy (Barry, 2001).

The *Gleason score* is a grading system used to determine the aggressiveness of prostate cancer (Gleason and Mellinger, 1974). The Gleason grade is estimated through the similarity of the tissue from the biopsies with normal tissue (lower Gleason grade) or with abnormal tissue (higher Gleason grade), the Gleason grade range from 1- 5 (see **Figure 6**) (Epstein, 2010). Since most of the cancer tissues are made of cells with different grades, two different regions are analyzed, and the Gleason score is determined by the sum of individual scores. Furthermore, the likelihood of cancer grows and quickly spread increases for higher Gleason scores (Humphrey, 2004). Gleason scores of 6 and bellow are considered to be low-grade and as so less aggressive. On the opposite, scores of 8-10 are determined high-grade, which implicates higher probability of metastasis development and lead to lethal tumors (Pierorazio *et al.,* 2013).

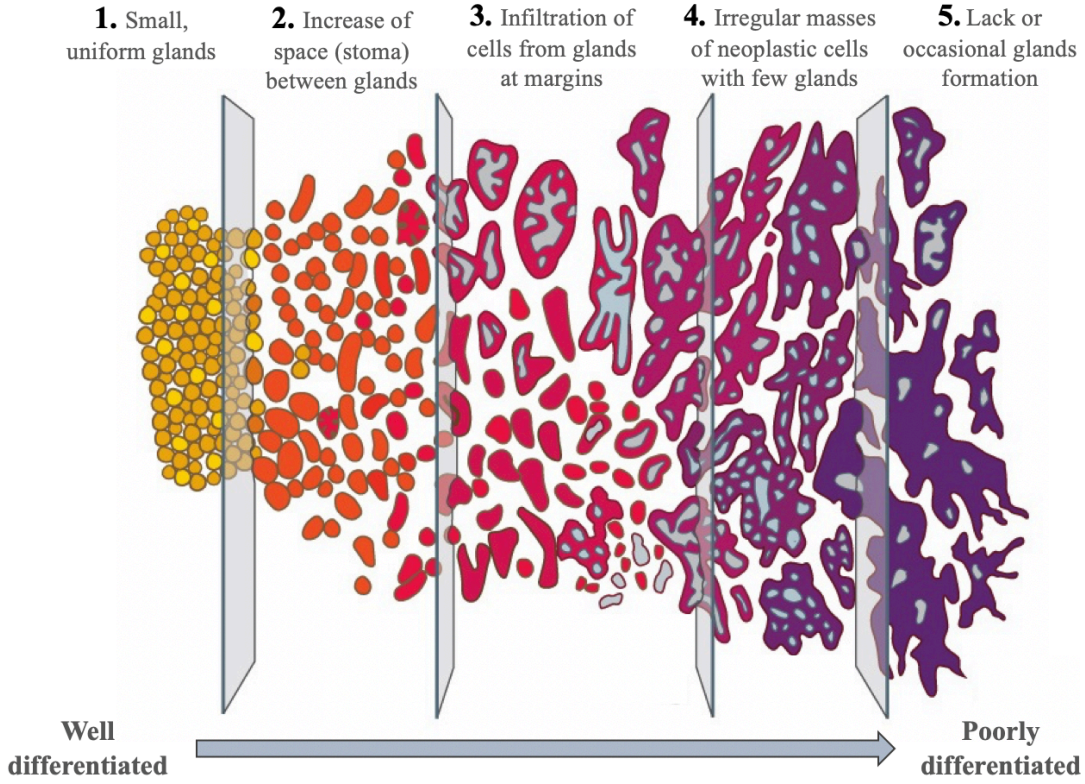

Figure 6. Schematic histopathological features of tissue appearance and characteristics with Gleason grade. Histopathological tissue appearance of each Gleason grade. Lower grades have higher similarity with normal tissues. Since, most of the cancer tissues are made of cells which have different grades, two different regions are analyzed, and the Gleason score is determined by the sum of individual scores.

Finally, despite the breakthroughs on the understanding of the molecular basis of aggressive and indolent prostate cancer, negligible improvements have occurred in the global outcome of patients. While the great majority of the efforts are directed to proteins and protein coding genes, the study of non-coding genes still deserves further investigation.

1.3.3 New Class of Biomarkers in PCa

Recently, urinary biomarkers were considered to be helpful in the detection and prognosis of prostate cancer. In fact, urine ought to be an excellent source for recovering and analyzing prostate cancer biomarkers because of the anatomical position of the prostate in relation to urethra. Besides, unlike other biological samples (*i.e.* blood or tissue), urine collection is inexpensive, and it is easy to obtain higher sample volumes without the need of invasive procedures. However, when targeting nucleic acids, one should consider the high content of nucleases and RNases in urine samples, the high level

of RNA fragmentation and instability (Martignano *et al*., 2017). Additionally, salinity, urea and hydration levels affect the properties of urine samples.

Several of these novel urinary biomarkers are being currently investigated for improved predictive value on prostate cancer detection: *Prostate cancer antigen 3* (*PCA3*) (Filella and Foj, 2016) and *Second Chromosome Locus Associated with Prostate-1* (*SChLAP1*) (Casadio *et al*., 2013), which are both long non-coding RNAs.

1.3.4 Long non-coding RNAs

Long non-coding RNAs (lncRNAs) are a class of RNA molecules with more than 200 base pairs (bp), which are not transcribed into proteins due to the lack of functional open reading frames (ORFs) (Prensner and Chinnaiyan, 2011). There are two main categories of lncRNAs based on their location in the genome, relatively to protein coding genes: intergenic and intragenic. This last subcategory can be further divided on intronic, exonic and overlapping lncRNAs (Derrien *et al*., 2012). Even though, merely 20% of the transcripts in the human genome are coding RNAs, little is known about lncRNAs and its function (Rinn and Chang, 2012). Among the roles played in cellular processes by lncRNAs are the regulation of gene expression (mostly transcription rather than posttranscriptional regulation), chromatin remodulation (Rinn *et al*., 2007), regulation of mRNAs stability (Gong and Maquat, 2011), pluripotency in steam cells (Guttman *et al*., 2011) and X chromosome inactivation (Lee, 2009).

1.3.5 lncRNAs in Prostate Cancer

The study of lncRNAs have been conquering attention for its potential as markers for cancer progression. One of the most well-known PCa markers is Prostate Cancer antigen 3, which was initially discovered through the expression profile of prostate samples (Nakanishi *et al*., 2008). The analysis of *PCA3* in urine samples can aid in the prediction of Gleason score and histopathological characteristics. Nevertheless, *PCA3* is not a good predictor of cancer outcomes, such as relapse and metastasis. Through another study in which 102 prostate samples were examined cancer, approximately 1,800 lncRNAs were found to be expressed in prostate tissues (Prensner *et al*., 2011).Among the transcripts identified, 121 lncRNAs were discovered, whose expression patterns allow the differentiation between benign, localized and metastatic prostate cancers, these lncRNAs are defined as Prostate Cancer Associated Transcripts (PCATs).

Special attention has been given to a lncRNA selectively upregulated in a subset of prostate cancers. The referred lncRNA was designated *SCHLAP1* after its location on Chromosome 2q31.3, a region that comprises a “gene desert”, so called due to the lack of

protein-coding genes (Prensner *et al*., 2014; Zhao *et al.*, 2014). This lncRNA is considered to be highly specific for prostate, since the results of RNA-seq of 27 different tissues from 95 humans have only shown minor levels of expression at testis, bladder and kidney samples (Fagerberg *et al*., 2014).

1.3.6 Second chromosome Locus Associated with Prostate 1

SChLAP1 gene is composed by 7 exons with a total length of 1,675 nucleotides and has a transcribed size of 24,484 kb. The primary transcript, known as isoform 1, is composed by 5 exons. However, 8 isoforms resulting from alternative splicing were discovered, of which the isoforms 1,2 and 3 account for more than 90% of the transcripts (Prensner *et al*., 2013). The working mechanism of *SChLAP1* in cancer was proved to be related with cell invasiveness and metastasis, consequence of the antagonizing effect on the SWI/SNF chromatin modifying complex (see **Figure 7**). In fact, loss and gain of function experiments reported that inactivation of SWI/SNF complex, that has a tumor suppressor activity, promoted cancer progression and in addition, multiple components of this complex were somatically inhibited in cancer (Roberts and Orkin, 2004). *In vivo* trials have demonstrated the implication of *SChLAP1* in tumor proliferation by injection of cells with *SChLAP1* knockdown, in mice. The reduction of both tumor growth kinetics and number of metastatic sites as well as the decrease of its dimensions are indications of the role played by this lncRNA (Prensner *et al*., 2013).

Besides, *SChLAP1* overexpression can also trigger cancer progression through a second pathway, related with the negative regulation of miR-198 (Li *et al*., 2018). Mitogen-activated protein kinases (MAPKs) play an important role in regulation of cell growth, differentiation and apoptosis. Several studies have demonstrated that the activation of MAPKs is strongly linked with cell growth, proliferation, differentiation and survival (Yang *et al*., 2009). By its turn, miR-198 potentially exerts a tumor suppressor activity by the inhibition of MAPK signaling pathway (Marin-Muller *et al*., 2013). Consequently, the expression miR-198 was found to be significantly lower in PCa tissues than in normal tissues. Further experiments have demonstrated that *SChLAP1* overexpression leads to a decrease in the miR-198 expression, thus once more evidencing its role in the cancer progression (Li *et al*., 2018).

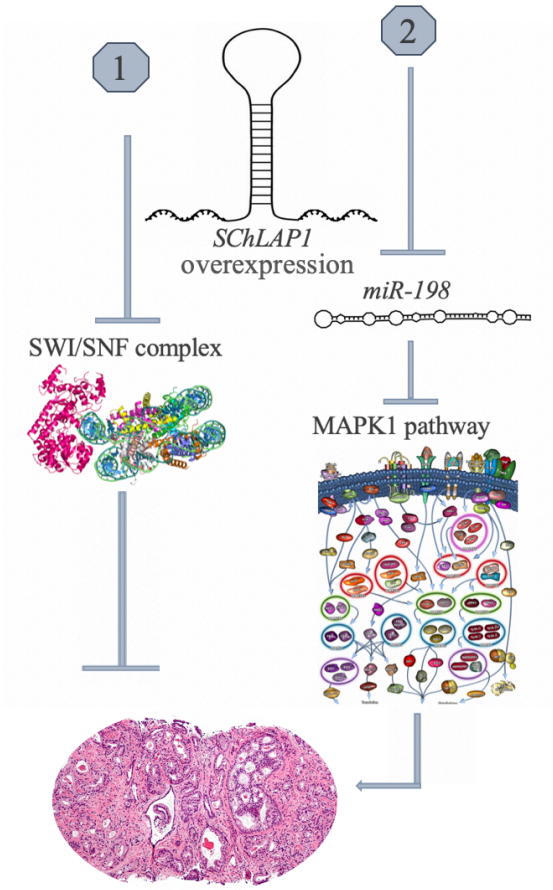

Figure 7. Working model of *SChLAP1* in prostate cancer. There are two pathways. In pathway 1, *SChLAP1* overexpression causes the loss of function of SWI/SNF multi-protein complex promoting cancer progression. In pathway 2, *SChLAP1* exerts a repressive role on miR-198 tumor suppressor activity, preventing it to modulate the MAPK1 pathway. Without the silencing of this pathway cancer progression is endorsed. Adapted from Prensner *et al.,* 2013.

1.3.7 Prostate Cancer Antigen 3

Prostate cancer antigen 3 is a lncRNA that is specific to prostate cancer (Jung, 2004; Schalken *et al*., 2003). This gene is overexpressed in prostate cancer cells, and it is present in up to 95% of PCa cases. Specifically, PC-3 cell line overexpresses 60 to 100 -fold this lncRNA (Tomlins, 2014). FDA approved in 2012 the RT-qPCR of *PCA3* as a detection technique for PCa, which is indicated for men with ages above 50 years with negative prior biopsies. The *PCA3* score reflects the ratio between *PCA3* with *PSA* mRNAs, in post-DRE. The higher scores are associated with a higher probability of cancer-positive biopsy after a prior negative result.

Lastly, *PCA3* has been extensively investigated as PCa-specific biomarker in urine samples. Even though *PCA3* reveals itself as a good predictor of biopsy status and histopathological characteristics, it does not fulfil the suitability for the prediction of

recurrence and metastasis. Since *SChLAP1* is an unambiguous marker for PCa progression and aggressiveness, the detection of both biomarkers could drive to better diagnosis and prognosis, avoiding stressful screening methods, such as DRE and aggressive treatments for indolent cancers.

1.4 Objectives

The development of new technologies for analysis of gene expression requires a multidisciplinary scientific approach relying on the development and optimization of molecular procedures coupled to innovative LOC principles and platforms. The Nanomedicine laboratory has focused on molecular genetics with particular interest in the development of user-friendly and low-cost molecular diagnostics, which then can be applied to LOC platforms. Currently, several projects are focused on the development of microfluidics for assessing relevant biomarkers.

Within this context, this project had two main objectives:

1) The development of isothermal amplification reactions for the detection of genetic biomarkers associated with cancer development and malignancy;

2) the integration of these reactions into a chip-based format capable of generating droplet and measurement for a quantitative digital amplification approach.

For these purposes, target selection and primer design were performed for PCR and LAMP reactions. Additionally, *in silico* optimization of PCR and LAMP reactions and the assessment of real-time semiquantitative calibration for different types of template were achieved. Finally, LAMP reactions were transposed for droplet systems to be used on digital LAMP assays.

2. MATERIALS AND METHODS

2.1 Materials

2.1.1 Equipment

- Balance Sartorius BP 610 (DWS, US)
- Gel Doc XR+ Molecular Imager system (Bio-Rad, US)
- LEGATO® 210 SYRINGE PUMP(KD Scientific, US)
- Nikon Eclipse Ti-U inverted microscope (Nikon, Japan)
- Pentax K100D Digital SLR Camera (Pentax, Japan)
- pH meter Basic 20 with combined glass electrode 5209 (Crison, Spain).
- Refrigerated SIGMA 3-16K Centrifuge (SciQuip, UK)
- Rotor-Gene RG3000 (Corbett Research, Australia)
- Sigma 1-14 Microfuge (SciQuip, UK)
- Stereo Microscope Leica Zoom 2000 (Leica, Germany)
- Stemi 305 stereo microscope (Zeiss, Germany)
- Thermal Cycler MyCycler (Bio-Rad, US)
- Thermal Cycler Tgradient (Biometra, Germany)
- TX4 Digital IR Vortex Mixer (VELP Scientifica, US)
- UV-Vis Spectrophotometer Cary 50 (Varian, US)
- UV-Vis Spectrophotometer Nanodrop ND-1000 (Nanodrop Technologies, US)
- Vortex MS 3 Digital (IKA, Germany)
- VWR Digital Heat Block (VWR, EUA)
- Wide Mini-Sub Cell GT electrophoresis cell (Bio-Rad, US)

2.1.2 Consumables

- Polystyrene thermoplastic sheets “Shrinky Dinks” (K &B Innovations, US)

2.1.3 Reagents

Table 2.1. List of reagents.

Reagent	CAS number	Distributor
Absolute ethanol	64-17-5	PanReac AppliChem
Acetic acid (Glacial)	64-19-7	Merck
Agarose	9012-36-6	VWR
Betaine	107-43-7	Sigma-Aldrich
Bromophenol Blue	115-39-9	Merck
Chloroform	67-66-3	Merck
Ethanol (96%)	64-17-5	Aga
Ethylenediaminetetraacetic acid (EDTA)	25102-12-9	Merck
Evagreen dye 20 X in water	-	Biotium
GelRed™	-	Biotium
Ficoll PM400	26873-85-8	Sigma-Aldrich
Isoamyl alcohol	123-51-3	Merck
Isopropyl Alcohol (IPA)	7732-18-5	Fisher Chemical
Silicone oil	63148-62-9	Sigma-Aldrich
Sodium Dodecyl Sulfate (SDS)	151-21-3	Merck
Span-80	1338-43-8	Sigma-Aldrich
5-Carboxytetramethylrhodamine (5-TAMRA)	91809-66-4	Sigma-Aldrich
Tris(hydroxymethyl)aminomethane (TRIS)	77-86-1	Sigma-Aldrich
TRIS- acetate	6850-28-8	Santa Cruz
Tween-20	9005-64-5	Sigma-Aldrich
QX200™ Droplet generation oil for Evagreen	-	Bio-Rad
Xylene Cyanol FF	2650-17-1	BDH Chemicals

2.1.4 Solutions

All the solutions and reagents were prepared or diluted in ultrapure, sterile filtered and autoclaved water.

- TE pH 7.4

10 mM Tris base (pH 7.4)
1 mM EDTA (pH 8)

Sterilize by autoclaving and filtration (0.22 μm).
Store at room temperature.

- TAE buffer (50x)

2 M Tris-Acetate
0.05 M EDTA
Store at room temperature

- Loading dye

0.25% Blue bromophenol
0.25% Xylene Cyanol
1.5 mg Ficoll
Store at room temperature

2.1.5 Biological Material

2.1.5.1 DNA size markers

- GeneRuler^{TM} DNA Ladder Mix, ready-to-use (Fermentas, Canada)

2.1.5.2 Enzymes

- Taq DNA polymerase (Thermo Fisher Scientific, US)
- *Bst* DNA polymerase, large fragment (New England Biolabs Inc., US)
- RNase H endoribonuclease (Fermentas, Canada)
- M-MuLV reverse transcriptase (Nzytech, Portugal)

2.1.5.3 Molecular Biology kits

- NZY M-MuLV First-Strand cDNA Synthesis Kit (Nzytech, Portugal)
- SYBR Green Real-Time PCR Kit (Invitrogen, US)

2.1.5.4 Oligonucleotides

LAMP primers were designed with PrimerExplorer V4 software (Eiken Chemical Co., Ltd.; Tokyo, Japan) based on an alignment of the *SChLAP1* isoforms sequences and

of the *PCA3* transcripts. The specificity of the designed primers was confirmed by n-BLAST on the National Center of Biotechnology Information (NCBI). The name and sequences of the primers are presented in **Table 2.2** and their location on the target sequences are shown in Annex section, **Figure A1** and **Figure A2**. All oligonucleotides were acquired from STAB VIDA (Lda, Caparica, Portugal).

Table 2.2. List of primers.

Name	Sequence (5´→3´)	Tm (ºC)	Target (GenBank Acc.No.)
c-Myc F3	TCTGAAGAGGACTTGTTGC	48.9	NM_002467
c-Myc B3	TTCAGTCTCAAGACTCAGC	48.9	
c-Myc FIP	CTTTTCCTTACGCACAAGAGTTCC-GGAAACGACGAGAACAG	-	
c-Myc BIP	ACGATTCCTTCTAACAGAAATGTCC - CAAGGTTGTGAGGTTGCA		
SChLAP1 F3*	GAAAAGGAAAGAATAAAAGCGAA	55.6	NR_104319.1
SChLAP1 B3*	TTTGGATAATGGGATTACAAAGA	55.5	
SChLAP1 FIP*	GGTTGTTCCAGACCCATATACACTC-AATGAAGAGTCATATGATTACCAAC	-	
SChLAP1 BIP*	GTCCTGGCTAACCTCATTATGTC-ATATCCACATTCACAATACAGAT		
PCA3 F3*	CTGGGAAGCATCTCAAGA	55.1	NR_132312.1
PCA3 B3*	AACATTGAATTCTTCCAGGTTA	55.4	
PCA3 FIP*	GACACTGAGGATGATGTTGATTAGA -TTATACTTACTAGCACACAGCAT	-	
PCA3 BIP*	ATTTCCCACTTTTGTGCCCA-ATCCTGTGATATTAATGGAATGAC		

* LAMP primers for *SChLAP1* and *PCA3* genes were designed using Primer Explorer V4 (http://primerexplorer.jp/elamp4.0.0/).

2.2 Methods

2.2.1 Cell culture

PC-3 cell line derived from a grade 4 prostatic adenocarcinoma from a 62 year old Caucasian male and HCT-116 cell line derived from a male with colonic carcinoma were cultured in RPMI 1640 (Invitrogen, US) cell culture medium, supp1emented with 10% (v/v) fetal bovine serum (FBS) (Invitrogen, US) and 1% (v/v) streptomycin-penicillin (Invitrogen, New York, US) and maintained at 37°C in a humidified atmosphere of 99% of 5% (v/v) CO_2.

2.2.2 Genomic DNA extraction from HCT-116 cell line with Phenol/ Chloroform protocol

Genomic DNA was extracted from HCT-116 cell line by the phenol/chloroform procedure.

1. Centrifuge the suspension of cells at 500 x g for 5 minutes at room temperature. Remove the supernatant;
2. Add 250 µL of TE pH=7.5 buffer to the pellet; Briefly mix to solubilize the pellet.
3. Add 250 µL of phenol follow a briefly mix;
4. Centrifuge at 10,000 rpm for 5 minutes at room temperature;
5. Collect the top aqueous phase into a new tube;
6. Add an equal volume of chloroform/isoamyl alcohol (24:1) to the aqueous phase;
7. Vigorously mix for 1 minute;
8. Centrifuge at 10,000 rpm for 5 minutes at room temperature;
9. Collect the top aqueous phase into a new tube;
10. Add 2 volumes of cooled absolute ethanol to the aqueous phase, to precipitate the DNA;
11. Incubate at -20ºC for 30 minutes;
12. Centrifuge at 10,000 x g for 10 minutes at 4ºC;
13. Discard the supernatant without disturb the pellet;
14. Air-dry the pellet;
15. Resuspend the pellet in 20-50 µL of milli-pore water.
16. Store at -20 ºC. DNA concentration and purity were determined by UV spectrophotometry, further DNA integrity analysis was performed via gel electrophoresis

2.2.3 RNA extraction from cell cultured PC-3 cell line with TRIsure protocol

RNA was extracted from PC-3 cell line by the guanidine thiocyanate procedure (RNA isolation with TRIsure protocol, BIO-38033, Bioline), following the manufacture specifications.

1. Homogenization

1.1 Centrifuge the suspension of cells at 200 xg for 5 minutes at room temperature.
1.2 Remove the supernatant;
1.3 Add 1mL of trizol to the pellet to lyse the cells (per ~ $5x10^6$ cells);

2. Phase Separation

2.1 Incubate samples for 5 minutes at room temperature;
2.2 Add 0.2mL of chloroform per 1mL of trizol used. Cap the tubes and shake vigorously for 15 seconds;
2.3 Incubate samples for 3 minutes at room temperature;
2.4 Centrifuge samples at 12.000 x g for 15 minutes at 4ºC. The sample will separate in a colorless upper aqueous phase, a pale green interphase and in an organic phase;

3. RNA Precipitation

3.1 Transfer the aqueous phase, very carefully, to a new tube, without disturbing the interphase;
3.2 Precipitate the RNA by adding 0.5mL of cold isopropyl alcohol per 1mL of trizol used; Incubate samples for 10 minutes at room temperature;
3.3 Centrifuge at 12.000 x g for 10 minutes at 4ºC;

4. RNA Wash

4.1 Remove the supernatant;
4.2 Wash the pellet by adding 1mL of cold 75% ethanol per 1mL of trizol used;
4.3 Agitate the tube until the pellet is dissolved;
4.5 Centrifuge at 7500 x g for 5 minutes at 4ºC;

5. Re-dissolving the RNA

5.1 Remove the supernatant;
5.2 Air dry the pellet;
5.3 Resuspend the pellet in 20uL of DEPC-treated water by pipetting up and down;

5.4 Store the RNA at -80ºC. RNA concentration and purity were determined by UV spectrophotometry, further RNA integrity analysis was performed via gel electrophoresis.

2.2.4 Enzyme mediated nucleic acid reactions

2.2.4.1 Reverse Transcription (rt)

Total RNA extracted from the PC-3 cell line was subjected to reverse transcription reaction NZY M- MuLV First-Strand cDNA Synthesis kit (Nzytech, Lisbon, Portugal) following the manufacture's specifications. Components were added into a microcentrifuge tube.

1. All reagents aliquots were allowed to defrost;
2. A reaction mix was prepared according to sub-section *2.2.4.7*;
3. Reaction mix was briefly mixed and vortexed;
4. The reaction mix was distributed to 0.2 ml microtube;
5. Template RNA sample was added to the reaction mixture according to the experimental design;
6. Reaction was incubated at 25 ºC for 10 minutes, followed by a 50 minutes incubation at 37 ºC;
7. The enzyme was heat inactivated of by heating at 85 ºC for 5 minutes, and then cooled at -20 ºC;
8. Add 1 µL of NZY RNase H (*E. coli*) and incubate at 37 ºC for 20 minutes;
9. Rapidly cool on ice for enzyme inactivation;
10. Store at -20 ºC. cDNA concentration was determined by UV spectrophotometry.

The cDNA product was directly used in PCR, LAMP and RT-LAMP reactions or diluted in water for further amplifications reactions.

2.2.4.2 Target amplification by Polymerase Chain Reaction (PCR)

PCR reaction for *c-Myc* gene was performed in order to obtain templates for the further LAMP reactions. Additionally, PCR reactions were also developed for *SChLAP1* and *PCA3* genes, aiming for their amplification, thus optimization of annealing temperature, primer and template concentration were performed. All the reaction conditions and further thermocycler's programs were prepared as described in sub-sections *2.2.4.7* and *2.2.4.8*, respectively.

1. All reagents aliquots were allowed to defrost;

2. A reaction mix was prepared according to sub-section *2.2.4.7* – different PCR conditions are described as a consequence of iterative optimization of PCR reactions;
3. Reaction mix was briefly mixed and vortexed;
4. The reaction mix was distributed to 0.2 ml microtube;
5. Template sample was added to the reaction mixture according to the experimental design;
6. Reaction was briefly mixed and vortexed and incubated in the thermocycler for amplification reaction, following the respective reaction temperature programs according to sub-section *2.2.4.8.*

2.2.4.3 Target amplification by Loop-mediated Isothermal Amplification (LAMP)

1. All reagents aliquots were allowed to defrost;
2. A reaction mix was prepared according to sub-section *2.2.4.7*– Standard LAMP of this chapter;
3. Reaction mix was briefly mixed and vortexed;
4. The reaction mix was distributed to 0.2 ml microtube;
5. Template sample was added to the reaction mixture according to the experimental design;
6. Reaction was briefly mixed and vortexed and incubated in the thermocycler at 95 °C for 5 min for denaturation and immediately transferred to ice for 1 minute;
7. *Bst* DNA polymerase was added to the reaction;
8. Reaction was briefly mixed and vortexed and incubated in the thermocycler for amplification reaction at 65 ºC for 1.5 hour for amplification reaction.

For *c-Myc* gene, *Bst* polymerase was directly added into the reaction mixture, thus after step 5 the reaction is mixed and incubated in the thermocycler (step 8).

In order to test LAMP compatibility with the components required for the droplet generation, 190 µL of silicone oil, 4.5% (v/v) Span-80 and 0.5% (v/v) Tween-20 were added to each reaction tube.

2.2.4.4 Real-time PCR

RT-PCR was performed in a Corbett Research Rotor-Gene RG3000 using SYBR GreenER Real-Time PCR Kit (Invitrogen, US) according to manufacturer's specifications in 10 µL reactions containing the reaction mix, described in sub-section

2.2.4.7 and 1× SYBR Green dye, following the respective reaction temperature programs according to sub-section *2.2.4.8*. All experiments were performed at least three times.

2.2.4.5 Real-time LAMP

RT-LAMP was performed in a 10 µL (for *c-Myc* gene) or 25 µL (for *SChLAP1*and *PCA3* genes) reaction mixture containing 1x Evagreen fluorescent dye (Biotium, US) as described in sub-section *2.2.4.7*. The final reaction mixture was transferred to a Corbett Research Rotor-Gene RG3000 and allowed to react for 90 min at 65 ºC with fluorescence measurement taken every minute. All experiments were performed at least three times.

2.2.4.6 Quantification of DNA amplification

PCR and LAMP amplification products were analyzed by 1.5 % agarose gel electrophoresis stained with GelRed™ (Biotium, US) and run for 90 minutes at 80V.

PCR Product quantification (copies per µL) was performed by pixel intensity/counting using ImageJ imaging software (https://imagej.nih.gov/ij/) (NIH, US). Determination of the copy number of amplifications was performed by linear regression analysis, by fitting the fluorescence intensity of the amplicon band to a calibration curve based on the fluorescence intensity of ladder bands.

Fluorescence-based real-time monitoring results were obtained through the normalization between 0 and 1 of the arbitrary fluorescence intensities, following the **Equation 1**:

$$\textbf{Eq (1)}. \quad zi = \frac{xi - \min(x)}{\max(x) - \min(x)}$$

Threshold time (T_T) values obtained for first fluorescence inflexion point.

2.2.4.7 Reaction mixtures

Standard reverse transcription conditions *	
NZYRT Master Mix (2X)	1X
NZYM-MuLV RT Enzyme Mix	2 µL
Template RNA (100 ng/µL) [a]	1 µL
DEPC-treated water	Up to 20 µL

[*] – Volumes described for a 20 µL reaction.

[a] – RNA from PC-3 cell line was used as template in a concentration of 100 ng/µL.

Optimal PCR conditions for *c-Myc* gene	
Dream Taq buffer (10X)	1X
dNTPs (10mM)	0.2 mM
Primer Forward (10pmol/µL)	0.4 µM
Primer Reverse (10pmol/µL)	0.4 µM
Dream Taq enzyme (5U/µL)	0.1 U
Template (cDNA)[a, b]	1 µL

[a] – gDNA of HCT-116 cell line was used as template in a concentration of 1000 ng/µL.

[b] – gDNA was replaced by water in the non-template controls

PCR conditions for annealing temperature optimization of *SChLAP1* and *PCA3* genes	
Dream Taq buffer (10 X)	1 X
dNTPs (10 mM)	0.8 mM
Primer F3 (10 pmol/µL)	0.8 µM
Primer B3(10 pmol/µL)	0.8 µM
Dream Taq enzyme (8U/µL)	1.6 U
Template (cDNA)[a, b]	2 µL

[a] – cDNA was used in two different concentrations, 100 ng/µL and 1000 ng/µL for *PCA3* and *SChLAP1* genes.

[b] – cDNA was replaced by water in the non-template controls.

PCR conditions for primer concentration optimization of *SChLAP1* and *PCA3* genes	
Dream Taq buffer (10X)	1X
dNTPs (10 mM)	0.8 mM
Primer F3 (10 pmol/µL) *	0.8 µM to 0.48 µM
Primer B3 (10 pmol/µL) *	0.8 µM to 0.48 µM
Dream Taq enzyme (8U/µL)	1.6 U
Template (cDNA)[a, b]	2 µL

[*] – Primer concentrations tested were: 0.8 µM, 0.72 µM, 0.64 µM, 0.56 µM and 0.48 µM.

[a] – cDNA was used in two different concentrations, 100 ng/µL and 1000 ng/µL for *PCA3* and *SChLAP1* genes.

[b] – cDNA was replaced by water in the non-template controls.

Optimal PCR conditions for *SChLAP1* and *PCA3* genes	
Dream Taq buffer (10X)	1X
dNTPs (10mM)	0.8 mM
Primer Forward (10pmol/µL)	0.48 µM
Primer Reverse (10pmol/µL)	0.48 µM
Dream Taq enzyme (8U/µL)	1.6 U
Template (cDNA)[a, b]	2 µL

[a] – cDNA was used in two different concentrations, 100 ng/µL for *PCA3* gene and 1000 ng/µL for *SChLAP1* gene.

[b] – cDNA was replaced by water in the non-template controls.

Standard LAMP conditions for *c-Myc* gene	
Buffer Bst (10 X)	1 X
dNTPs (5mM)	0.45 mM
Primer FIP (10pmol/µL)	1.6 µM
Primer BIP (10pmol/µL)	1.6 µM
Primer F3 (10pmol/µL)	0.2 µM
Primer B3 (10pmol/µL)	0.2 µM
Betaine (5M)	0.8 M
MgCl2 (25mM)	3 mM
Bst enzyme (8U/µL)	1.6 U
Template [a, b]	1 µL
Evagreen 20 X [*]	1 X

[a] – Template was replaced by water in the non-template controls.

[b] – gDNA from HCT-116 (1000 ng/µL) or different dilutions of PCR product from of c-Myc (5.38E+10 copies/µL) were used as template.

[*] – Evagreen dye was only added to the reaction mixture for RT-LAMP and ddLAMP reactions. For standard LAMP reaction, the corresponding volume was replaced by water.

Standard LAMP conditions for *SChLAP1* and *PCA3* genes	
Buffer Bst (10 X)	1 X
dNTPs (5mM)	0.7 mM
Primer FIP (10pmol/µL)	0.64 µM
Primer BIP (10pmol/µL)	0.64 µM
Primer F3 (10pmol/µL)	0.2 µM
Primer B3 (10pmol/µL)	0.2 µM
Betaine (5M)	0.36 M
MgCl2 (25mM)	2 mM
Bst enzyme (8U/µL)	0.32 U
Template [a,b]	1 µL
Evagreen 20 X	1 X [d] / 0.2 X to 2 X [e]

[a] – Template was replaced by water in the non-template controls.

[b] – cDNA of PC-3 cell line was used as template in the following concentrations: 1000ng/µL, 500ng/µL, 100ng/µL, 50ng/µL, 10ng/µL and 1ng/µL, for the RT-LAMP studies of template concentration effect.

[c] – cDNA and purified PCR products of S*ChLAP1* were used as templates in the following concentrations: 1000ng/µL, 500ng/µL, 100ng/µL, 50ng/µL, 10ng/µL and 1ng/µL, for the experiments that aimed for the evaluation of different Evagreen dye concentrations on the amplification efficiency of LAMP reaction towards different type of template molecules.

[d] – Evagreen dye was only added to the reaction mixture for RT-LAMP reactions. For standard LAMP reaction, the corresponding volume was replaced by water.

[e] – Concentrations of Evagreen dye of 0.2 X, 0.5 X, 1X and 2 X were used on the RT-LAMP experiments that aimed for the evaluation of different Evagreen dye concentrations on the amplification efficiency of LAMP reaction towards different type of template molecules.

RT-PCR conditions for of *SChLAP1* and *PCA3* genes	
qPCR Green Master mix (2 X)	1 X
Primer F3 (10 pmol/µL)	0.48 µM
Primer B3(10 pmol/µL)	0.48 µM
Template (cDNA)[a, b]	1 µL

[a] – Template was replaced by water in the non-template controls.

[b] – cDNA of PC-3 cell line was used as template in the following concentrations: 1000ng/µL, 500ng/µL, 100ng/µL, 50ng/µL, 10ng/µL and 1ng/µL, for the RT-PCR studies of template concentration effect.

2.2.4.8 Reaction programs

Standard Reverse transcription		
Step	**Temperature**	**Time**
Initial incubation	25 ºC	10 minutes
Reverse transcription	37 ºC	50 minutes
Heat inactivation	85 ºC	5 minutes
Hold	4 ºC	Forever
RNase H incubation	37 ºC	20 minutes
Enzyme inactivation	-20 ºC	1 minute

Optimal PCR conditions for *c-Myc* gene			
Step	**Temperature**	**Time**	**Cycles**
Initial denaturation	95 ºC	5 minutes	1
Denaturation	95 ºC	30 seconds	
Annealing	55 ºC	30 seconds	34
Extension	72 ºC	45 seconds	
Hold	4 ºC	Forever	1

Standard LAMP condition for *c-Myc* gene		
Step	**Temperature**	**Time**
Amplification	65 ºC	60 minutes
Hold	4 ºC	Forever

PCR conditions for annealing temperature optimization of *SChLAP1* and *PCA3* genes			
Step	**Temperature**	**Time**	**Cycles**
Initial denaturation	95 ºC	3 minutes	1
Denaturation	95 ºC	20 seconds	
Annealing	53.0 to 63.0 ºC	30 seconds	40
Extension	72 ºC	15 seconds	
Hold	4 ºC	Forever	1

Optimal PCR conditions for *SChLAP1* and *PCA3* genes *			
Step	**Temperature**	**Time**	**Cycles**
Initial denaturation	95 ºC	3 minutes	1
Denaturation	95 ºC	20 seconds	
Annealing	53.7 [a] / 61.0 [b] ºC	30 seconds	40
Extension	72 ºC	15 seconds	
Hold	4 ºC	Forever	1

[*] – Reaction program also used in the experiments of primer concentration optimization and RT-PCR experiments.

[a] – Annealing temperature used for *SChLAP1* reaction.

[b] – Annealing temperature used for *PCA3* reaction.

Standard LAMP condition for *SChLAP1* and *PCA3* genes		
Step	Temperature	Time
Primer's hybridization	95 ºC	5 minutes
	-20 ºC	1 minute
Amplification	65 ºC	90 minutes
Hold	4 ºC	Forever

End-point LAMP condition for *c-Myc* gene		
Step	Temperature	Time
Amplification	65 ºC	2.5 hours

2.2.5 Stirring-based droplet system

2.2.5.1 Stirring-based droplet generation

The generation of droplets for further compartmentalization of the LAMP reaction was achieved by the generation of water-in-oil emulsions by stirring on vortex. The aqueous phase was comprised of water and TAMRA dye, instead of all the necessary reagents for the amplification reactions. Droplet generation procedure was performed according to the previous literature reports, with minor modifications (Tawfik and Griffiths, 1998).

For the generation of droplets, a proportion of 1:20 of water to oil was used. The continuous phase consists in silicone oil (Sigma 37667) and the dispersed phase consists of water, TAMRA dye (Invitrogen, T6105), Tween-20 at 0.5% v/v (Sigma, P1754) and Span-80 at 4.5% v/v (Sigma, S6760). The aqueous phase was freshly prepared by dissolving 4.5% (v/v) Span-80 and 0.5% (v/v) Tween-20 in 10 µL water already containing TAMRA dye. In a sterile microcentrifuge tube of 0.5mL (ABDOS Labware, P10201), 190 µL of silicone oil were stirred at 1500 rpm on vortex (Velp Scientifica, TX4 Digital IR Vortex Mixer) while 1 µL of the aqueous phase was dripped into the oil every 15 seconds until all the 10 µL were added. Following 1 minute of stirring at 3000 rpm. Furthermore, size stability of the droplets was analyzed at 65 ºC. For this, 5 time points with 15 minutes interval were used.

2.2.5.2 Droplet size

The size distribution was analyzed via fluorescence microscopy (Nikon Eclipse Ti-U inverted microscope). For this, the bottom phase of the emulsion was diluted 1:50 in water, following 5 µL of the diluted sample were placed into a glass with SiU8 frame with 50 µm of thickness, to visualize the droplets, instead of the typical blade and coverslip assembly. The images were treated with ImageJ software. The microscope settings are described in sub-section *2.2.7.*

2.2.5.3 Transposal of LAMP reaction to a droplet-based system

Droplets were generated by stirring on vortex as mentioned in the sub-section *2.2.5.1,* with the exception that LAMP reaction mixture with Evagreen dye 1x (prepared as described in sub-section *2.2.4.7*) was used as the aqueous phase, instead of water with TAMRA. After the LAMP reaction was emulsified, the 0.2 mL tube was placed in the thermocycler (program described in sub-section *2.2.4.8*). The amplification was

monitored every 15 minutes, until 1 hour of reaction. For each time point, a non-template control and a positive control of LAMP reaction were observed in microscope, for this the bottom phase of the emulsion was diluted by 1:50 with water and placed into the glass with SiU8 frame. The microscope settings for the image acquirement are described in the sub-section *2.2.7.*

2.2.5.4 Recovery of the LAMP reaction products

LAMP amplification was also monitored via gel electrophoresis. In order to recover the amplification products, droplets were breakdown by centrifugation at 9000 x g for 5 minutes (Shao et al., 2011). The upper phase (oil) was discarded and the bottom phase (reaction mixture) was analyzed by agarose gel electrophoresis.

2.2.6 Microfluidic chip-based digital LAMP

2.2.6.1 Chip fabrication and operation conditions for droplet generation

The microfluidic chip was fabricated with a laser ablation mechanism in a polystyrene (PS) commercial sheets and further hot press bonding technique was used to the 3D assemble of the multiple layers containing the microchannels. The 3D assembled chip was then heated at 163 ºC in order to shrink. The chip design and fabrication were accomplished by Dr. Veigas B. (DCV/CENIMAT).

The droplets were generated as following:

1. Microfluidics tubes are connected to the pump syringes; one syringe is filled with the continuous phase (QX200^{TM} Droplet generation oil for Evagreen) and the other syringe is filled with 20 µL of LAMP reaction with 1X Evagreen dye (prepared as described in sub-section *2.2.4.7*).

2. The tube connected to the oil syringe is attached into the inlet of the continuous phase. Also, the oil recover tube is attached into the outlet channel.

3. Oil is infused into the chip until the totality of the chamber is filled, with a flux of 50 µL/min.

4. The tube with the LAMP reaction is attached into the inlet of the dispersed phase.

5. Set the oil flux (*Qc*) at 20 µL/min.

6. Turn on the reaction flux (*Qd*) at 1 µL/min.

7. When the chamber was almost filled with droplets, *Qc* is settled to zero.

8. After droplets stop arriving to the chamber, *Qd* can also be settled to zero.

9. Tubes are detached from the inlets and outlet, which are further sealed with hot glue.

10. Chip is placed on a heat block at 65ºC for 2.5 hours (reaction program described in sub-section *2.2.4.8*).

Following the end-point amplification reaction, amplification detection is performed on chip, by fluoresce microscopy. The images were taken with microscope settings described in the sub-section *2.2.7.*

2.2.6.2 Chip-based digital LAMP algorithm

1. On the image J software, set the measurement conditions as Area and Grey Mean Value (GMV);

2.Set the scale bar for 1.6 μm/pixel;

3. Open the Roi manager and select the circular tool;

4. Encircle all the droplets in the image (except the ones that are not entirely visible or that present overlap with other droplets). For each image, has to be taken 3 measures of the background. Also, a minimum of 400 droplets have to measured, per experiment;

5. Normalize the grey mean value of the droplets to the average of the GMV of the background;

6. Convert the area of the droplets for diameter;

7. Plot the normalized GMV in function of the droplet's diameter;

8. Count the droplets above the threshold line (y=0.001x+1.14);

9. Determine the fraction of positive droplets;

10. Estimate the number of positive and negative events with Poisson's statistics;

11. Model the fraction of positive droplets with Poisson partitioning statistics.

12. Estimate the initial concentration of the target sample through Poisson modeling.

2.2.7 Microscope settings

Determination of droplet size	
Parameter	**Setting**
Image format	640 x 480, 2x2 binning
Ampliation	40 x
Gain	1 x
Filter	G2-A (G)
Exposure	15 milliseconds

Stirring-based droplet - LAMP amplification	
Parameter	**Setting**
Image format	640 x 480, 2x2 binning
Ampliation	20 x
Gain	1 x
Filter	DAPI-FITC (B)
Exposure	5.82 seconds

Chip-based droplet - LAMP amplification	
Parameter	**Setting**
Image format	1280 x 1024, 2x2 no binning
Ampliation	4 x
Gain	1 x
Filter	DAPI-FITC (B)
Exposure	15 seconds

3. RESULTS AND DISCUSSION

3.1 Droplet-based digital LAMP reaction development

Nucleic acids amplification technologies (NAATs) are regarded as essential tools in clinical diagnosis, being PCR the most exploited amplification method (Pekin *et al*., 2011). Since NAATs implementation, several developments have occurred in order to increase the sensibility, efficiency, cost and time effectiveness of these reactions. Among these improvements, digital nucleic acids amplification technique has become a popular approach for quantitatively detect DNA/RNA molecules, in a wide range of biomedical applications (Pekin *et al*., 2011). Likewise, for standard and quantitative amplifications methods, digital PCR remains the most common way to conduct digital nucleic acids detection. Despite all its potential, droplet-based PCR amplification still faces difficulties related to lab-on-chip integration (Rane *et al*., 2015).

Isothermal amplification methods have been developed in order to outmatch the limitations above mentioned while reducing integration complexity. From these, LAMP reaction has been currently developed and integrated into LOC systems since it shows higher sensitivity, specificity while reducing reaction times (Notomi, 2000).

In this chapter is described the assessment of LAMP reaction compatibility and implicated factors towards a droplet-based amplification approach aiming for digital target quantification.

3.1.1 Vortex-base droplet generation

Digital amplification approaches consist into breaking down a solution of the nucleic acids target with the reaction components into a large number of discrete compartments (Zanoli and Spoto, 2012). After parallel amplification on all these reaction compartments/micro-reactors, accurate quantification of the nucleic acid molecule of interest can be obtained through the statistical analysis of the fraction of positive events (Rane *et al*., 2015). A vortex-based droplet generation approach was performed for rapid creation of the reaction droplets, which were used to study the LAMP reaction compatibility with the components required for droplet generation and further ability for amplification to occur inside the droplets. Thus, the first experiment had two main tasks: characterize the size and stability of the droplets towards heating at 65ºC.

The droplet generation was accomplished as described in **subsection *2.2.5.1***. The emulsion generated after stirring consists in two phases, an upper phase with oil and a bottom phase with the droplets and the emulsifiers, which is easily distinguished from the

oil phase due to its turbidity and viscosity (**Figure 8**). This effect is mainly due to the insolubility of the emulsifiers into the silicone oil. In fact, literature reports present several systems were mineral oil is used as the continuous phase. The use of silicone oil was considered so as to allow future integration of isothermal amplification methods with digital microfluidics chips.

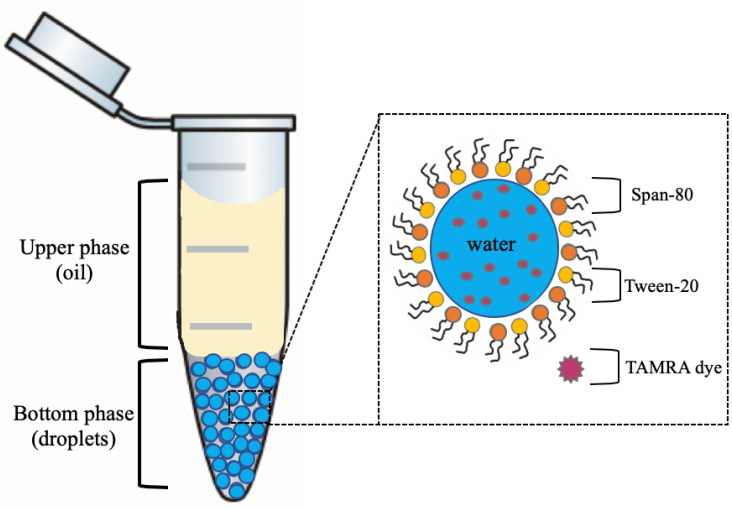

Figure 8. Schematic representation of emulsion attained by stirring on vortex. The mixture is composed by an upper phase of oil and a bottom layer were droplets are settled. The droplets are composed by an inner aqueous phase with TAMRA dye that is surrounded by a layer of Span-80 and Tween-20 emulsifiers.

To confirm if the droplets generated had the right conformation (aqueous inner phase surrounded by oil), a water-soluble fluorophore was added to the aqueous mixture. After the incubation at 65ºC, droplets were observed via optical and fluorescence microscopy, microscope settings are described in **subsection *2.2.7* (Figure 9**).

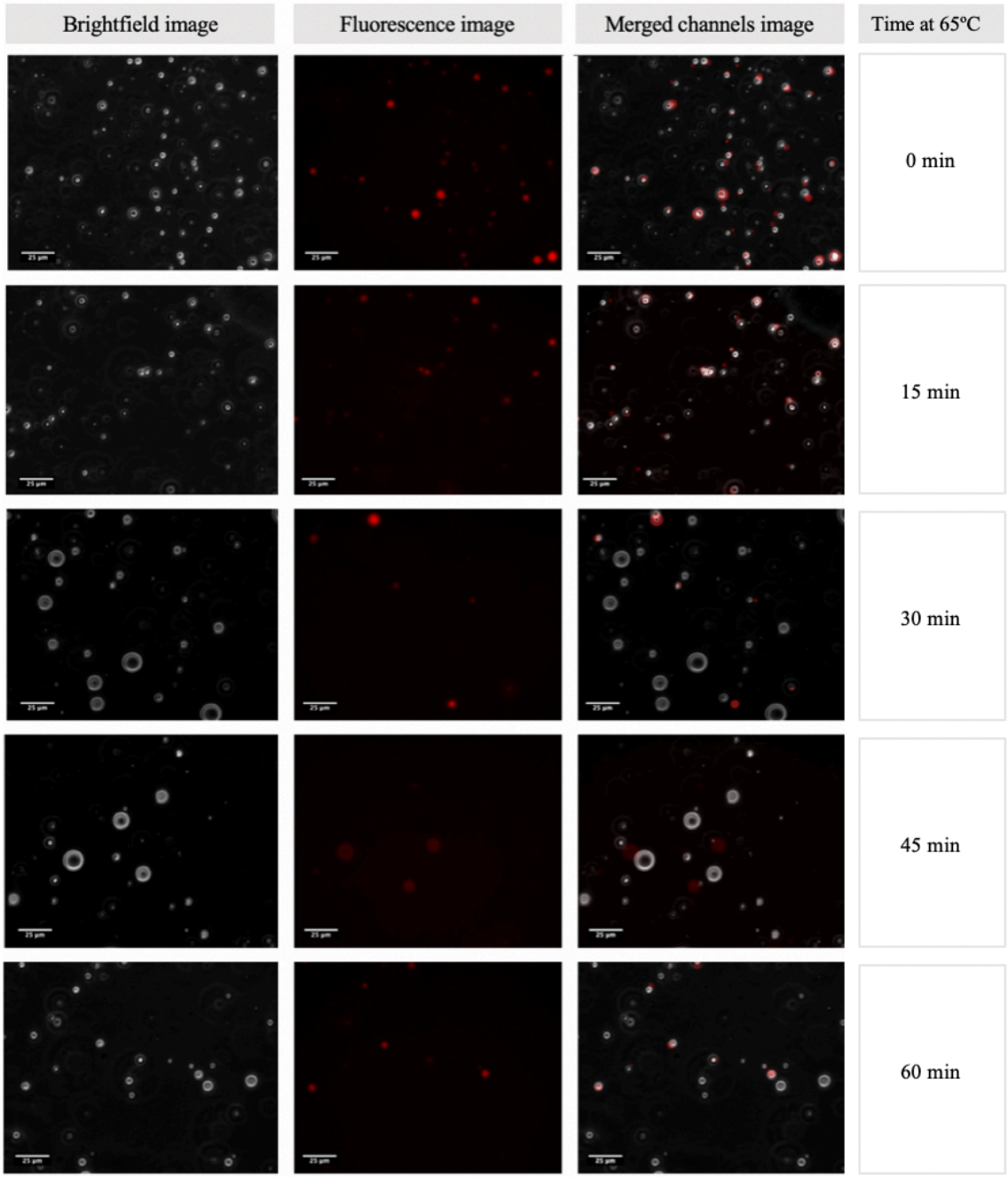

Figure 9. Droplet formation with time at 65ºC. The images were obtained with an 40x objective. The optical microscopy images (left panel) were taken with 15 milliseconds of exposure and fluorescence microscopy images (central panel) were taken with 2 seconds of exposure with the green channel (excitation between 510 to 560nm). The images on the left panel results from the overlap of the brightfield image with the green channel (fluorescence image). All the images contain a scale bar of 25µm.

The presence of fluorescence inside the droplets confirms that the hydrophilic content is in the inner phase (**Figure 9**, central section). On the contrary, if air was encased instead of the aqueous phase, the background would have higher fluorescence than the droplets. Despite the right droplet arrangement, it is noticeable that not all the droplets on the brightfield image are visible in the fluorescence image, which might be caused by multiple focus plans and multilayer arrangement of droplets. Additionally, some fluorescence signals do not match the position of any droplet (brightfield image) when both channels are merged, which might be caused by the movement of the droplets.

The size of the droplets was analyzed at 65 ºC (optimal LAMP temperature) to assess stability under continuous heating. For this, 5 time points with 15 minutes interval were used **(**see Annex, **Figure A3)**. After incubation droplet size distribution was analyzed via fluorescence microscopy (see **subsection *2.2.5.2***) - **Figure 10.**

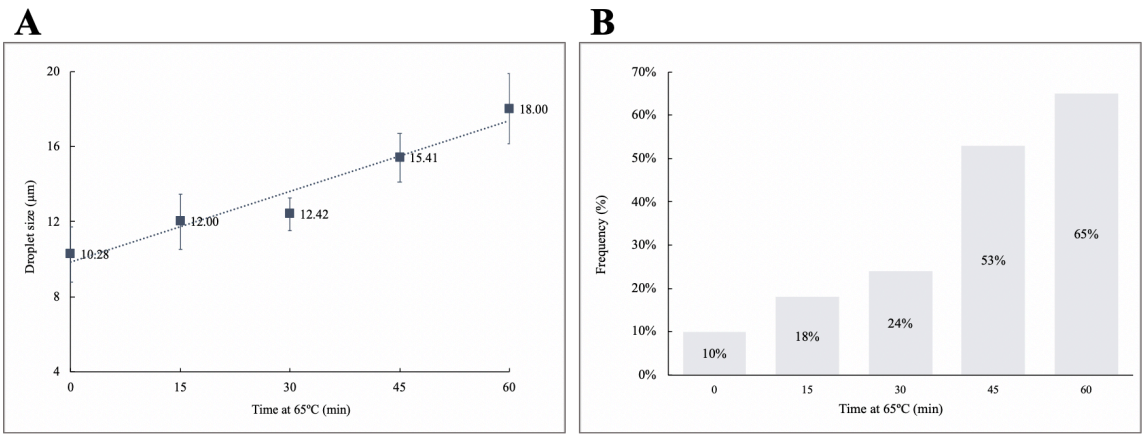

Figure 10. Size distribution of the droplets towards different times at 65ºC. **(A)**Weighted average size of the droplets (■) in function of time at 65ºC. The error bars correspond to the standard error of the mean (SEM). The coefficient of variation is 11%. The trendline (••••) equation is y = 0.1257x + 9.852 with R^2 = 0.94. **(B)** Frequency of droplets with size equal or higher than 17 µm (■) within the time at 65ºC.

It is noticeable an increase in the size of the droplets over time, specially above 30 minutes of incubation (**Figure 10A**). This is in line with recent reports that demonstrate a temperature dependence of the physical properties of the droplets (Khater *et al*., 2019). More precisely, temperature leads to a decrease in both the viscosity and the superficial tension between the oil and aqueous phases, resulting in an increase of droplet size (Khater *et al*., 2019; Nguyen *et al.,* 2007).

It is known that droplets try to minimize the contact area with the continuous phase (oil) via one of two mechanisms: first coagulation possibly followed by coalescence and,

second, Ostwald ripening, both causing an increase on droplets size (Sadtler, Imbert and Dellacherie, 2002). These phenomena may be observable through the increase of the frequency of droplets with larger sizes, especially for sizes ≥ 17 μm (**Figure 10B**). In fact, the frequency size of these droplets triples for incubation periods longer than 30 minutes.

Following the development and characterization of the stirring-based droplets, which will serve as microreactors for LAMP, the next experiment aimed at assessing the compatibility of this droplet system and components with LAMP. As such, LAMP reaction of a well-studied gene, *c-Myc*, was performed and analyzed by agarose gel electrophoresis - **Figure 11**.

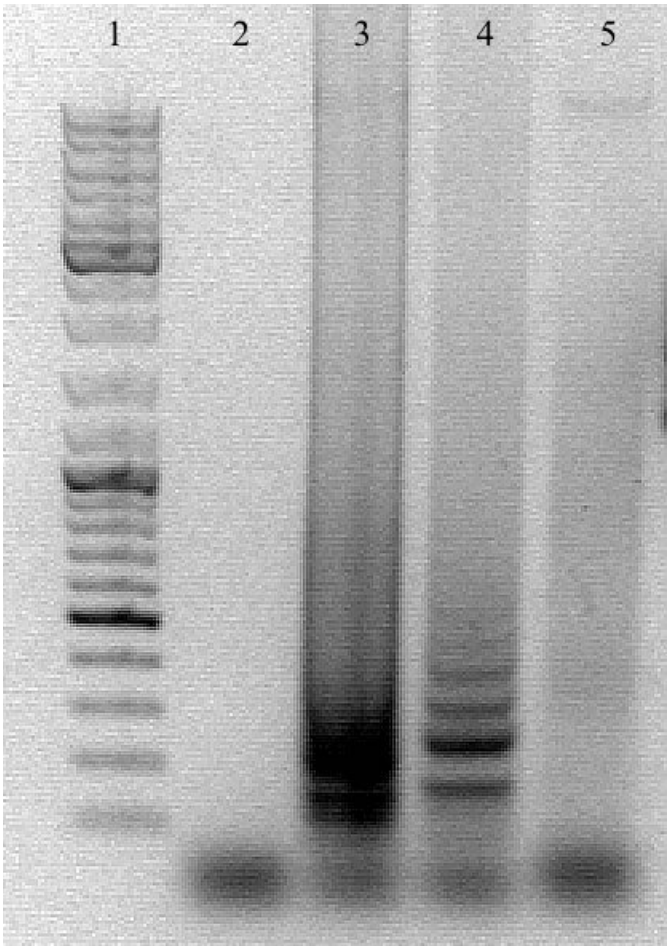

Figure 11. Products of LAMP amplification of *c-Myc* gene with the components necessary for droplet generation. Comparison between a standard LAMP reaction with an amplification with droplet generation components (Silicone oil 5cSt, Tween-20 and Span-80) for c-Myc gene. The electrophoresis was performed in a 1.5% agarose gel and run at 60V for 90 min. (1) Ladder (2) Non-template control for the LAMP reaction of c-Myc (3) Amplification c-Myc gene (4) Amplification c-Myc gene with Silicone oil 5cSt, 4.5% Span-80 and 0.5% Tween-20 (5) Non-template control with Silicone oil 5cSt, 4.5% Span-80 and 0.5% Tween-20.

Figure 11 (lane 4) shows the presence of a typical LAMP amplification band on the template control indicating that oil and emulsifiers required for droplet formation are compatible with LAMP. The apparent differences in band intensity may be attributed to the need for an extra step to recover the sample from the oil and emulsifiers mixture.

3.1.2 Vortex-based LAMP reaction

After the verification that LAMP reaction is compatible with the reagents required for droplet generation, the next step was to evaluate LAMP inside the droplets, *i.e.* droplet-based LAMP amplification **(**see **subsection *2.2.5.3***). The optical and fluorescence microscopy images are presented in **Figure 12.**

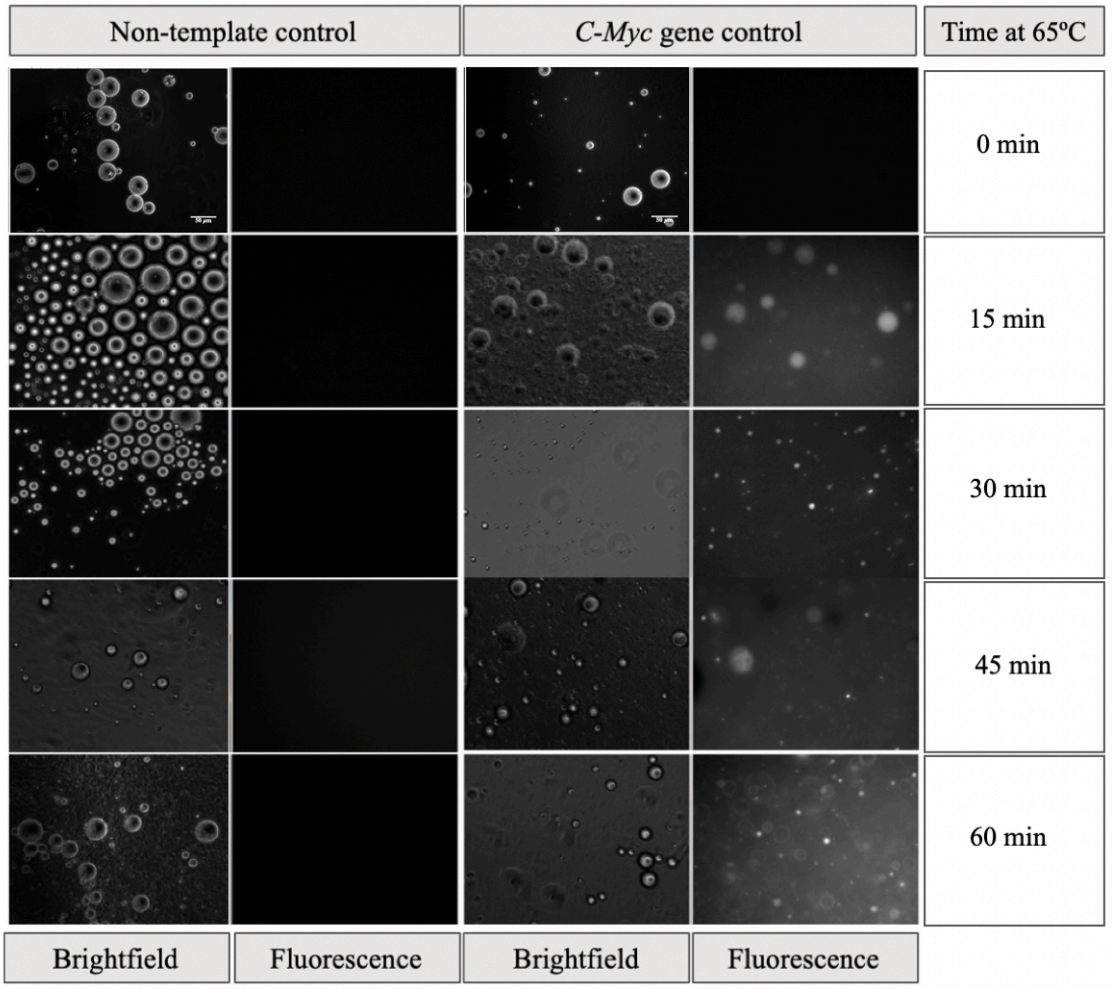

Figure 12. Optical and fluorescence images of the droplets within time at 65ºC. The images were obtained with an 20x objective. Optical microscopy images of non-template control are on the first column and *c-Myc* amplification control brightfield images are on the third column. Fluorescence microscopy images (second and fourth columns) were taken with 5.82 seconds of exposure with the green channel (excitation between 510 to 560nm). The first image of each brightfield column contain a scale bar of 50µm.

Figure 12 shows the presence of fluorescent droplets on *c-Myc* gene controls while absent in the non-template control, demonstrating that LAMP is fully compatible with the droplet-based approach. These microscopy results do not allow a quantitative analysis of the reaction or serve the purpose of being used in digital LAMP applications. However, the microscopy images allow some qualitative insights about the reaction profile. For example, the ratio between the average fluorescence intensity of the droplets with background fluorescence over time and comparison of the reaction profile with real-time LAMP (RT-LAMP) (see **Figure 13**).

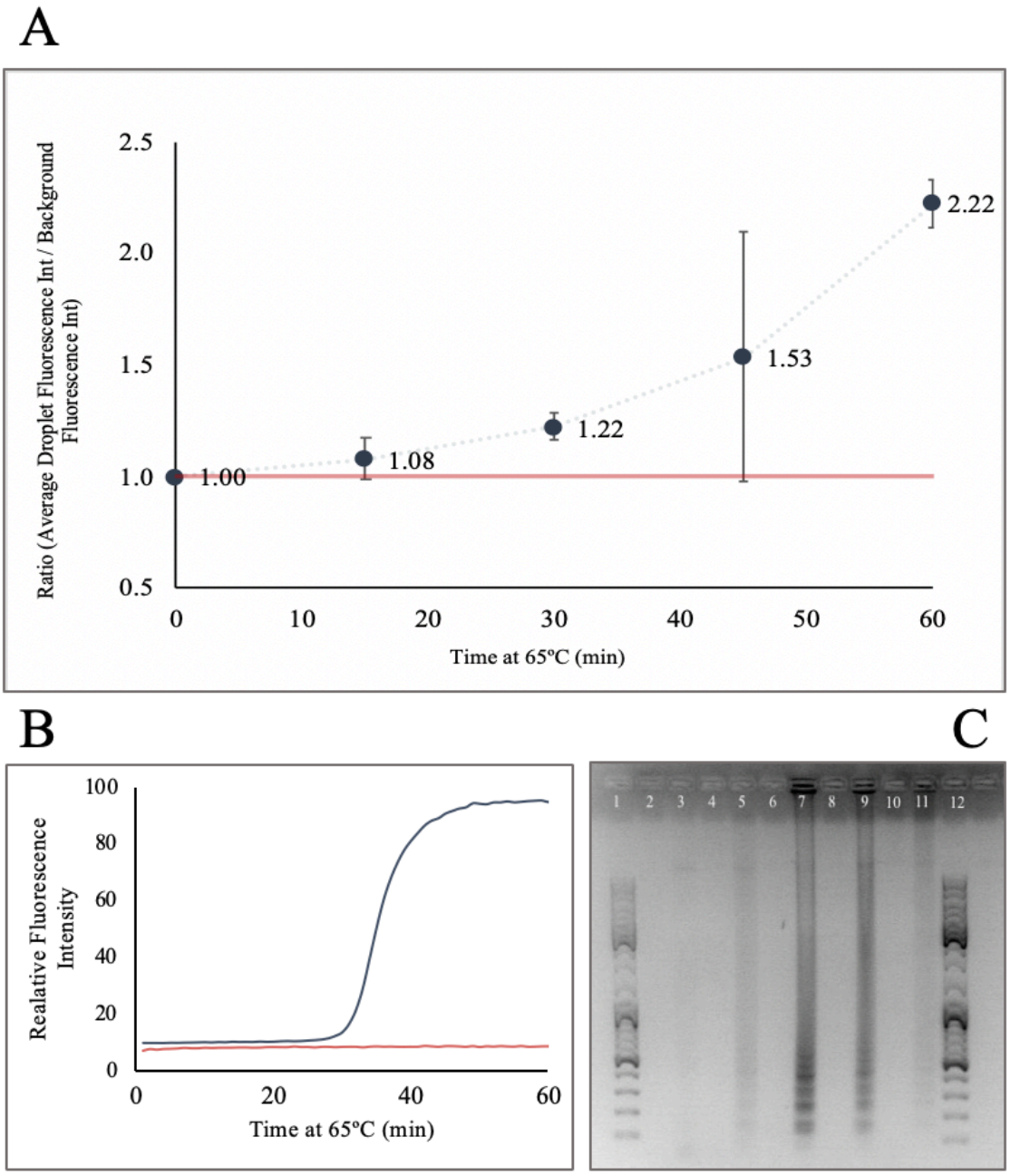

Figure 13. Evaluation of dLAMP amplification of *c-Myc* gene. (A) Ratio of average droplets fluorescence intensity with background intensity over reaction time at 65ºC. (-●-) represents the ratio between the average fluorescence intensity of droplets with *c-Myc* template with background over time. (–) represents the ratio for the non-template control. The error bars correspond to the standard deviation for tree independent experiments (N=3). **(B)** Real-time LAMP curves of *c-Myc* gene amplification (–) and Non-template control (–) for in silico system. **(C)** Image of the gel electrophoresis of the LAMP products of discrete amplification times. Non-template controls (NTC) and c-Myc template controls (PC) were monitored between 0 and 60 minutes, in intervals of 15 minutes. The electrophoresis was performed in a 1.5% agarose gel and run at 60V for 90 min. (1) Ladder (2) NTC 0 minutes at 65ºC (3) PC 0 minutes at 65ºC (4) NTC 15 minutes at 65ºC (5) PC 15 minutes at 65ºC (6) NTC 30 minutes at 65ºC (7) PC 30 minutes at 65ºC (8) NTC 45 minutes at 65ºC (9) PC 45 minutes at 65ºC (10) NTC 60 minutes at 65ºC (11) PC 60 minutes at 65ºC (12) Ladder.

Figure 13 indicates that LAMP occurred inside the droplets, since the average fluorescence intensity of droplets, with *c-Myc* template, increases 2 times ± 0.11 after 60 minutes, whereas fluorescence of non-template droplets remained constant over time (**Figure 13A**). These results are comparable to the data obtained from the standard fluorescence-based DNA monitorization technique (RT-LAMP). The amplification curve for *c-Myc* gene was obtained for the typical *in situ* amplification system, since the turbidity of this droplet-based methodology interferes with the use of the device for real-time fluorescence tracing. The amplification curve (**Figure 13B**) indicates a clear intensification of fluorescence from 30 to 45 minutes, time at which the reaction achieves its endpoint (maximum fluorescence), thus corresponding to the maximum amount of *c-Myc* amplification products.

Following the visualization of the droplets in microscope, emulsions were broken down in the centrifuge (see **subsection *2.2.5.4*),** after which LAMP products we analyzed in an agarose gel electrophoresis (**Figure 13C**). The presence of positive amplification bands on the *c-Myc* template controls and absence of bands on the non-template controls corroborates the occurrence of LAMP amplification. Additionally, it is also noticeable an increase in the intensity of the LAMP amplification bands over time. In **Figure 13C** a clear rise in amplification products is observed from 30 to 45 minutes, at which the reaction seems to have achieved a maximum (with the exception of the band for 60 min, were a problem loading the gel had occurred). A strict inference cannot be made, since this detection method is susceptible to the amount of DNA loaded into the gel, which cannot be guaranteed.

In this section we were able to transpose the LAMP amplification reactions into a droplet-based amplification approach. The amplification seems to occur without a significant difference in reaction kinetics. However, it is clear that some aspects need further improvement, such as reduction of size dispersion and monolayer arranging of droplets (noticeable aspects on brightfield images). These traits are preventing the transposal of this stirring-based droplet generation methodology into digital LAMP quantitative applications, where there is a strict demand for an equal distribution of the reaction mixture and a requirement for the analyses of the totality of these compartments (Gansen *et al*., 2012). Neither of these requirements are being fulfilled with this droplet system. To this end, a different approach needs to be addressed in order to circumvent the referred limitations.

3.2 Microfluidic chip-based droplet generation

Chip-based microfluidics technology is regarded as the current gold standard for droplet generation technology and it has been emerging as an advantageous tool for biological, biomedical and diagnostics fields (Nayak *et al*., 2008). Droplet-based microfluidics is a subcategory that uses immiscible fluids to generate discrete fractions of aqueous solutions. Droplet-based microfluidic systems can employ a great variety of devices geometries, among them is the T-junction configuration, in which the inlet channel, that contains the continuous phase, perpendicularly intersects the middle channel containing the dispersed phase (Giuffrida and Spoto, 2017). This method produces highly monodisperse droplets that can be used in a diverse range of applications, including the synthesis of biomolecules, drug delivery and diagnostic testing. Digital amplification consists into breaking down a solution of the nucleic acids target with the reaction components into a large number of discrete reaction compartments, where the number of target molecules inside each compartment follows a Poisson distribution (Zanoli and Spoto, 2012). Following an end-point amplification, the absolute determination of initial target molecules is estimated by modeling the fraction of positive partitions.

In spite of the predominance of PCR-based methods as gold standard tools in molecular diagnostics, significant efforts into implementing NAATs in deployable, portable and PoC devices are still being addressed. The implementation of isothermal amplification methods in LOC systems (being LAMP-on-a-chip the most studied) have contributed to major instrumental simplification and time-to-result reduction (Pardy *et al.*, 2017). Nevertheless, the fabrication techniques of microfluidic devices still require improvement, to become simple, fast and cost-effective.

In this section, will be presented an alternative design and fabrication process for production of a microfluidics device and its further application aiming for droplet digital LAMP (ddLAMP), towards a quantitative approach for gene expression analysis.

3.2.1 Chip fabrication

Most of the microfluidic devices require complicated fabrication processes, such as photolithography, hot embossing and injection molding. Despite the achievement of high-quality channels, these fabrication processes are still time consuming and lack design flexibility, needed in a R&D setting. In research laboratories, that constantly need to change/optimize chip designs, the improvement of prototyping time and cost are much valued. With this mind-set, the chip fabrication process (**Figure 14A and 14B**) was developed with a laser ablation mechanism (Li *et al.,* 2011), in a polystyrene (PS) commercial sheets and further hot press bonding technique was applied (**subsection**

2.2.6.1). PS films are particularly beneficial for microfluidic devices due to its high transparency, easy obtention, biochemical compatibility and good material rigidity (Wang *et al*., 2011). The PS substrate is commercially available, low-cost and allows to complete the process from chip design to working device within minutes. The laser ablation mechanism with a CO_2 laser occurs when the beam laser hits the surface of the thermoplastic sheets inducing melting, decomposition and vaporization of the material and leaving a void in the workpiece (Cao, Bontrager-Singer and Zhu, 2015). The μF channels are created in a few seconds and then are assembled into a 3D structure that is bonded with a thermo pressing method. The integration of this material and fabrication technique allows for fast chip production (under 30 minutes) and for extra flexibility, since changes to the design can be implemented digitally with no additional costs.

Chip design was upgraded to an all-in-one (droplet generation, amplification reaction and detection) integrated chip, instead to the design of commercial devices, that require a specific equipment for each operation. This approach eliminates steps such as the mask fabrication, as well as the corresponding microfabrication equipment and processes required in conventional methods. The chip design and fabrication were executed by Dr. Veigas (DCV/CENIMAT).

3.2.2 Chip design and operation conditions

The proposed design aims to develop an integrated chip for droplet generation, amplification and result measurement. The laser cutting conditions were defined to produce channels with 200 μm of width. The part of the chip dedicated to droplet generation comprises channels with a T-junction geometry, where the dispersed phase (reaction mixture and template molecules) and continuous phase (oil) meet perpendicularly ($\theta = 90°$). This geometry is widely used due to its simplicity and capacity to produce monodisperse droplets (Zhu and Wang, 2017). Droplet incubation and measurements are performed on the central part of the chip. The size of the chamber was iteratively increased in order to allow the accommodation of the total reaction volume, needed to the desire ddLAMP application (**Figure 14C**). The chemical nature of the droplets makes them fluctuate, causing a monolayer arrangement on the upper part of the chambers, making it easier for picture acquisition and further image processing techniques. Also, the outlet channel has to be connected to the bottom section of the chamber, which prevents droplet escaping and enables oil recovering (**Figure 14**).

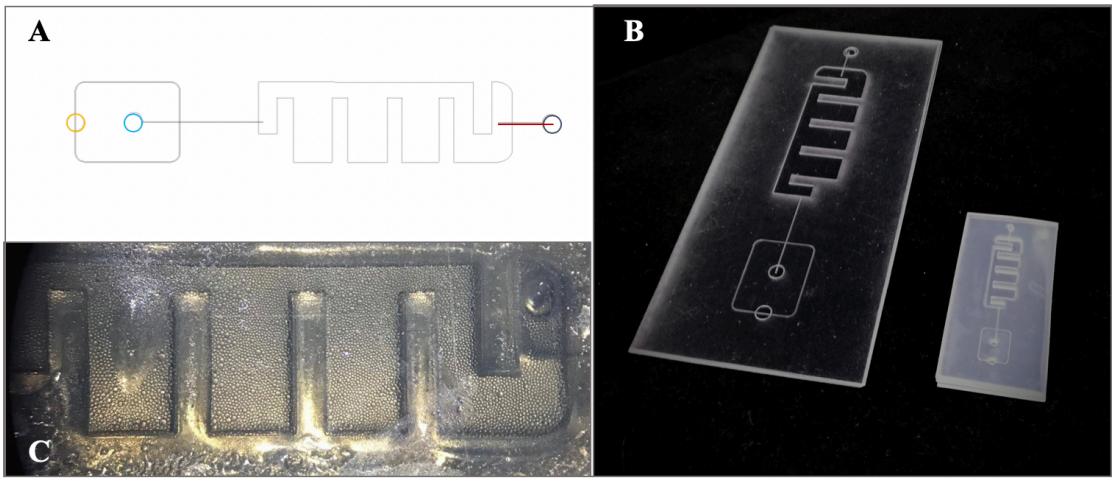

Figure 14. Chip design and fabrication. (A) Chip design. The chip is composed by tree layers, an upper one where are the inlets and outlet, a middle layer represented with (—) and a lower layer with the outlet channel represented with (—). The ◯ represents the inlet of the oil, ◯ the inlet of the aqueous phase (reagent components and target molecules) and ◯ the outlet for the oil. **(B)** Chip appearance before and after the shrinkage. The shrink is isotopically in plane and reduces around 66% of the original size. Additionally, occurs an increase in the height of the features over 500%. **(C)** A close-up view of the device.

The continuous phase flow rate (*Qc*) and dispersed phase flow rate (*Qd*) were controlled by a syringe pump with flow rates set at *Qc* = 20 µL/min and *Qd* = 1 µL/min. Small changes to the initially *Qd*/*Qc* ratio were made to modulate droplet sizes (see **subsection *2.2.6.1***) (Sontti and Atta, 2019). These flow rates were optimized to generate droplets with a size of approximately 150 µm of diameter (corresponding to ~1 nL of volume) to resemble the droplets produced by Bio-Rad droplet generator apparatus, the current gold standard for ddPCR (Gene-quantification.de, 2019). Droplets volume depends on the viscosity of the oil phase, the surfactants used, and the specific geometry of the microfluidic device adopted to generate droplets, all these factors are the same for both this chip and Bio-Rad droplet generator (Gene-quantification.de, 2019). This chip-based droplet system accomplished to produce droplets with 170 µm of diameter (~1.5 nL of volume) and with low size dispersion (**Figure 15**). The coefficient of variation (CV) is defined as (**Equation 2**):

$$\textbf{Eq (2)}. \quad CV = \frac{Standard\ deviation}{Mean}$$

A droplet size CV of 3% was achieved, which represents a significatively decrease when compared to the CV of 11% that was obtained with the stirring on vortex approach (see Annex, **Figure A4**). The attained CV value was close to the reports for this T-type junction droplet generation system (usually under 2%) (Xu *et al.*, 2006).

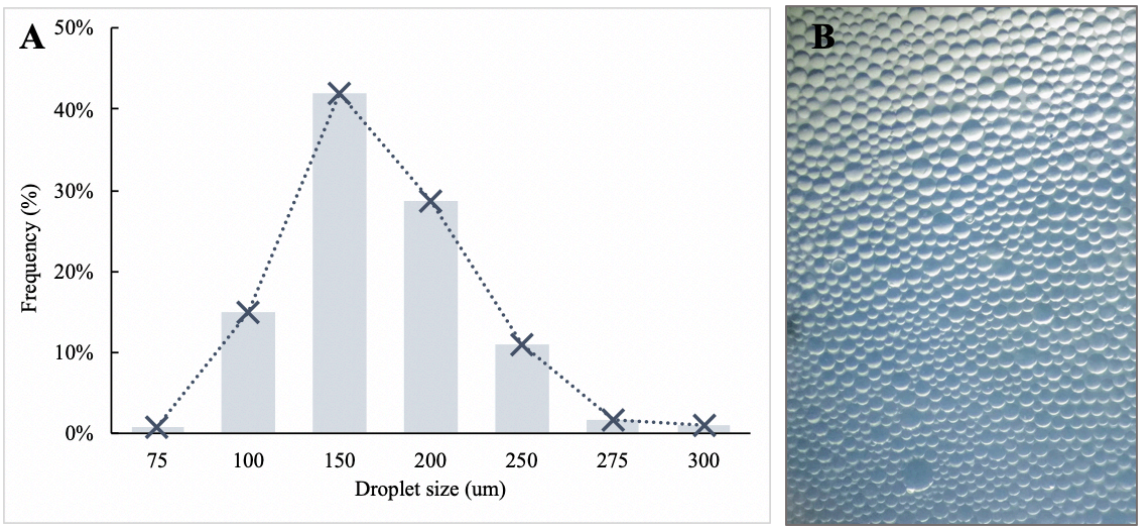

Figure 15 Frequency distribution of droplet sizes. (A) Droplet size analyses. The droplets present a weighted average size of 170 µm, a coefficient of variation equals to 3% and a SEM of 0.27. The results represent the measurement of the droplets attained for all the experiments during the development of this project. The mean volume encaged by these droplets is 1.5 nL. **(B)** A close-up view of the droplet monolayer inside the chip**.**

The discussed chip-base droplet generation system has clearly overcome the limitations faced by the stirring on vortex approach **(**see **Results section 3.1**). The chip-based droplets have an average size of circa 170 µm and a reaction volume of 1.5 nL, similar to those reported for dLAMP and ddPCR (Gene-quantification.de, 2019). Also, the droplets show a narrow polydispersity (CV=3%) and present monolayer arrangement inside the chip. All of these aspects were not feasible by the stirring on vortex approach, thus thwarting the effective droplet generation system for digital LAMP. Additionally, the chip-based system not only provides the essential conditions for molecular biology applications but also presents an improved method for rapid chip fabrication. What is more, the innovative design allows droplet generation, amplification reaction and droplet measurement all in a single device. This chip-based device was applied to a digital LAMP approach for amplification of *c-Myc* gene and, eventual, target quantification.

3.2.3 Chip-based digital LAMP

Following the design and fabrication of the device, the system was transposed aiming for a digital LAMP approach towards *c-Myc* gene amplification. Digital amplification techniques are based on the partitioning of the amplification reaction into many small reaction vessels, where end-point amplification is conducted. The determination of the initial concentration of target molecules, in the sample, is achieved through a Poisson statistical analysis of the positive droplets (droplets that contain at least one target molecule) and negative droplets (droplets that displayed zero target molecules) (see **subsection *2.2.6.2***) (Vogelstein and Kinzler, 1999). The first logical step was the definition of the threshold, which is used to distinguished between positive and negative droplets based on their fluorescence amplitude. Positive droplets inherently exhibit increased fluoresce in comparison to negative droplets, due to the presence of Evagreen, a dsDNA binding dye in the amplification reaction. However, the fluorescence amplitude of Evagreen fluctuates with factors such as droplet size, amplicon size, amplification efficiency and primer-dimer formation (Gene-quantification.de, 2019). Consequently, these aspects should be taken in account into the threshold definition, to guarantee a correct droplet score. In order to define the threshold that distinguished positive droplets from negative droplets, experiments without target template molecules were performed. (**Figure 16**).

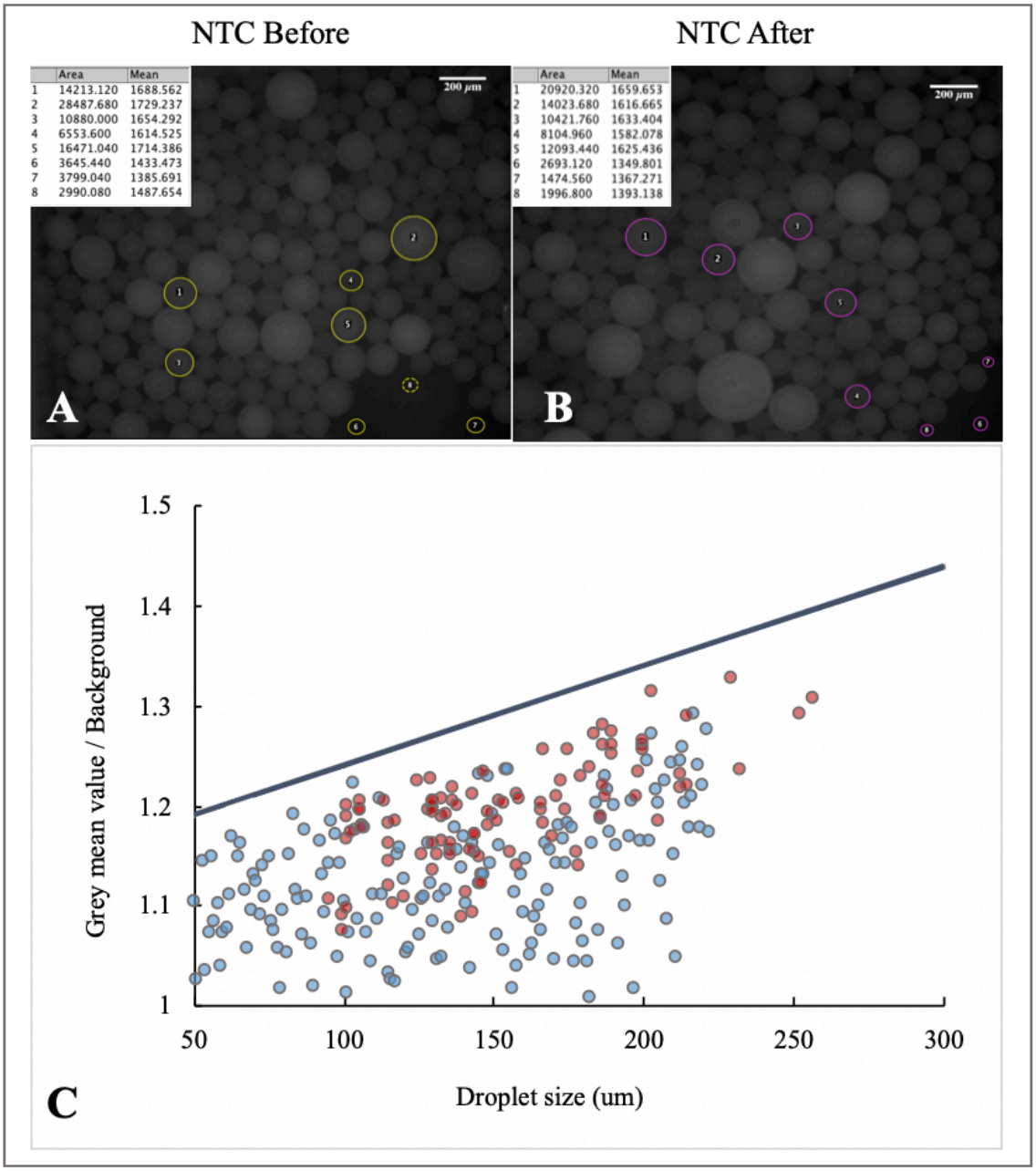

Figure 16. Threshold definition. (A) Image of the droplets without template before end-point amplification. **(B)** Image of the droplets without template after end-point amplification. The ◯ and ◯ exemplify the process used to obtain the data for the threshold definition. The list of values (Area and mean) on top of each image are the measurements results for the droplet's area and corresponding mean grey value obtained with ImageJ software. The scale bar on both (A and B) images marks 200 µm. **(C)** Corrected grey mean value (droplet GMV/ background GMV) with droplet size. ● represent the droplets before end-point reaction and ● represents the droplets after end-point reaction. The threshold (—) equation is y = 0.001x+1.14.

The results presented in **Figure 16** were obtained through the correction of the grey mean value of each droplet to the GMV of the image background and further plotting the corrected GMV against the droplet's diameter. A clear correlation between fluorescence and droplet size is noticeable (Corbisier *et al*., 2015) implying that the threshold line must have a two-dimensional equation with a positive slope value. In fact, droplets with greater sizes have a higher volume, increasing the optical path and hence their intrinsic fluorescence. They also present an increased probability of encage more than one target molecule, thus more Evagreen molecules will bind and therefore increasing the basal fluorescence (Gene-quantification.de, 2019). The effect of the formation of primer-dimers was also evaluate by measuring the GMV of non-template controls before and after end-point reaction (**Figure 16A, 16B**). The results seem to indicate that primer-dimers do not significantly increase the basal fluorescence of the droplets, since for the same droplet sizes, the higher fluorescence values are present in both before and after end-point reactions (**Figure 16C**). Bearing in mind the discussed results, the threshold was iteratively defined taking into account all the attained baseline measurements, in order to distinctively distinguished positive from negative droplets. The threshold equation **(3)** is:

$$\textbf{Eq}\ (\textbf{3}). \quad y = 0.001x + 1.14$$

In order to verify if the defined threshold allows to distinguish droplets with and without target molecules, two end point droplet LAMP reactions were performed, a non-template control and a positive control (**Figure 17**).

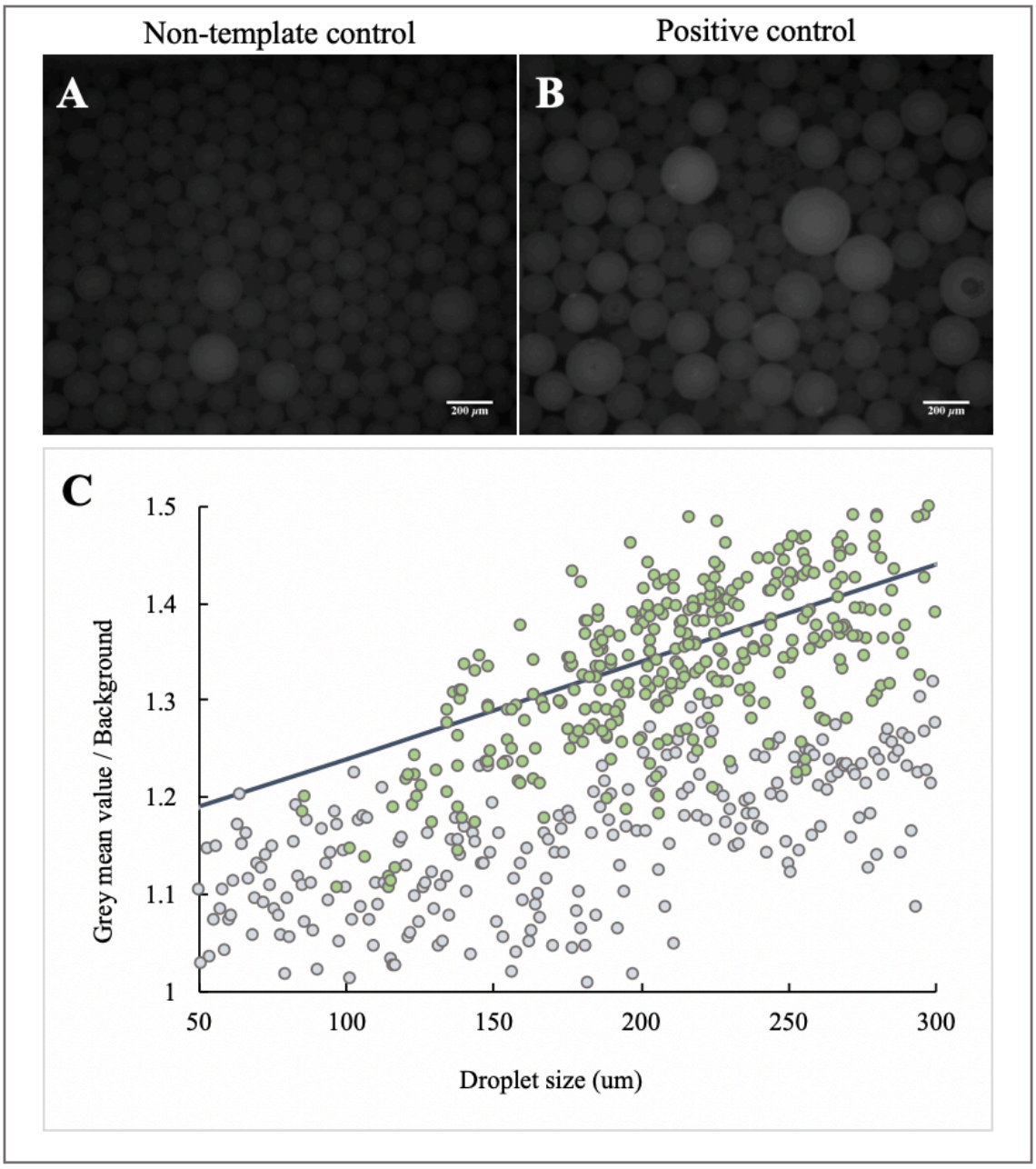

Figure 17. Assessment of the threshold differentiation ability to distinguish between negative and positive droplets. (A) Droplets of the non-template control experiment. Scale bar grades 200 µm. **(B)** Droplets of the positive control experiment. Scale bar grades 200 µm **(C)** Corrected grey mean value (droplet GMV/ background GMV) with droplet size. ● represent the NTC droplets and ● represents the droplets after end-point reaction. The threshold (—) equation is y = 0.001x+1.14.

The results indicate that the threshold is able to differentiate positive from negative droplets, since only droplets from the positive control sample have corrected grey mean values above the previously defined threshold. The fact that not all the positive control sample droplets present a fluorescence intensity above the threshold is related with the Poisson distribution of target molecules, indicating that some of these droplets lack target template molecules.

3.2.4 Application on target quantification

Digital amplification methods are end-point measurements that outmatched the need for a DNA calibrant, and they have been reported as alternative methods to determinate the copy number and/or concentration of specific sequences in a sample (Corbisier *et al*., 2015). In order to assess the quantification capability of the developed chip-based system for ddLAMP approach, several serial dilutions of a *c-Myc* PCR product were tested (logarithm of dilution factor ranging from -6 to -12). The copy number for each dilution was calculated based on the previous quantification of the original target sample via gel electrophoresis (see **subsection *2.2.4.6***) – see Annex, **Figure A5**.

End-point amplification reactions were conducted for all the template dilutions, followed by fluorescence image taking and processing. For each condition, area and grey mean value parameters were measured. After the fluorescence normalization to the background, the number of droplets above the threshold (positive droplets) and the number of droplets below the threshold (negative droplets) were scored (**Figure 18**).

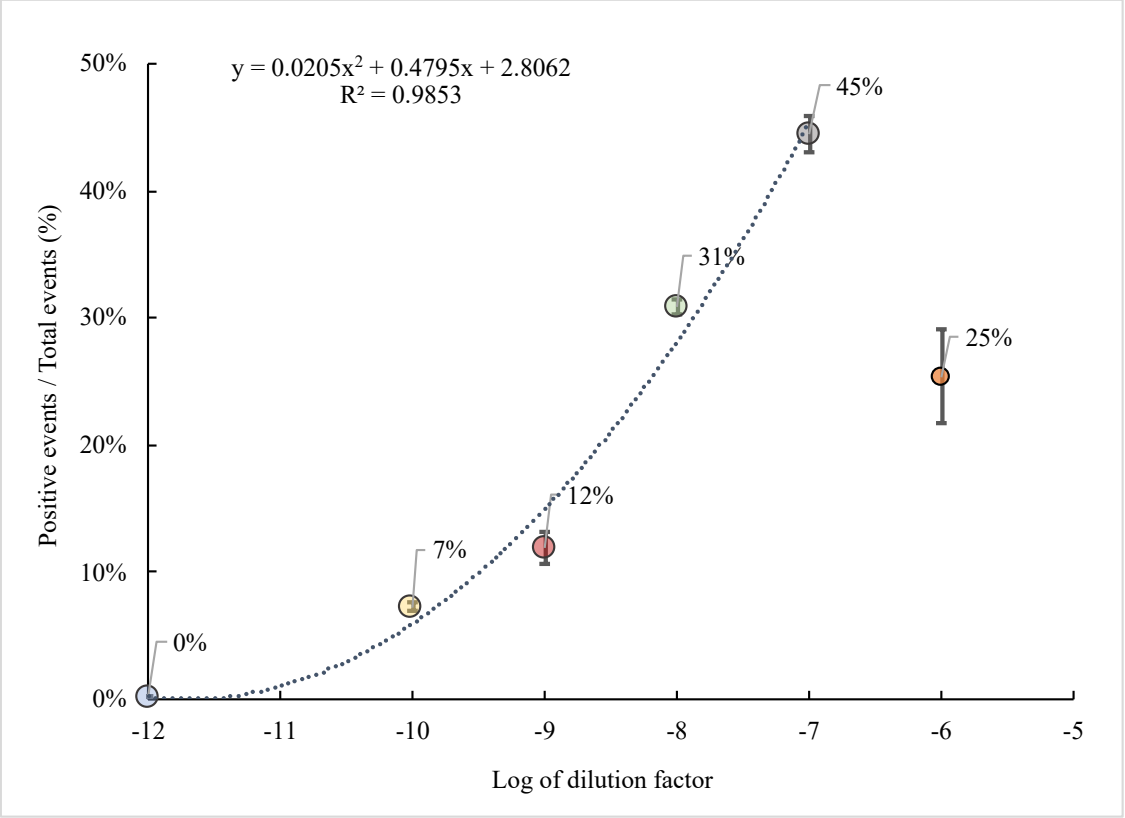

Figure 18. Fraction of positive events for different target dilutions. The results represented the fraction of positive droplets in a total of 400 measured droplets. The error bars correspond to the standard deviation values: 0.18%, 0.35%, 1.24%, 0.53%, 1.41% and 3.71% % of two independent experiments (n=2). The trendline present a polynomial equation: y= 0.0205x2 + 0.4795x + 2.8062 and a $R^2 = 0.98$. (●) represents the 10^{-12} dilution, (●) represents the 10^{-10} dilution, (●) represents the 10^{-9} dilution, (●) represents the 10^{-8} dilution, (●) represents the 10^{-7} dilution and (●) represents the 10^{-6} dilution.

Figure 18 shows the increase of the fraction of positive droplets (E_{pos}) as function of the logarithm of the dilution factor, indicating that the chip-based system is able to distinguish different target concentrations. The increase of E_{pos} occurs due to a raise in the number of targets and, consequently, the probability of a droplet containing at least one target - **Equation 4**:

$$\textbf{Eq (4).} \quad E_{pos}\ (\%) = \frac{Number\ of\ positive\ droplets\ \ (N_{pos})}{Total\ number\ of\ droplets\ (N)} \cdot 100$$

The observable decay on the E_{pos} for the log of dilution factor -6 (**Figure 18** - ●) seems to indicate a possible reaction inhibition by excessive amount of template, consequence of the number of copies encaged per droplet. In fact, this dilution

corresponds to an average of 180 copies per droplet (CPD). **Figure 19A** shows the CPD for each template dilution calculated via **Equation (5)**:

$$\textbf{Eq (5)}. \quad CPD = \frac{Total\ number\ of\ target\ molecules}{Total\ number\ of\ droplets\ (N)}$$

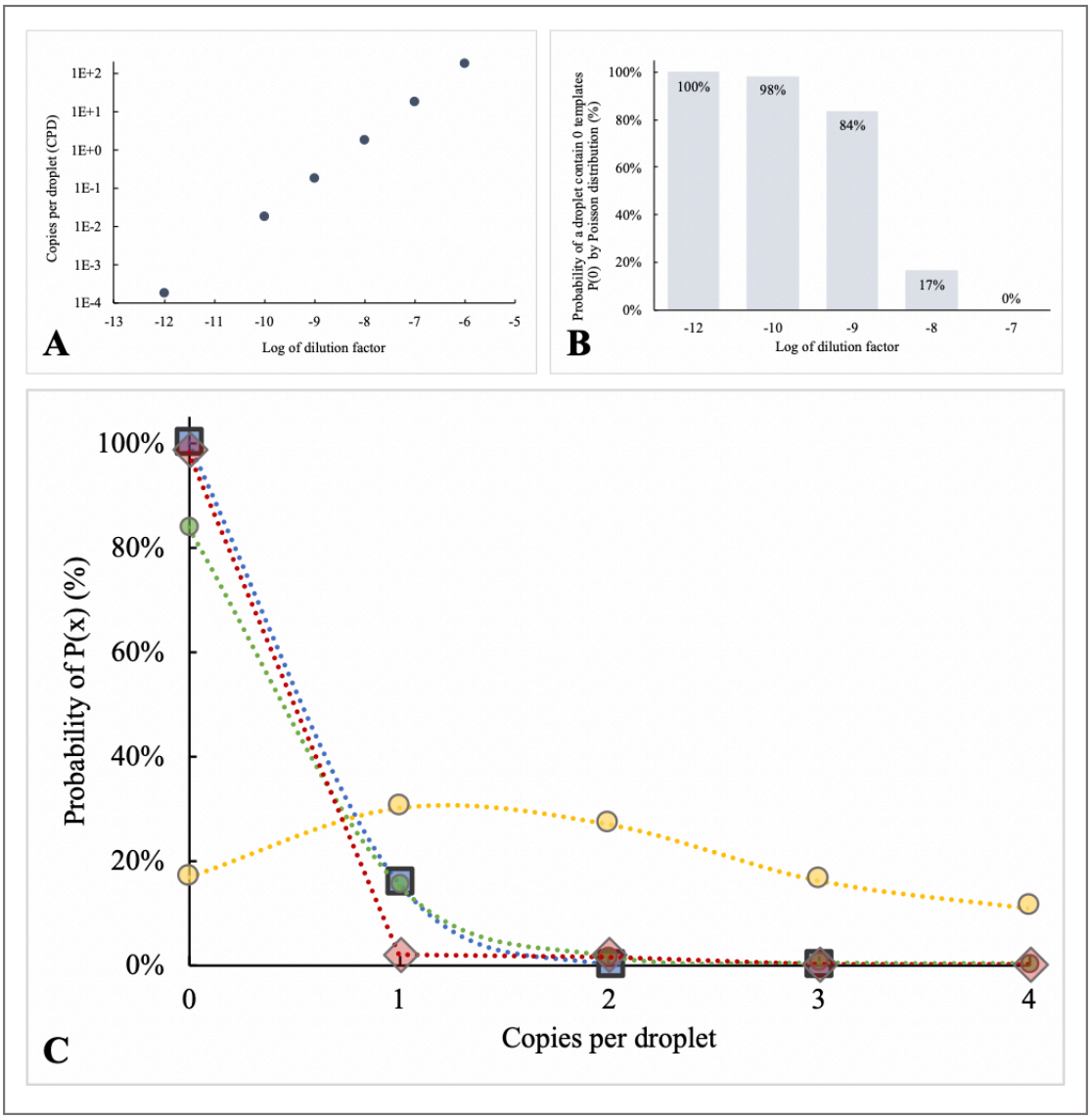

Figure 19. Poisson partitioning statistics. (A) Correlation between the number of copies per droplet (CPD) and the logarithm of template dilution factor. **(B)** Probability of a droplet contain zero target molecules for each template dilution, by the Poisson statistics. **(C)** Poisson-estimated probability in function of the number of copies per droplet, for each template dilution. (■) represents the 10^{-12} dilution, (◆) represents the 10^{-10} dilution, (●) represents the 10^{-9} dilution and (●) represents the 10^{-8} dilution.

Since the digital amplification methods rely on Poisson distribution, the absolute determination of initial target molecules has to be estimated by modeling the fraction of positive partitions as a Poisson distribution. This assumes that both reaction components and target molecules are randomly distributed in all droplets. Randomly distribution implies that a target molecule got an equal probability of being distributed into any of the droplets, meaning that target molecules move independently and do not interact with each other. This assumption is the core of all digital amplification approaches. As a consequence of the random distribution, some droplets will be lacking nucleic acids templates and other droplets will contain one or more target molecules thus, the fraction of positive droplets must be corrected to Poisson partitioning statistics. So, the probability for droplets contain an exact number of target molecules (zero, one, two, three or more targets per droplet) needs to be determined, to this end is used the **Equation** (**6**):

$$\textbf{Eq (6)}. \quad Pr(n) = \frac{C^n . e^{-C}}{n!}$$

Figure 19B represents the probability given by the Poisson statistics of a droplet contain zero target molecules (Pr (0)) for each template dilution. As expected, the probability of a droplet contains zero target molecules increases with the increasement of the dilution factor. In **Figure 19C** is represented the probability, also given by Poisson statistics, of a droplet containing zero, one, two, three or more target molecules for the samples with logarithm of dilutions factors of -12, -10, -9, -8 and -7. Sample with dilution factor of 10^{-8} (**Figure 19C** - ●) shows a similar probability of a droplet contains 1 or 2 template molecules (30% and 27%, respectively) and also an approximate probability for droplets containing 0 or 3 template molecules (17% and 16%, respectively), which is expectable having into account that this template dilution corresponds to an average of 1.8 copies per droplet. However, for the dilutions of -7 (CPD=18) and -6 (CPD=180), the Poisson statistics cannot be applied, since this method requires the existence of droplets without template molecules, and as so that has no probability to occur when the average number of copies per droplet is 18 or 180. Usually, this requirement stops being fulfilled at CPDs above 8, corresponding to the referred dilutions (Gene-quantification.de, 2019).

After the end-point amplification reactions and further scoring the positive and negative results, the observed fraction of positive droplets (E_{pos}) must be modeled by Poisson partitioning statistics. To this end, the Poisson probability of a droplet contain zero target molecules is used to correct the observed number of positive droplets (correction to the Poisson partitioning statistics) (**Figure 20**). The corrected fraction of positive droplets was obtained with **Equation** (**7**):

$$\textbf{Eq (7).} \quad E_{pos}^{C}\,(\%) = 1 - \left(\frac{N_{neg}\,.\,Pr(0)}{N}\right).100$$

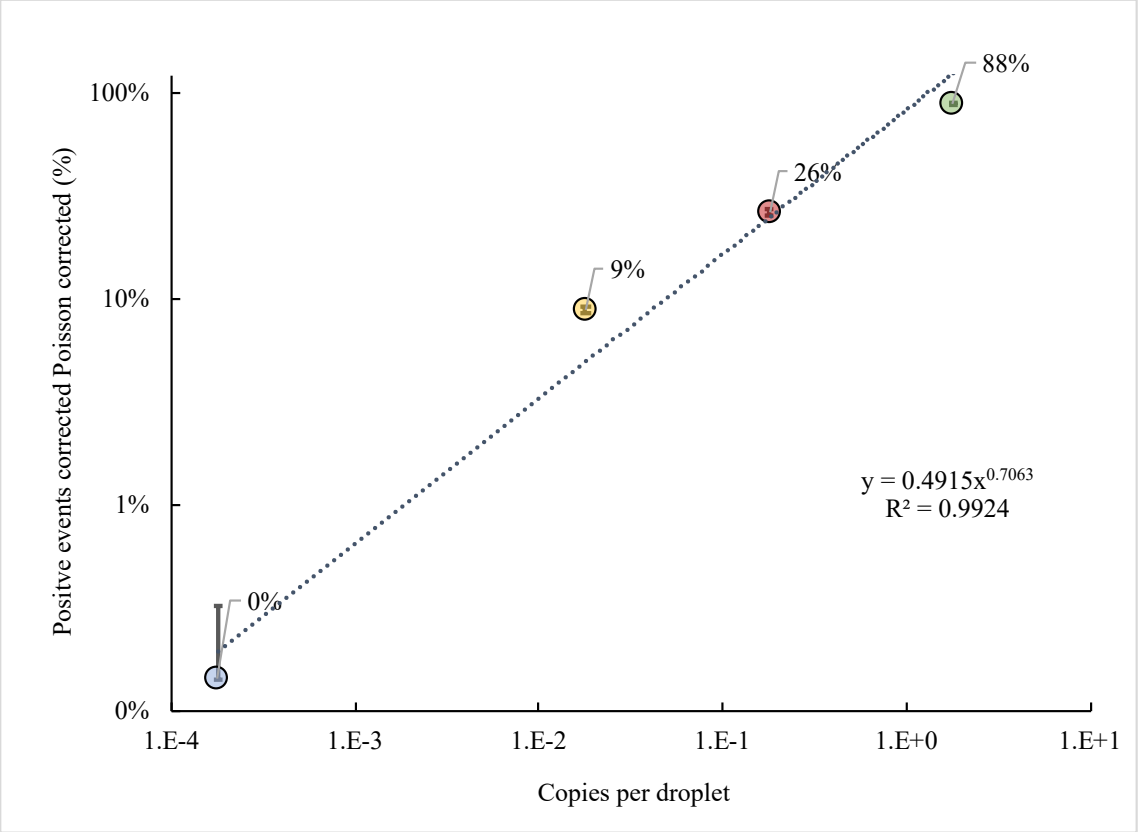

Figure 20. Fraction of positive events attained with Poisson-based correction for different target dilutions. The fraction of positive events corrected to the Poisson statistics are represented with a logarithmic scale. The error bars correspond to the standard deviation values: 0.18%, 0.35%, 1.03% and 0.09% of two independent experiments (n=2) with 400 measured droplets for each experiment. The trendline present an exponential equation: $y = 0.4915x^{0.7063}$ and a $R^2 = 0.99$. (●) represents the 10^{-12} dilution, (●) represents the 10^{-10} dilution, (●) represents the 10^{-9} dilution and (●) represents the 10^{-8} dilution.

Figure 20 shows a high linear correlation ($R^2 = 0.99$) between the Poisson corrected fraction of positive droplets (in logarithmic scale) and CPD. This correlation indicates the capability of this system for on chip direct target quantification. The results show only 4 orders of magnitude of target dilutions. Due to the restriction of Poisson correction for conditions where the probability of droplets having no template being >0, the fraction of positive droplets can only be corrected for template dilutions down to 10^{-8} dilution factor (corresponding to 1.8 copies per droplet). Taking this into consideration, the working dilution range is theoretically constrained to 4 orders of magnitude of template dilution. To further increase the detection range, the number of droplets has to be increased by a 10-fold factor for each order of template dilution magnitude.

In order to assess if this chip-based ddLAMP system allows to perform target concentration analyses, the attained results (Poisson corrected) were used to estimate the concentration of each target dilution sample. The following **Equation (8)** was used:

$$\textbf{Eq (8)}. \quad C = -In\left(\frac{N_{neg}}{N}\right) / V_{droplet}$$

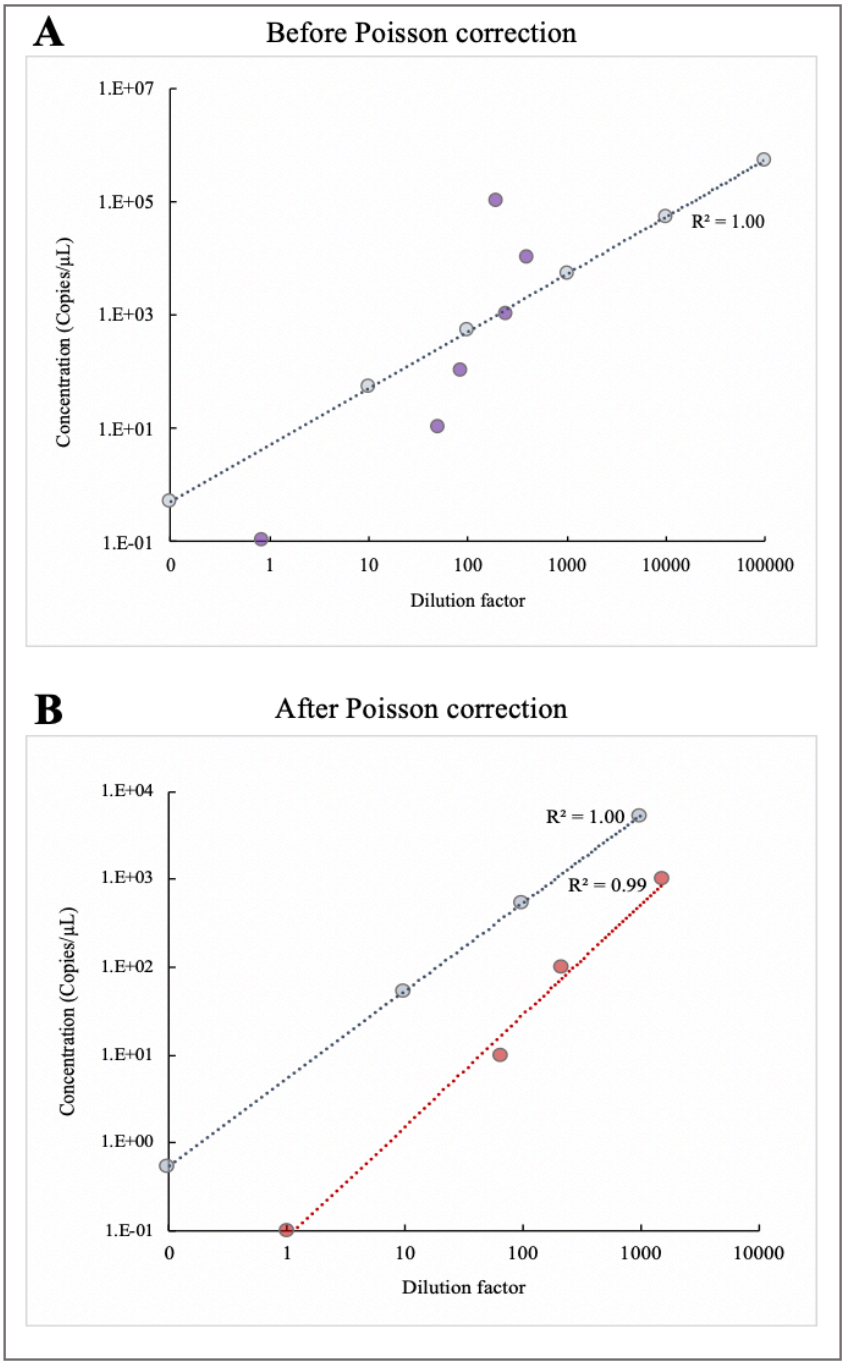

Figure 21. Comparison between the template concentration for each dilution attained by the chip-based system and gel electrophoresis. (A) Results of concentration (copies/µL) attained by chip-based

ddLAMP system without Poisson correction (●) in comparison to the concentration obtained via gel electrophoresis (●). **(B)** Results of concentration (copies/µL) attained by chip-based ddLAMP system with Poisson correction (●) in comparison to the concentration obtained via gel electrophoresis (●). The trendline for the power adjustment has a R^2= 0.99.

Figure 21 clearly indicates the need for Poisson correction in order to attain a correct score of the positive and negative droplets, thus allowing for a precise target quantification, which is also demonstrated by the robust power correlation (R^2=0.99) (**Figure 21B**). On the contrary, no correlation is attained between the concentrations estimate by the chip-based system without the Poisson correction and the concentrations based on the gel electrophoresis (**Figure 21A**). These results highlight the importance of the Poisson correction for the correct concentration assessment.

Finally, the discussed chip-based ddLAMP approach demonstrated the capability to distinguish between different target concentrations as well as to providing sample quantification. However, some aspects should still be improved in order to enhance the score assessment, such as optimization of droplet generation to remove size dispersity, optimization of the LAMP reaction conditions (*i.e.* primers' concentrations) lowering the basal fluorescence of the droplets, use an external reference dye to normalize the initial fluorescence of the droplets. Additionally, for an improved quantification capacity the calibration curve should be done with more dilutions and more droplet readings, thus increasing the robustness of the quantification. The detection range could also be raised by increasing the number of droplets.

3.3 Amplification of prostate cancer biomarkers

In this section, the development of isothermal amplification reactions aiming at further integration into the previously described chip-based format for digital LAMP is described. Considering that the effectiveness of LAMP to quantitatively monitor gene expression is still allusive (Aoi, Hosogai and Tsuneda, 2006; Toumazou *et al.,* 2013), the gold-standard RT-qPCR was adopted for comparation.

3.3.1 Development and optimization of SChLAP1 and PCA3 PCR reaction conditions

Two specific PCR reactions were developed for the *Second Chromosome Locus Associated with Prostate 1* and *Prostate Cancer Antigen 3*. The PCR amplification of a 226 bp amplicon for *SChLAP*1 gene and a 213 bp amplicon for *PCA3* were developed using primers from a set of four primers aimed for a LAMP amplification architecture,

with Primer Explorer V4. Target template was obtained via RNA extraction of the PC-3 cell-line with the TRIsure protocol (see Annex, **Table A3**). Following the synthesis and quantification of the cDNA, development and optimization of PCR reactions of *SChLAP1* and *PCA3* genes were performed, and products analyzed via agarose gel electrophoresis - **Figure 22**.

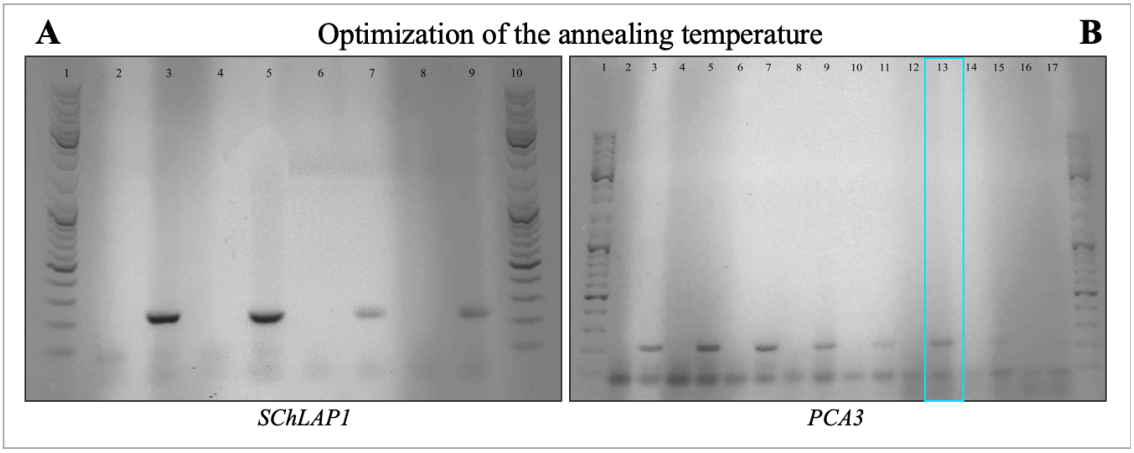

Figure 22 Optimization of the annealing temperature of *SChLAP1* and *PCA3* gene for PCR amplification reaction. Gel electrophoresis was performed in a 1.5% agarose gel and run at 80V for 90 minutes. (**A**) Optimization of the annealing temperature for *SChLAP1* gene. **(1)** Ladder **(2)** Non-template control (NTC) **(3)** Amplification control (PC) of *SChLAP1* with annealing temperature of 53ºC and 2000ng of cDNA as template **(4)** NTC **(5)** PC with annealing of 53.7ºC and 2000ng of cDNA as template **(6)** NTC **(7)** PC with annealing e of 53ºC and 200ng of cDNA as template **(8)** NTC **(9)** PC with annealing of 53.7 ºC with 200ng of cDNA as template **(10)** Ladder. **(B)** Optimization of the annealing temperature for *PCA3* gene. **(1)** Ladder **(2)** NTC with annealing temperature of 53ºC **(3)** PC with annealing temperature of 53ºC and 200ng of cDNA as template **(4)** NTC 53.7ºC **(5)** PC with annealing of 53.7ºC and 2000ng of cDNA as template **(6)** NTC 54.9ºC **(7)** PC with annealing of 54.9ºC and 2000ng of cDNA as template **(8)** NTC 56.7 ºC **(9)** PC with annealing of 56.7 ºC with 2000ng of cDNA as template **(10)** NTC 59.1ºC **(11)** PC with annealing of 59.1 ºC with 2000ng of cDNA as template **(12)** NTC 61ºC **(13)** PC with annealing of 61 ºC with 200ng of cDNA as template **(14)** NTC 62ºC **(15)** PC with annealing of 62 ºC with 2000ng of cDNA as template **(16)** NTC 63ºC **(17)** PC with annealing of 63 ºC with 2000ng of cDNA as template.

For *SChLAP1* gene the best annealing temperatures were found to be between 53ºC and 53.7ºC (**Figure 22A**). These temperatures have shown to reduce unspecific amplification products and primer dimer formation; relevant when monitoring the amplification in real-time with intercalating dyes. Also, no clear reduction in endpoint product was found for the higher annealing temperature, allowing for increased specificity without loss in sensitivity. For *PCA3* gene the best annealing temperature was found to be at 61ºC (**Figure 22B**, □ box). This amplification condition has shown to reduce the amount of amplification product. However, there is a clear reduction in unspecific products and primer dimer formation. These two annealing temperatures (53,7ºC for *SChLAP1* and 61ºC for *PCA3*) were used to further optimize the primer concentration for each gene (reaction conditions were performed as described in **subsection *2.2.4.7***) (**Figure 23**).

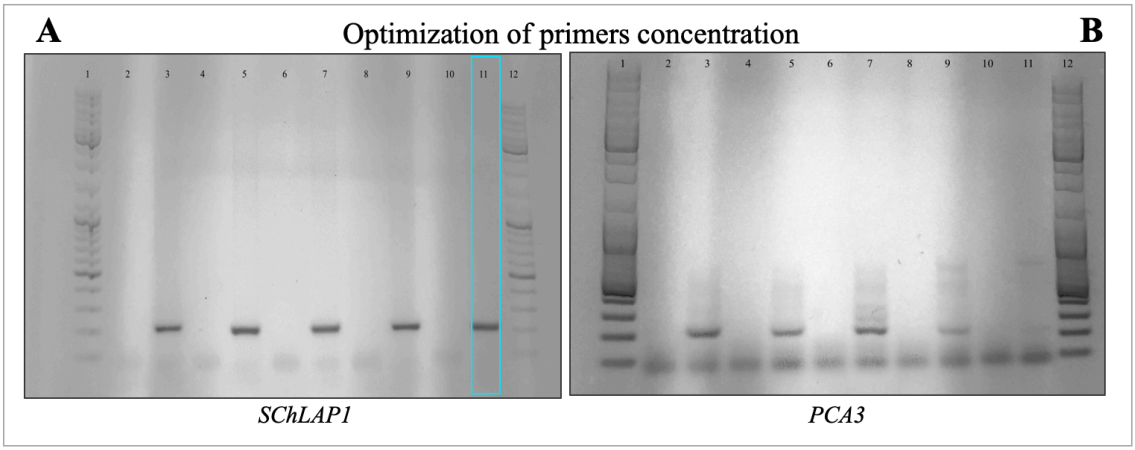

Figure 23. Optimization of the primer concentration of *SChLAP1* and *PCA3* gene for PCR amplification reaction. The electrophoresis was performed in a 1.5% agarose gel and run at 80V for 90 minutes. (**A**) Optimization of the primers concentration for *SChLAP1* gene. (1) Ladder (2) NTC (3) Amplification of *SChLAP1* gene control (PC) with 800nM of primers (4) NTC (5) PC with 720nM of primers (6) NTC (7) PC with 640nM of primers (8) NTC (9) PC with 560nM of primers (10) NTC (11) PC with 480nM of primers (12) Ladder. . (**B**) Optimization of the primers concentrations for *PCA3* gene. (1) Ladder (2) NTC (3) Amplification *PCA3* gene control (PC) with 800nM of primers (4) NTC (5) PC with 720nM of primers (6) NTC (7) PC with 640nM of primers (8) NTC (9) PC with 560nM of primers (10) NTC (11) PC with 480nM of primers (12) Ladder.

For *SChLAP1* gene amplification reaction, the primer dimer band disappears at primer concentrations bellow 480nM (see **Figure 23A**, □ box). At this concentration a single amplification product is observed matching the expected amplicon size for the *SChLAP1* gene (226bp). The same optimization was performed for the *PCA3* PCR reaction (Figure **23B**). For this reaction, despite the decrease in the primer concentration, there is no reduction in primer dimer production nor an observable reduction in unspecific amplification bands. Furthermore, the reduction of primers led to a lower amplification efficiency, which is observed by the decrease in the intensity of amplification band. Additionally, all amplification bands presented smear, which could be an indicator of excessive amount of template (**Figure 23B**). In order to verify if the smear was caused by excessive amount of template cDNA, PCR reactions were performed with the same conditions but with a ten-fold reduction of template concentration (200ng) (**Figure 24)**.

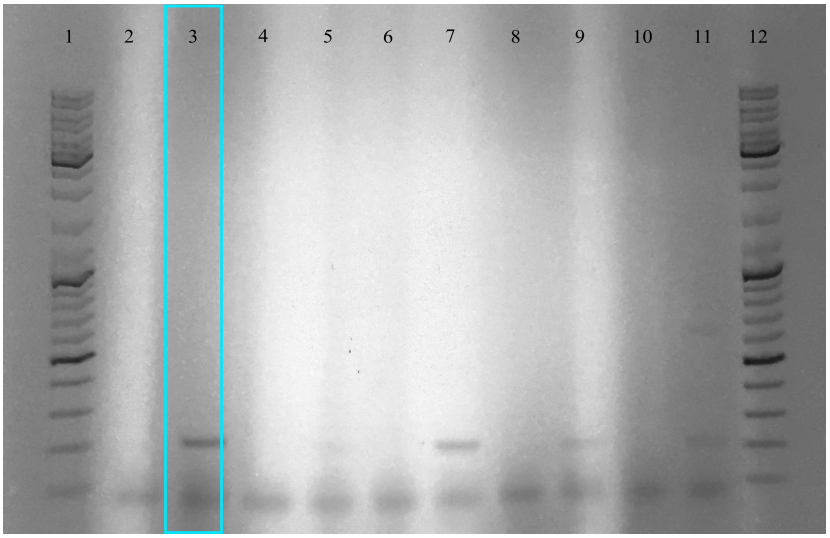

Figure 24. Optimization of the annealing temperature of *PCA3* gene for PCR amplification reaction with 10-times less template. The electrophoresis was performed in a 1.5% agarose gel and run at 80V for 90 min. (1) Ladder (2) NTC (3) Amplification *PCA3* gene with 800nM of primers (4) NTC (5) Amplification of *PCA3* gene with 720nM of primers (6) NTC (7) Amplification of *PCA3* gene with 640nM of primers (8) NTC (9) Amplification of *PCA3* gene with 560nM of primers (10) NTC (11) Amplification of *PCA3* gene with 480nM of primers (12) Ladder.

Figure 24 shows that reduction of template cDNA allowed for the amplification of *PCA3* gene (213bp). Also, the decrease in the concentration of primers did not influence primer dimer formation. However, it reduces the intensity of the amplification band, implying that for lower primer concentrations there may be a reduction in amplification efficiency. Even this might not be ideal for real-time monitoring, these were the conditions used for the subsequent experiments (see **Figure 24**, box in □). Amplification products were further analyzed via Sanger sequencing, confirming that amplicons correspond to *SChLAP1* and *PCA3* (see Annex, **Figure A6**).

Altogether, data show the successful optimization of PCR conditions for *SChLAP1* and *PCA3* genes. The importance of this optimization process relies not only on the development of more efficient reactions, but also into reducing factors, such as primer dimer and unspecific products, that could interfere in the real-time fluorescence-based amplification measurements.

3.3.2 Development of SChLAP1 and PCA3 LAMP amplification reactions

LAMP is performed under isothermal conditions and at a relatively low temperature, making it an excellent alternative to PCR-based methods for PoC applications. In this thesis, LAMP reactions were developed aiming for the amplification and quantification of two lncRNAs (*SChLAP1* and *PCA3*) with clinical value as prostate cancer predictors, for further incorporation into microfluidics devices. For this, both cDNA from PC-3 cell line and PCR products were tested as templates for the reactions. The conditions used are described in **subsection *2.2.4.7***. In **Figure 25** is represented a typical result of LAMP amplification.

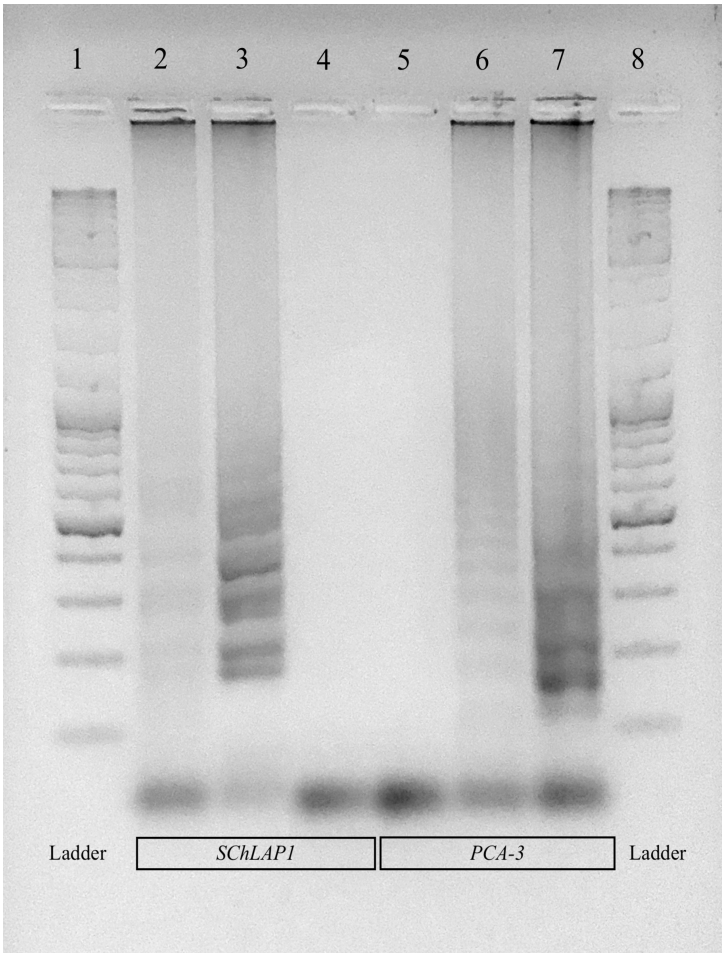

Figure 25. Typical result of LAMP amplification products. Result of *SChLAP1* and *PCA3* LAMP amplification products, with 1000ng cDNA or 200ng of PCR product as template. The electrophoresis was performed in a 1.5% agarose gel and run at 60V for 90 min. (1) Ladder (2) Amplification *SChLAP1* gene with cDNA as template (3) Amplification *SChLAP1* gene with PCR product as template (4) Non-template control for the LAMP reaction of *SChLAP1* (5) Non-template control for the LAMP reaction of *PCA3* (6) Amplification of *PCA3* gene with cDNA as template (7) Amplification of *PCA3* gene with PCR product as template (8) Ladder.

Figure 25 shows a positive amplification result for both *SChLAP1* and *PCA3* target genes with the characteristic ladder-like LAMP product pattern, which is caused due to the numerous concatemers of different sizes, that are formed in course of the LAMP reaction (Martzy *et al*., 2017). Both LAMP reactions do not present contamination, which is observed trough the absence of bands in the non-template controls. Further validation of *SChLAP1* and *PCA3* LAMP specificity was not studied, since direct Sanger sequencing cannot be performed. Specificity studies can be accomplished using TaqMan probes, restriction patterns analysis and fragment sequencing. At this time there was no possibility to perform any of the above-mentioned techniques. However, the lower band of the amplification control allows some considerations about the amplification specificity. In fact, the distance between B2 and F2 primers matches the size of the dumbbell structure, corresponding to the lowest size band. So, the presence of a band with the same size as the distance between B2 and F2 could indicate a specific amplification. For *SChLAP1* gene, the smallest band corresponds to the expected length between B2 and F2, which is 165bp. For *PCA3,* the same occurs, a region of 148bp - see **Figure 25 (**lanes 6 and 7).

The next step was the optimization of Evagreen dye in order to allow the detection of the amplification through fluorescence without significantly compromise reaction efficiency (**Figure 26**). Real time-LAMP (RT-LAMP) experiments were performed in triplicates (n=3) for *SChLAP1* gene.

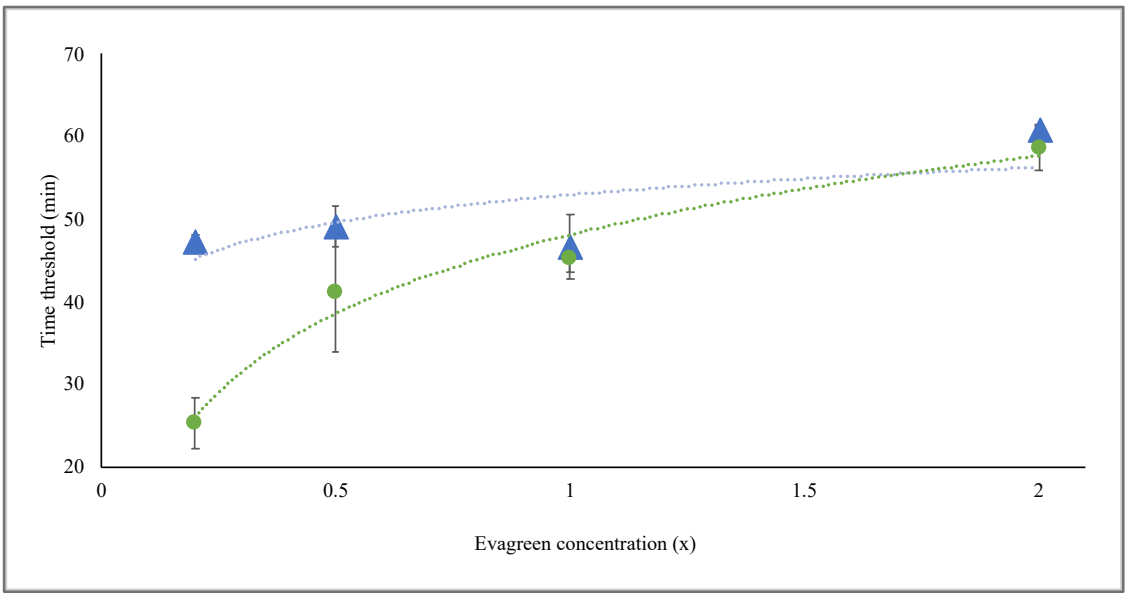

Figure 26. Influence of Evagreen dye in the time threshold of LAMP reaction Time threshold in minutes of RT-LAMP reaction in function of Evagreen concentration for two types of template: cDNA (…▲…),

PCR product of S*ChLAP1* (…●…). The error bars presented are the standard deviation of three experiments performed (n=3).

For all templates, an increase in the time threshold at higher concentrations of Evagreen dye is observed. This is in line with the literature, which shows that intercalating agents adversely affect enzyme activity (Mao, Leung and Xin, 2007). This effect is more pronounced in reactions that depend on enzymes with strand displacement activity, which is the case of *Bst* polymerase.

Figure 26 shows that reactions using cDNA as template are the least affected, showing a $\Delta T_{threshold}$ of 13 minutes between concentrations of Evagreen spanning from 0.2x to 2x, while for PCR product this variation is around 2.5-fold higher (see Annex, **Table A4**). Additionally, each RT-LAMP product was analyzed via fluorescence spectroscopy to quantify the difference between a positive and negative amplification signal. Hereupon, Evagreen at a concentration of 1x was selected for further experiments. As for template, the reaction was found to work with cDNA, allowing for an easy implementation of LAMP into the standard protocols in gene expression analysis.

3.3.3 Real-time PCR and LAMP amplification of SChLAP1 and PCA3

Amplification efficiency of the LAMP amplification was evaluated by real-time fluorescence-based monitoring and further compared with the current gold standard tool (PCR). For the RT-PCR amplification, SybrGreen dye was used instead of Evagreen dye, since Evagreen dye causes unspecific amplification. In fact, literature has already reported that SybrGreen is a better intercalating agent for PCR reactions than Evagreen dye (Mao, Leung and Xin, 2007). The results of the effect of each intercalating agent on the PCR for *PCA3* gene are presented in **Figure 27**.

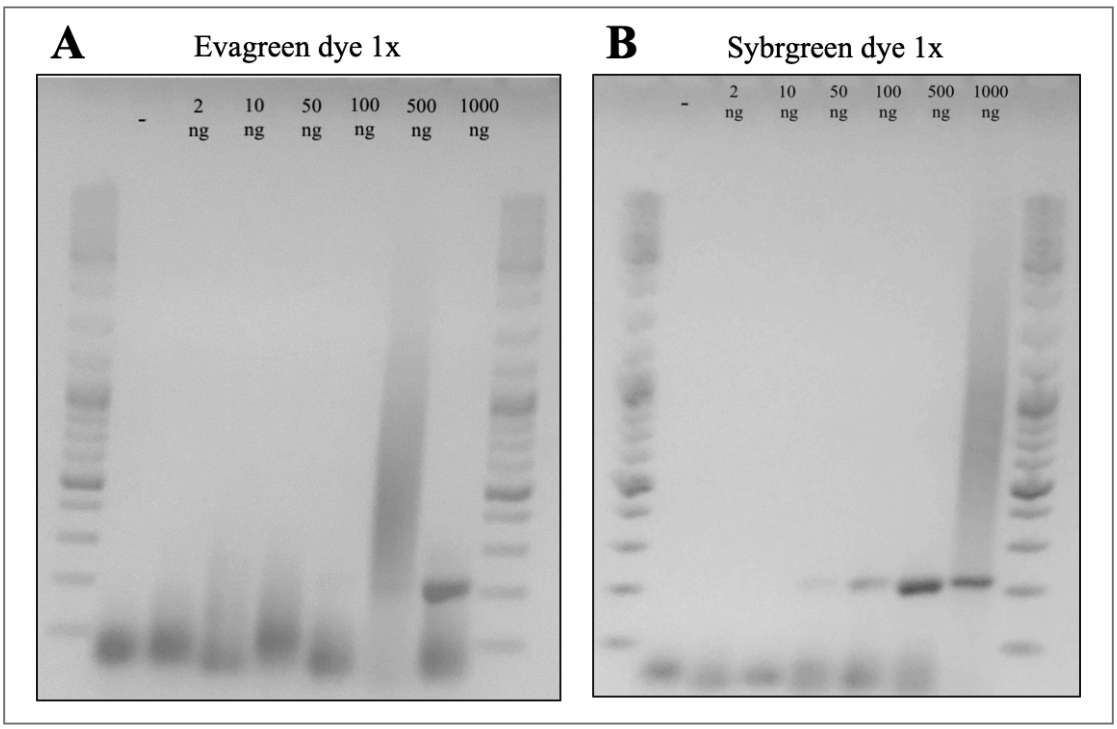

Figure 27. Effect of intercalating dyes (Evagreen and Sybrgreen) in the efficiency of the PCR reaction. The electrophoresis was performed in a 1.5% agarose gel and run at 60V for 90 min. (A) Effect of Evagreen dye 1x for different concentrations of cDNA template in the PCR amplification of *PCA3* gene. (1) Ladder (2) Non-template control (3) Amplification *PCA3* gene with 2ng of cDNA as template and 1x Evagreen dye (4) Amplification of *PCA3*gene with 10ng of cDNA and 1x Evagreen dye (5) Amplification of *PCA3* gene with 50ng of cDNA and 1x Evagreen dye (6) Amplification of *PCA3* gene with 100ng of cDNA and 1x Evagreen dye (7) Amplification of *PCA3* gene with 500ng of cDNA and 1x Evagreen dye (8) Amplification of *PCA3*gene with 1000ng of cDNA and 1x Evagreen dye (9) Ladder. (B) Effect of Sybrgreen dye 1x for different concentrations of cDNA template in the PCR amplification of *PCA3* gene. (1) Ladder (2) Non-template control (3) Amplification *PCA3* gene with 2ng of cDNA as template and SybrGreen dye (4) Amplification of *PCA3* gene with 10ng of cDNA and SybrGreen dye (5) Amplification of *PCA3* gene with 50ng of cDNA and SybrGreen dye (6) Amplification of *PCA3* gene with 100ng of cDNA and SybrGreen dye (7) Amplification of *PCA3* gene with 500ng of cDNA and SybrGreen dye (8) Amplification of *PCA3* gene with 1000ng of cDNA and SybrGreen dye (9) Ladder.

Trough the comparation of the amplification bands with each intercalating agent it is noticeable that SybrGreen is the more appropriate intercalating agent, due to the absence of unspecific bands and primer dimer formation. The smear present at the condition of 1000ng of cDNA template might be caused due to excessive amount of template (**Figure 27B)**.

The RT-PCR amplifications for *SChLAP1* and *PCA3* genes were performed accordingly to the procedure described in **subsection *2.2.4.4***. The results are discussed as time threshold (in minutes) and not as cycle threshold, which is the conventional way to represent the RT-PCR results, in order to allow the comparation between PCR and LAMP reaction efficiencies, towards different template concentrations (**Figure 28**).

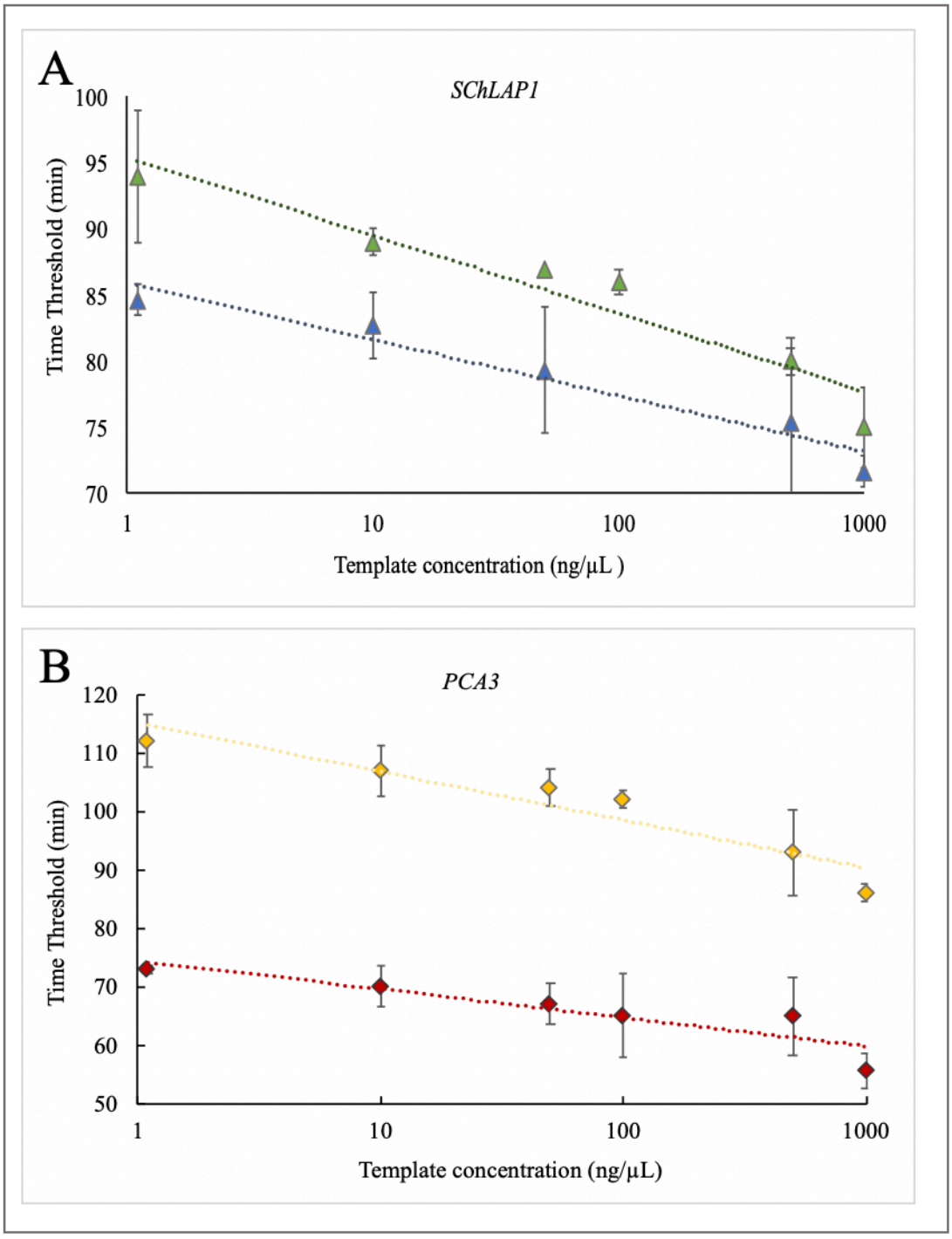

Figure 28. Time threshold of RT-PCR and RT-LAMP reactions for *SChLAP1* and *PCA3* genes for different template concentrations. The results presented are the mean of three independent experiments and the error bars presented are the standard deviation of three experiments performed (n=3). The template concentrations are represented in a logarithmic scale. **(A)** Time threshold in minutes of RT-PCR of *SChLAP1* gene (…▲…). The logarithmic trendline (……) has the an R^2=0.92. Time threshold in minutes of RT-LAMP of *SChLAP1* gene (…▲…). The logarithmic trendline (……) has an R^2=0.95. **(B)** Time threshold in minutes of RT-PCR of *PCA3* (…◆…) gene. The logarithmic trendline (……) has an R^2=0.90. Time threshold in minutes of RT-LAMP of *PCA3* gene (…◆…). The logarithmic trendline (……) has an R^2=0.81.

For both genes and amplification reactions, there is a clear correlation between target concentration and threshold time (**Figure 28**). *SChLAP1* gene presents a slight variation of the threshold time with template concentration (ΔT_T=19 minutes for RT-PCR and ΔT_T=13 minutes for RT-LAMP) in comparison to *PCA3* (ΔTt=26 minutes for RT-PCR and ΔT_T=17 minutes for RT-LAMP), indicating higher amplification efficiency of *SChLAP1* gene (see Annex, **Table A5**). Additionally, the robustness of the amplification of *SChLAP1* gene is also denoted by the logarithmic correlation R^2=0.92 and R^2=0.95 in comparison to R^2=0.90 and R^2=0.81 for *PCA3* gene RT-PCR and RT-LAMP reactions, respectively. Further analysis of amplification products was preformed via gel electrophoresis (see Annex, **Figure A7**). Also, LAMP reaction efficiency seems to be higher than the PCR counterpart, since there is a noticeable reduction in the ΔT_T, for both genes.

Successful LAMP amplification of *SChLAP1* and *PCA3* genes was achieved. The amplification reaction was further optimized for fluorescence based real-time monitorization, and a clear correlation between initial cDNA concentration and T_T was found. As such, it was possible to develop a quantitative method for cDNA amplification in real-time comparable to the standard RT-PCR. The developed LAMP reactions have shown slightly higher amplification efficiencies when compared to the gold standard RT-PCR. Also, a significant reduction in overall reaction time was achieved. To the best of our knowledge this is the first time that these target genes have been amplified and monitored in real-time via the LAMP amplification architecture. Furthermore, because LAMP has been applied to the quantification of cDNA target templates, the strategy here proposed can be easily extended to the monitorization of gene expression levels. Significant progress is still needed to integrate these reactions into the previously developed digital LAMP chip-based approach. Regardless the optimizations still required, this isothermal amplification method is compatible with the droplet-based digital LAMP approach and hence a suitable alternative to PCR counterpart.

4. CONCLUSION AND FURTHER PERSPECTIVES

The continuous developments in Biotechnology have put forward innovative powerful tools that may significantly contribute to improve the way we investigate and manage medical conditions. Particularly, novel genetic testing technologies have been developed, with the ultimate goal of providing suitable alternatives for point-of-care diagnosis. Most of these new sensing technologies still rely on PCR-based amplification methods, with concomitant costs in terms of time and money.

In the context of this thesis, it was intended to develop and optimize an integrated system for both isothermal amplification and quantitative assessment, that would allow the evaluation of biomarkers with particular relevance on prostate cancer diagnosis. Studies were conducted in order to analyze the compatibility of the components required for droplet generation with LAMP reaction. Overall, results demonstrate that amplification occurs without a significant difference in reaction kinetics when reagents for droplet generation are used. Further experiments assessed the incorporation of LAMP reaction into the droplets generated by vortex. Despite the capability to distinguish between positive and negative reactions, this vortex-based approach does not allow a straightforward quantitative assessment of template concentration. This is mostly due to the wide dispersion of droplets and absence of monolayer arrangement.

Taking into consideration that digital amplification methods require an equal distribution of the reaction mixture and the capability of the devices to allow the measurement of the totality of the droplets, a novel chip-based approach was attempted. The developed fabrication process and material used aids in circumventing the current limitations of design flexibility and extensive fabrication time, presented by the conventional microfluidics devices. In addition to the advantages of the fabrication process, this chip-based system also demonstrated the ability distinguish between different target concentrations as well as to properly quantify them.

The improvements conveyed by the chip design allowed the development and optimization of LAMP reactions for two prostate cancer biomarkers - *SChLAP1* or *PCA3*. The real-time fluorescence monitoring studies showed that both LAMP reactions allow amplification from as little as 1ng of cDNA with an overall reduction in time and slight improvement in the amplification efficiency than RT-qPCR.

Still, there is plenty of room for improvement, but the results herein presented seem to demonstrate that these reactions can be easily extended to the monitorization of gene expression levels. Implementation of these reactions into the developed chip-based system could constitute a suitable alternative to PCR. However, some aspects to enhance

the score assessment still require some further optimization. This might be achieved by assessing the impact of factors contributing to enhance the basal fluorescence of the droplets, such as size and primer-dimer formation.

Once these optimizations are in place, the performance of this platform ought to be assesses using clinical samples and compared to current techniques.

5. REFERENCES

Abd El Galil, K., El Sokkary, M., Kheira, S., Salazar, A., Yates, M., Chen, W. and Mulchandani, A. (2005). Real-Time Nucleic Acid Sequence-Based Amplification Assay for Detection of Hepatitis A Virus. *Applied and Environmental Microbiology*, 71(11), pp.7113-7116.

Ahmad, F., Seyrig, G., Tourlousse, D., Stedtfeld, R., Tiedje, J. and Hashsham, S. (2011). A CCD-based fluorescence imaging system for real-time loop-mediated isothermal amplification-based rapid and sensitive detection of waterborne pathogens on microchips. *Biomedical Microdevices*, 13(5), pp.929-937.

Ahrberg, C., Manz, A. and Chung, B. (2016). Polymerase chain reaction in microfluidic devices. *Lab on a Chip*, 16(20), pp.3866-3884.

An, L., Tang, W., Ranalli, T., Kim, H., Wytiaz, J. and Kong, H. (2005). Characterization of a Thermostable UvrD Helicase and Its Participation in Helicase-dependent Amplification. *Journal of Biological Chemistry*, 280(32), pp.28952-28958.

Aoi, Y., Hosogai, M. and Tsuneda, S. (2006). Real-time quantitative LAMP (loop-mediated isothermal amplification of DNA) as a simple method for monitoring ammonia-oxidizing bacteria. *Journal of Biotechnology*, 125(4), pp.484-491.

Barry, M. (2001). Prostate-Specific–Antigen Testing for Early Diagnosis of Prostate Cancer. *New England Journal of Medicine*, 344(18), pp.1373-1377.

Bray, F., Ferlay, J., Soerjomataram, I., Siegel, R., Torre, L. and Jemal, A. (2018). Global cancer statistics 2018: GLOBOCAN estimates of incidence and mortality worldwide for 36 cancers in 185 countries. *CA: A Cancer Journal for Clinicians*, 68(6), pp.394-424.

Burchill, S., Perebolte, L., Johnston, C., Top, B. and Selby, P. (2002). Comparison of the RNA-amplification based methods RT–PCR and NASBA for the detection of circulating tumour cells. *British Journal of Cancer*, 86(1), pp.102-109.

Cao, Y., Bontrager-Singer, J. and Zhu, L. (2015). A 3D microfluidic device fabrication method using thermopress bonding with multiple layers of polystyrene film. *Journal of Micromechanics and Microengineering*, 25(6), p.065005.

Casadio, V., Calistri, D., Salvi, S., Gunelli, R., Carretta, E., Amadori, D., Silvestrini, R. and Zoli, W. (2013). Urine Cell-Free DNA Integrity as a Marker for Early Prostate Cancer Diagnosis: A Pilot Study. *BioMed Research International*, 2013, pp.1-5.

Center, M., Jemal, A., Lortet-Tieulent, J., Ward, E., Ferlay, J., Brawley, O. and Bray, F. (2012). International Variation in Prostate Cancer Incidence and Mortality Rates. *European Urology*, 61(6), pp.1079-1092.

Chen, F., Zhao, Y., Fan, C. and Zhao, Y. (2015). Mismatch Extension of DNA Polymerases and High-Accuracy Single Nucleotide Polymorphism Diagnostics by Gold Nanoparticle-Improved Isothermal Amplification. *Analytical Chemistry*, 87(17), pp.8718-8723.

Cho, E., Yang, L., Levy, M. and Ellington, A. (2005). Using a Deoxyribozyme Ligase and Rolling Circle Amplification To Detect a Non-nucleic Acid Analyte, ATP. *Journal of the American Chemical Society*, 127(7), pp.2022-2023.

Choi, J., Liu, Z., Hu, J., Tang, R., Gong, Y., Feng, S., Ren, H., Wen, T., Yang, H., Qu, Z., Pingguan-Murphy, B. and Xu, F. (2016). Polydimethylsiloxane-Paper Hybrid Lateral Flow Assay for Highly Sensitive Point-of-Care Nucleic Acid Testing. *Analytical Chemistry*, 88(12), pp.6254-6264.

Chuang, T., Wei, S., Lee, S. and Lin, C. (2012). A polycarbonate based surface plasmon resonance sensing cartridge for high sensitivity HBV loop-mediated isothermal amplification. *Biosensors and Bioelectronics*, 32(1), pp.89-95.

Coburn, S., Bray, F., Sherman, M. and Trabert, B. (2017). International patterns and trends in ovarian cancer incidence, overall and by histologic subtype. *International Journal of Cancer*, 140(11), pp.2451-2460.

Compton, J. (1991). Nucleic acid sequence-based amplification. *Nature*, 350(6313), pp.91-92.

Connelly, J., Rolland, J. and Whitesides, G. (2015). “Paper Machine” for Molecular Diagnostics. *Analytical Chemistry*, 87(15), pp.7595-7601.

Consedine, N., Horton, D., Ungar, T., Joe, A., Ramirez, P. and Borrell, L. (2007). Fear, Knowledge, and Efficacy Beliefs Differentially Predict the Frequency of Digital Rectal Examination Versus Prostate Specific Antigen Screening in Ethnically Diverse Samples of Older Men. *American Journal of Men's Health*, 1(1), pp.29-43.

Corbisier, P., Pinheiro, L., Mazoua, S., Kortekaas, A., Chung, P., Gerganova, T., Roebben, G., Emons, H. and Emslie, K. (2015). DNA copy number concentration measured by digital and droplet digital quantitative PCR using certified reference materials. *Analytical and Bioanalytical Chemistry*, 407(7), pp.1831-1840.

Craw, P. and Balachandran, W. (2012). Isothermal nucleic acid amplification technologies for point-of-care diagnostics: a critical review. *Lab on a Chip*, 12(14), p.2469.

Cui, Y., Feng, X., Wang, Y., Pan, H., Pan, H. and Kong, D. (2019). An integrated-molecular-beacon based multiple exponential strand displacement amplification strategy for ultrasensitive detection of DNA methyltransferase activity. *Chemical Science*, 10(8), pp.2290-2297.

Dalton, W. (2006). Cancer Biomarkers--An Invitation to the Table. *Science*, 312(5777), pp.1165-1168.

Dean, F. (2001). Rapid Amplification of Plasmid and Phage DNA Using Phi29 DNA Polymerase and Multiply-Primed Rolling Circle Amplification. *Genome Research*, 11(6), pp.1095-1099.

Demidov, V. (2002). Rolling-circle amplification in DNA diagnostics: the power of simplicity. *Expert Review of Molecular Diagnostics*, 2(6), pp.542-548.

Derrien, T., Johnson, R., Bussotti, G., Tanzer, A., Djebali, S., Tilgner, H., Guernec, G., Martin, D., Merkel, A., Knowles, D., Lagarde, J., Veeravalli, L., Ruan, X., Ruan, Y., Lassmann, T., Carninci, P., Brown, J., Lipovich, L., Gonzalez, J., Thomas, M., Davis, C., Shiekhattar, R., Gingeras, T., Hubbard, T., Notredame, C., Harrow, J. and Guigo, R. (2012). The GENCODE v7 catalog of human long noncoding RNAs: Analysis of their gene structure, evolution, and expression. *Genome Research*, 22(9), pp.1775-1789.

Du, W., Li, L., Nichols, K. and Ismagilov, R. (2009). SlipChip. *Lab on a Chip*, 9(16), p.2286.

Eisenstein, M. (2005). Breaking the silence. *Nature Methods*, 2(2), pp.90-90.

Epstein, J. (2010). An Update of the Gleason Grading System. *Journal of Urology*, 183(2), pp.433-440.

Etzioni, R. (2002). Overdiagnosis Due to Prostate-Specific Antigen Screening: Lessons From U.S. Prostate Cancer Incidence Trends. *CancerSpectrum Knowledge Environment*, 94(13), pp.981-990.

Fagerberg, L., Hallström, B., Oksvold, P., Kampf, C., Djureinovic, D., Odeberg, J *et al*., (2014). Analysis of the Human Tissue-specific Expression by Genome-wide Integration of Transcriptomics and Antibody-based Proteomics. *Molecular & Cellular Proteomics*, 13(2), pp.397-406.

Fan, F., Du, P., Kan, B. and Yan, M. (2015). The Development and Evaluation of a Loop-Mediated Isothermal Amplification Method for the Rapid Detection of Salmonella enterica serovar Typhi. *PLOS ONE*, 10(4), p.e0124507.

Fang, X., Chen, H., Yu, S., Jiang, X. and Kong, J. (2011). Predicting Viruses Accurately by a Multiplex Microfluidic Loop-Mediated Isothermal Amplification Chip. *Analytical Chemistry*, 83(3), pp.690-695.

Filella, X. and Foj, L. (2016). Prostate Cancer Detection and Prognosis: From Prostate Specific Antigen (PSA) to Exosomal Biomarkers. *International Journal of Molecular Sciences*, 17(11), p.1784.

Fire, A. and Xu, S. (1995). Rolling replication of short DNA circles. *Proceedings of the National Academy of Sciences*, 92(10), pp.4641-4645.

Francesko, A., Cardoso, V. and Lanceros-Méndez, S. (2019). Lab-on-a-chip technology and microfluidics. *Microfluidics for Pharmaceutical Applications*, pp.3-36.

Gansen, A., Herrick, A., Dimov, I., Lee, L. and Chiu, D. (2012). Digital LAMP in a sample self-digitization (SD) chip. *Lab on a Chip*, 12(12), p.2247.

Gene-quantification.de. (2019). [online] Available at: https://www.gene-quantification.de/bio-rad-ddpcr-app-guide-6407.pdf [Accessed 1 Sep. 2019].

Gill, P., Amini, M., Ghaemi, A., Shokouhizadeh, L., Abdul-Tehrani, H., Karami, A. and Gilak, A. (2007). Detection of Helicobacter pylori by enzyme-linked immunosorbent assay of thermophilic helicase-dependent isothermal DNA amplification. *Diagnostic Microbiology and Infectious Disease*, 59(3), pp.243-249.

Gill, P., Ramezani, R., Amiri, M., Ghaemi, A., Hashempour, T., Eshraghi, N., Ghalami, M. and Tehrani, H. (2006). Enzyme-linked immunosorbent assay of nucleic acid sequence-based amplification for molecular detection of M. tuberculosis. *Biochemical and Biophysical Research Communications*, 347(4), pp.1151-1157.

Ginocchio, C., Kemper, M., Stellrecht, K. and Witt, D. (2003). Multicenter Evaluation of the Performance Characteristics of the NucliSens HIV-1 QT Assay Used for Quantitation of Human Immunodeficiency Virus Type 1 RNA. *Journal of Clinical Microbiology*, 41(1), pp.164-173.

Giuffrida, M. and Spoto, G. (2017). Integration of isothermal amplification methods in microfluidic devices: Recent advances. *Biosensors and Bioelectronics*, 90, pp.174-186.

Gleason, D. and Mellinger, G. (1974). Prediction of Prognosis for Prostatic Adenocarcinoma by Combined Histological Grading and Clinical Staging. *Journal of Urology*, 111(1), pp.58-64.

Gong, C. and Maquat, L. (2011). lncRNAs transactivate STAU1-mediated mRNA decay by duplexing with 3′ UTRs via Alu elements. *Nature*, 470(7333), pp.284-288.

Grosso, P., Carrara, S., Stagni, C. and Benini, L. (2010). Cancer marker detection in human serum with a point-of-care low-cost system. *Sensors and Actuators B: Chemical*, 147(2), pp.475-480.

Hanahan, D. and Weinberg, R. (2011). Hallmarks of Cancer: The Next Generation. *Cell*, 144(5), pp.646-674.

Helming, K., Wang, X., Wilson, B., Vazquez, F., Haswell, J., Manchester, H., Kim, Y., Kryukov, G., Ghandi, M., Aguirre, A., Jagani, Z., Wang, Z., Garraway, L., Hahn, W. and Roberts, C. (2014). ARID1B is a specific vulnerability in ARID1A-mutant cancers. *Nature Medicine*, 20(3), pp.251-254.

Hiltunen, J., Liedert, C., Hiltunen, M., Huttunen, O., Hiitola-Keinänen, J., Aikio, S., Harjanne, M., Kurkinen, M., Hakalahti, L. and Lee, L. (2018). Roll-to-roll fabrication of integrated PDMS–paper microfluidics for nucleic acid amplification. *Lab on a Chip*, 18(11), pp.1552-1559.

Hoffman, R. (2011). Screening for Prostate Cancer. *New England Journal of Medicine*, 365(21), pp.2013-2019.

Hong, M., Zha, L., Fu, W., Zou, M., Li, W. and Xu, D. (2011). A modified visual loop-mediated isothermal amplification method for diagnosis and differentiation of main pathogens from Mycobacterium tuberculosis complex. *World Journal of Microbiology and Biotechnology*, 28(2), pp.523-531.

Hsieh, K., Patterson, A., Ferguson, B., Plaxco, K. and Soh, H. (2012). Rapid, Sensitive, and Quantitative Detection of Pathogenic DNA at the Point of Care through Microfluidic Electrochemical Quantitative Loop-Mediated Isothermal Amplification. *Angewandte Chemie*, 124(20), pp.4980-4984.

Humphrey, P. (2004). Gleason grading and prognostic factors in carcinoma of the prostate. *Modern Pathology*, 17(3), pp.292-306.

Ilic, D., Djulbegovic, M., Jung, J., Hwang, E., Zhou, Q., Cleves, A., Agoritsas, T. and Dahm, P. (2018). Prostate cancer screening with prostate-specific antigen (PSA) test: a systematic review and meta-analysis. *BMJ*, p.k3519.

Jung, M. (2004). Re: Hessels D, Klein Gunnewiek JMT, van Oort I, Karthaus HFM, van Leenders GJL, van Balken B, Kiemeney LA, Witjes JA, Schalken JA. DD3PCA3-based molecular urine analysis for the diagnosis of prostate cancer. Eur Urol 2003;44:8?16. *European Urology*, 46(2), pp.271-272.

Khater, A., Mohammadi, M., Mohamad, A. and Nezhad, A. (2019). Dynamics of temperature-actuated droplets within microfluidics. *Scientific Reports*, 9(1).

Kiddle, G., Hardinge, P., Buttigieg, N., Gandelman, O., Pereira, C., McElgunn, C., Rizzoli, M., Jackson, R., Appleton, N., Moore, C., Tisi, L. and Murray, J. (2012). GMO detection using a bioluminescent real time reporter (BART) of loop mediated isothermal amplification (LAMP) suitable for field use. *BMC Biotechnology*, 12(1).

Klein, D. (2002). Quantification using real-time PCR technology: applications and limitations. Trends in Molecular Medicine, 8(6), pp.257-260.

Kolluri, N., Klapperich, C. and Cabodi, M. (2018). Towards lab-on-a-chip diagnostics for malaria elimination. *Lab on a Chip*, 18(1), pp.75-94.

Kopp, M. (1998). Chemical Amplification: Continuous-Flow PCR on a Chip. *Science*, 280(5366), pp.1046-1048.

Kumar-Sinha, C. and Chinnaiyan, A. (2018). Precision oncology in the age of integrative genomics. Nature Biotechnology, 36(1), pp.46-60.

Le, T., Nguyen, N., Truong, N. and De, N. (2012). Development of Mitochondrial Loop-Mediated Isothermal Amplification for Detection of the Small Liver Fluke Opisthorchis viverrini (Opisthorchiidae; Trematoda; Platyhelminthes). *Journal of Clinical Microbiology*, 50(4), pp.1178-1184.

Lee, J. (2009). Lessons from X-chromosome inactivation: long ncRNA as guides and tethers to the epigenome. *Genes & Development*, 23(16), pp.1831-1842.

Lee, M., Chen, Y. and Peng, C. (2009). Evaluation of reverse transcription loop-mediated isothermal amplification in conjunction with ELISA–hybridization assay for molecular detection of Mycobacterium tuberculosis. *Journal of Microbiological Methods*, 76(2), pp.174-180.

Li, H., Fan, Y., Kodzius, R. and Foulds, I. (2011). Fabrication of polystyrene microfluidic devices using a pulsed CO2 laser system. *Microsystem Technologies*, 18(3), pp.373-379.

Li, J. and Macdonald, J. (2015). *Advances in isothermal amplification: novel strategies inspired by biological processes,* 64(1), pp. 196-211.

Li, Y., Luo, H., Xiao, N., Duan, J., Wang, Z. and Wang, S. (2018). Long Noncoding RNA SChLAP1 Accelerates the Proliferation and Metastasis of Prostate Cancer via Targeting miR-198 and Promoting the MAPK1 Pathway. *Oncology Research Featuring Preclinical and Clinical Cancer Therapeutics*, 26(1), pp.131-143.

Liu, C., Geva, E., Mauk, M., Qiu, X., Abrams, W., Malamud, D., Curtis, K., Owen, S. and Bau, H. (2011). An isothermal amplification reactor with an integrated isolation membrane for point-of-care detection of infectious diseases. *The Analyst*, 136(10), p.2069.

Lo, W. and Baeumner, A. (2007). Evaluation of Internal Standards in a Competitive Nucleic Acid Sequence-Based Amplification Assay. *Analytical Chemistry*, 79(4), pp.1386-1392.

Lucchi, N., Gaye, M., Diallo, M., Goldman, I., Ljolje, D., Deme, A., Badiane, A., Ndiaye, Y., Barnwell, J., Udhayakumar, V. and Ndiaye, D. (2016). Evaluation of the Illumigene Malaria LAMP: A Robust Molecular Diagnostic Tool for Malaria Parasites. *Scientific Reports*, 6(1) pp.3037-3045.

Mao, F., Leung, W. and Xin, X. (2007). Characterization of EvaGreen and the implication of its physicochemical properties for qPCR applications. *BMC Biotechnology*, 7(1), p.76.

Marin-Muller, C., Li, D., Bharadwaj, U., Li, M., Chen, C., Hodges, S., Fisher, W., Mo, Q., Hung, M. and Yao, Q. (2013). A Tumorigenic Factor Interactome Connected through Tumor Suppressor MicroRNA-198 in Human Pancreatic Cancer. *Clinical Cancer Research*, 19(21), pp.5901-5913.

Martignano, F., Rossi, L., Maugeri, A., Gallà, V., Conteduca, V., De Giorgi, U., Casadio, V. and Schepisi, G. (2017). Urinary RNA-based biomarkers for prostate cancer detection. *Clinica Chimica Acta*, 473, pp.96-105.

Martzy, R., Kolm, C., Brunner, K., Mach, R., Krska, R., Šinkovec, H., Sommer, R., Farnleitner, A. and Reischer, G. (2017). A loop-mediated isothermal amplification (LAMP) assay for the rapid detection of Enterococcus spp. in water. *Water Research*, 122, pp.62-69.

Mori, Y. and Notomi, T. (2009). Loop-mediated isothermal amplification (LAMP): a rapid, accurate, and cost-effective diagnostic method for infectious diseases. *Journal of Infection and Chemotherapy*, 15(2), pp.62-69.

Mullis, K., Faloona, F., Scharf, S., Saiki, R., Horn, G. and Erlich, H. (1987). Specific Enzymatic Amplification of DNA In Vitro: The Polymerase Chain Reaction. *Cold Spring Harbor Symposia on Quantitative Biology*, 51(0), pp.263-273.

Nakanishi, H., Groskopf, J., Fritsche, H., Bhadkamkar, V., Blase, A., Kumar, S., Davis, J., Troncoso, P., Rittenhouse, H. and Babaian, R. (2008). PCA3 Molecular Urine Assay Correlates With Prostate Cancer Tumor Volume: Implication in Selecting Candidates for Active Surveillance. *Journal of Urology*, 179(5), pp.1804-1810.

Nayak, N., Lam, Y., Yue, C. and Sinha, A. (2008). CO2-laser micromachining of PMMA: the effect of polymer molecular weight. *Journal of Micromechanics and Microengineering*, 18(9), p.095020.

Nguyen, N., Ting, T., Yap, Y., Wong, T., Chai, J., Ong, W., Zhou, J., Tan, S. and Yobas, L. (2007). Thermally mediated droplet formation in microchannels. *Applied Physics Letters*, 91(8), p.084102.

Notomi, T. (2000). Loop-mediated isothermal amplification of DNA. *Nucleic Acids Research*, 28(12), pp.63e-63.

Omran, A. (2005). The Epidemiologic Transition: A Theory of the Epidemiology of Population Change. *Milbank Quarterly*, 83(4), pp.731-757.

Pardy, T., Tulp, I., Kremer, C., Rang, T. and Stewart, R. (2017). Integrated self-regulating resistive heating for isothermal nucleic acid amplification tests (NAAT) in Lab-on-a-Chip (LoC) devices. *PLOS ONE*, 12(12), p.e0189968.

Park, B., Oh, S., Jung, J., Choi, G., Seo, J., Kim, D., Lee, E. and Seo, T. (2017). An integrated rotary microfluidic system with DNA extraction, loop-mediated isothermal amplification, and lateral flow strip based detection for point-of-care pathogen diagnostics. *Biosensors and Bioelectronics*, 91, pp.334-340.

Pekin, D., Skhiri, Y., Baret, J., Le Corre, D., Mazutis, L., Ben Salem, C., Millot, F., El Harrak, A., Hutchison, J., Larson, J., Link, D., Laurent-Puig, P., Griffiths, A. and Taly, V. (2011). Quantitative and sensitive detection of rare mutations using droplet-based microfluidics. *Lab on a Chip*, 11(13), p.2156.

Pernar, C., Ebot, E., Wilson, K. and Mucci, L. (2018). The Epidemiology of Prostate Cancer. *Cold Spring Harbor Perspectives in Medicine*, 8(12), p.a030361.

Piepenburg, O., Williams, C., Stemple, D. and Armes, N. (2006). DNA Detection Using Recombination Proteins. *PLoS Biology*, 4(7), p.e204.

Pierorazio, P., Walsh, P., Partin, A. and Epstein, J. (2013). Prognostic Gleason grade grouping: data based on the modified Gleason scoring system. *BJU International*, 111(5), pp.753-760.

Prensner, J. and Chinnaiyan, A. (2011). The Emergence of lncRNAs in Cancer Biology. *Cancer Discovery*, 1(5), pp.391-407.

Prensner, J., Iyer, M., Sahu, A., Asangani, I., Cao, Q., Patel, L., Vergara, I *et al*., (2013). The long noncoding RNA SChLAP1 promotes aggressive prostate cancer and antagonizes the SWI/SNF complex. *Nature Genetics*, 45(11), pp.1392-1398.

Raja, N., Russell, C. and George, A. (2019). *Urinary markers aiding in the detection and risk stratification of prostate cancer*, 7(4), pp.436-442.

Rane, T., Chen, L., Zec, H. and Wang, T. (2015). Microfluidic continuous flow digital loop-mediated isothermal amplification (LAMP). *Lab on a Chip*, 15(3), pp.776-782.

Ravi, N., Rizzi, G., Chang, S., Cheung, P., Utz, P. and Wang, S. (2019). Quantification of cDNA on GMR biosensor array towards point-of-care gene expression analysis. *Biosensors and Bioelectronics*, 130(1), pp.338-343.

Ridley, R., White, J., McAleese, S., Goman, M., Alano, P., de Vries, E. and Kilbey, B. (1991). DNA polymerase δ: gene sequences fromPlasmodium falciparumindicate that this enzyme is more highly conserved than DNA polymerase α. *Nucleic Acids Research*, 19(24), pp.6731-6736.

Rinn, J., Kertesz, M., Wang, J., Squazzo, S., Xu, X., Brugmann, S., Goodnough, L., Helms, J., Farnham, P., Segal, E. and Chang, H. (2007). Functional Demarcation of Active and Silent Chromatin Domains in Human HOX Loci by Noncoding RNAs. *Cell*, 129(7), pp.1311-1323.

Ríos, Á., Zougagh, M. and Avila, M. (2012). Miniaturization through lab-on-a-chip: Utopia or reality for routine laboratories? A review. *Analytica Chimica Acta*, 740(1), pp.1-11.

Roberts, C. and Orkin, S. (2004). The SWI/SNF complex — chromatin and cancer. *Nature Reviews Cancer*, 4(2), pp.133-142.

Rusling, J., Kumar, C., Gutkind, J. and Patel, V. (2010). Measurement of biomarker proteins for point-of-care early detection and monitoring of cancer. *The Analyst*, 135(10), p.2496.

Ruzycka, M., Cimpan, M., Rios-Mondragon, I. and Grudzinski, I. (2019). Microfluidics for studying metastatic patterns of lung cancer. *Journal of Nanobiotechnology*, 17(1), p.71.

Sadtler, V., Imbert, P. and Dellacherie, E. (2002). Ostwald Ripening of Oil-in-Water Emulsions Stabilized by Phenoxy-Substituted Dextrans. *Journal of Colloid and Interface Science*, 254(2), pp.355-361.

Salvi, S., Gurioli, G., Martignano, F., Foca, F., Gunelli, R., Cicchetti, G., De Giorgi, U., Zoli, W., Calistri, D. and Casadio, V. (2015). Urine Cell-Free DNA Integrity Analysis for Early Detection of Prostate Cancer Patients. *Disease Markers*, 2015, pp.1-6.

Sandbhor Gaikwad, P. and Banerjee, R. (2018). Advances in point-of-care diagnostic devices in cancers. *The Analyst*, 143(6), pp.1326-1348.

Sanders, R., Huggett, J., Bushell, C., Cowen, S., Scott, D. and Foy, C. (2011). Evaluation of Digital PCR for Absolute DNA Quantification. *Analytical Chemistry*, 83(17), pp.6474-6484.

Sayad, A., Ibrahim, F., Mukim Uddin, S., Cho, J., Madou, M. and Thong, K. (2018). A microdevice for rapid, monoplex and colorimetric detection of foodborne pathogens using a centrifugal microfluidic platform. *Biosensors and Bioelectronics*, 100, pp.96-104.

Sayad, A., Ibrahim, F., Uddin, S., Pei, K., Mohktar, M., Madou, M. and Thong, K. (2016). A microfluidic lab-on-a-disc integrated loop mediated isothermal amplification for foodborne pathogen detection. *Sensors and Actuators B: Chemical*, 227, pp.600-609.

Schalken, J., Hessels, D. and Verhaegh, G. (2003). New targets for therapy in prostate cancer: differential display code 3 (DD3PCA3), a highly prostate cancer–specific gene. *Urology*, 62(5), pp.34-43.

Schuler, F., Siber, C., Hin, S., Wadle, S., Paust, N., Zengerle, R. and von Stetten, F. (2016). Digital droplet LAMP as a microfluidic app on standard laboratory devices. *Analytical Methods*, 8(13), pp.2750-2755.

Shan, X., Zhang, Y., Zhang, Z., Chen, M., Su, Y., Yuan, Y., Alam, M., Yan, H. and Shi, L. (2012). Rapid detection of food-borne Listeria monocytogenes by real-time quantitative loop-mediated isothermal amplification. *Food Science and Biotechnology*, 21(1), pp.101-106.

Shao, K., Ding, W., Wang, F., Li, H., Ma, D. and Wang, H. (2011). Emulsion PCR: A High Efficient Way of PCR Amplification of Random DNA Libraries in Aptamer Selection. *PLoS ONE*, 6(9), p.e24910.

Shapiro, C. (2018). Cancer Survivorship. *New England Journal of Medicine*, 379(25), pp.2438-2450.

Shen, F., Davydova, E., Du, W., Kreutz, J., Piepenburg, O. and Ismagilov, R. (2011). Digital Isothermal Quantification of Nucleic Acids via Simultaneous Chemical Initiation of Recombinase Polymerase Amplification Reactions on SlipChip. *Analytical Chemistry*, 83(9), pp.3533-3540.

Song, J., Mauk, M., Hackett, B., Cherry, S., Bau, H. and Liu, C. (2016). Instrument-Free Point-of-Care Molecular Detection of Zika Virus. *Analytical Chemistry*, 88(14), pp.7289-7294.

Sontti, S. and Atta, A. (2019). Numerical Insights on Controlled Droplet Formation in a Microfluidic Flow-Focusing Device. *Industrial & Engineering Chemistry Research,* 17(71), pp.4210-4226.

Sreejith, K., Ooi, C., Jin, J., Dao, D. and Nguyen, N. (2018). Digital polymerase chain reaction technology – recent advances and future perspectives. *Lab on a Chip*, 18(24), pp.3717-3732.

Suebsing, R., Prombun, P., Srisala, J. and Kiatpathomchai, W. (2013). Loop-mediated isothermal amplification combined with colorimetric nanogold for detection of the microsporidianEnterocytozoon hepatopenaeiin penaeid shrimp. *Journal of Applied Microbiology*, 114(5), pp.1254-1263.

Tawfik, D. and Griffiths, A. (1998). Man-made cell-like compartments for molecular evolution. *Nature Biotechnology*, 16(7), pp.652-656.

Tomlins, S. (2014). Urine PCA3 and TMPRSS2:ERG Using Cancer-specific Markers to Detect Cancer. *European Urology*, 65(3), pp.543-545.

Toumazou, C., Shepherd, L., Reed, S., Chen, G., Patel, A., Garner, D., Wang, C., Ou, C., Amin-Desai, K., Athanasiou, P., Bai, H., Brizido, I., Caldwell, B., Coomber-Alford, D., Georgiou, P., Jordan, K., Joyce, J., La Mura, M., Morley, D., Sathyavruthan, S., Temelso, S., Thomas, R. and Zhang, L. (2013). Simultaneous DNA amplification and detection using a pH-sensing semiconductor system. *Nature Methods*, 10(7), pp.641-646.

Van Gemen, B., van Beuningen, R., Nabbe, A., van Strijp, D., Jurriaans, S., Lens, P. and Kievits, T. (1994). A one-tube quantitative HIV-1 RNA NASBA nucleic acid amplification assay using electrochemiluminescent (ECL) labelled probes. *Journal of Virological Methods*, 49(2), pp.157-167.

Vashist, S., Luppa, P., Yeo, L., Ozcan, A. and Luong, J. (2015). Emerging Technologies for Next-Generation Point-of-Care Testing. *Trends in Biotechnology*, 33(11), pp.692-705.

Veigas, B., Branquinho, R., Pinto, J., Wojcik, P., Martins, R., Fortunato, E. and Baptista, P. (2014). Ion sensing (EIS) real-time quantitative monitorization of isothermal DNA amplification. *Biosensors and Bioelectronics*, 52(1), pp.50-55.

Vincent, M., Xu, Y. and Kong, H. (2004). Helicase-dependent isothermal DNA amplification. *EMBO reports*, 5(8), pp.795-800.

Vogelstein, B. and Kinzler, K. (1999). Digital PCR. *Proceedings of the National Academy of Sciences*, 96(16), pp.9236-9241.

Walker, G., Fraiser, M., Schram, J., Little, M., Nadeau, J. and Malinowski, D. (1992). Strand displacement amplification—an isothermal,in vitroDNA amplification technique. *Nucleic Acids Research*, 20(7), pp.1691-1696.

Wang, C., Lien, K., Wang, T., Chen, T. and Lee, G. (2011a). An integrated microfluidic loop-mediated-isothermal-amplification system for rapid sample pre-treatment and detection of viruses. *Biosensors and Bioelectronics*, 26(5), pp.2045-2052.

Wang, C., Lien, K., Wu, J. and Lee, G. (2011). A magnetic bead-based assay for the rapid detection of methicillin-resistant Staphylococcus aureus by using a microfluidic system with integrated loop-mediated isothermal amplification. *Lab on a Chip*, 11(8), p.1521.

Wang, J., Lu, P., Yan, J., Zhang, Y., Huang, L., Ali, Z., Liu, B., Li, Z. and He, N. (2016). Rapid and Sensitive Detection of RNA Viruses Based on Reverse Transcription Loop-Mediated Isothermal Amplification, Magnetic Nanoparticles, and Chemiluminescence. *Journal of Biomedical Nanotechnology*, 12(4), pp.710-716.

Wang, Y., Balowski, J., Phillips, C., Phillips, R., Sims, C. and Allbritton, N. (2011). Benchtop micromolding of polystyrene by soft lithography. *Lab on a Chip*, 11(18), p.3089.

Widschwendter, M., Jones, A., Evans, I., Reisel, D., Dillner, J., Sundström, K., Steyerberg, E., Vergouwe, Y., Wegwarth, O., Rebitschek, F., Siebert, U., Sroczynski, G., de Beaufort, I., Bolt, I., Cibula, D., Zikan, M., Bjørge, L., Colombo, N., Harbeck, N., Dudbridge, F., Tasse, A., Knoppers, B., Joly, Y., Teschendorff, A. and Pashayan, N. (2018). Epigenome-based cancer risk prediction: rationale, opportunities and challenges. *Nature Reviews Clinical Oncology*, 15(5), pp.292-309.

Winstel, V., Xia, G. and Peschel, A. (2014). Pathways and roles of wall teichoic acid glycosylation in Staphylococcus aureus. *International Journal of Medical Microbiology*, 304(3-4), pp.215-221.

Wong, Y., Othman, S., Lau, Y., Radu, S. and Chee, H. (2018). Loop-mediated isothermal amplification (LAMP): a versatile technique for detection of micro-organisms. *Journal of Applied Microbiology*, 124(3), pp.626-643.

World Health Organization. (2019). *Global Health Observatory (GHO) data*. [online] Available at: https://www.who.int/gho/en/ [Accessed 1 Sep. 2019].

Xu, J., Li, S., Tan, J., Wang, Y. and Luo, G. (2006). Preparation of highly monodisperse droplet in a T-junction microfluidic device. *AIChE Journal*, 52(9), pp.3005-3010.

Yang, Y., Weng, C., Ho, C. and Yen, G. (2009). Resveratrol analog-3,5,4′-trimethoxy-trans-stilbene inhibits invasion of human lung adenocarcinoma cells by suppressing the MAPK pathway and decreasing matrix metalloproteinase-2 expression. *Molecular Nutrition & Food Research*, 53(3), pp.407-416.

Yi, M., Ling, L., Neogi, S., Fan, Y., Tang, D., Yamasaki, S., Shi, L. and Ye, L. (2014). Real time loop-mediated isothermal amplification using a portable fluorescence scanner for rapid and simple detection of Vibrio parahaemolyticus. *Food Control*, 41(1), pp.91-95.

Yin, J., Suo, Y., Zou, Z., Sun, J., Zhang, S., Wang, B., Xu, Y., Darland, D., Zhao, J. and Mu, Y. (2019). Integrated microfluidic systems with sample preparation and nucleic acid amplification. Lab on a Chip, 19(17), pp.2769-2785.

Yuan, D., Kong, J., Li, X., Fang, X. and Chen, Q. (2018). Colorimetric LAMP microfluidic chip for detecting three allergens: peanut, sesame and soybean. *Scientific Reports*, 8(1), pp.1005-1012.

Zanoli, L. and Spoto, G. (2012). Isothermal Amplification Methods for the Detection of Nucleic Acids in Microfluidic Devices. *Biosensors*, 3(1), pp.18-43.

Zhang, C., Xu, J., Ma, W. and Zheng, W. (2006). PCR microfluidic devices for DNA amplification. *Biotechnology Advances*, 24(3), pp.243-284.

Zhang, H., Xu, Y., Fohlerova, Z., Chang, H., Iliescu, C. and Neuzil, P. (2019). LAMP-on-a-chip: Revising microfluidic platforms for loop-mediated DNA amplification. *TrAC Trends in Analytical Chemistry*, 113, pp.44-53.

Zhang, L., Zhang, Y., Wang, C., Feng, Q., Fan, F., Zhang, G., Kang, X., Qin, X., Sun, J., Li, Y. and Jiang, X. (2014). Integrated Microcapillary for Sample-to-Answer

Nucleic Acid Pretreatment, Amplification, and Detection. *Analytical Chemistry*, 86(20), pp.10461-10466.

Zhang, X., Lowe, S. and Gooding, J. (2014). Brief review of monitoring methods for loop-mediated isothermal amplification (LAMP). *Biosensors and Bioelectronics*, 61(1), pp.491-499.

Zhang, Y. and Ozdemir, P. (2009). Microfluidic DNA amplification—A review. *Analytica Chimica Acta*, 638(2), pp.115-125.

Zhao, S., Prensner, J., Erho, N., Ghadessi, M., Yousefi, K., Wellman, H., Mehra, R., Den, R., Dicker, A., Klein, E., Jenkins, R., Chinnaiyan, A., Davicioni, E. and Feng, F. (2014). Identification and Validation of the Long Noncoding RNA SChLAP1 as a Prognostic Biomarker in Prostate Cancer. *International Journal of Radiation Oncology*Biology*Physics*, 90(1), p.S2.

Zhao, Y., Chen, F., Li, Q., Wang, L. and Fan, C. (2015). Isothermal Amplification of Nucleic Acids. *Chemical Reviews*, 115(22), pp.12491-12545.

Zhou, C., Check, D., Lortet-Tieulent, J., Laversanne, M., Jemal, A., Ferlay, J., Bray, F., Cook, M. and Devesa, S. (2015). Prostate cancer incidence in 43 populations worldwide: An analysis of time trends overall and by age group. *International Journal of Cancer*, 138(6), pp.1388-1400.

Zhu, G., Yang, K. and Zhang, C. (2013). Sensitive detection of methylated DNA using the short linear quencher–fluorophore probe and two-stage isothermal amplification assay. *Biosensors and Bioelectronics*, 49(1), pp.170-175.

Zhu, P. and Wang, L. (2017). Passive and active droplet generation with microfluidics: a review. *Lab on a Chip*, 17(1), pp.34-75.

Zhu, Q., Gao, Y., Yu, B., Ren, H., Qiu, L., Han, S., Jin, W., Jin, Q. and Mu, Y. (2012). Self-priming compartmentalization digital LAMP for point-of-care. *Lab on a Chip*, 12(22), p.4755.

Ziros, P., Kokkinos, P., Allard, A. and Vantarakis, A. (2015). Development and Evaluation of a Loop-Mediated Isothermal Amplification Assay for the Detection of Adenovirus 40 and 41. *Food and Environmental Virology*, 7(3), pp.276-285.

6. ANNEX

Table A1. Summary of the properties of important isothermal amplification methods in comparison with PCR.

Property	PCR	NASBA	SDA	RCA	HDA	RPA	LAMP
Required enzymes	1 (*Taq* polymerase)	2 or 3 (Reverse transcriptase and RNA polymerase, RNase H)	2 (DNA polymerase and NEase)	2 (Ligase, DNA polymerase)	2 (DNA polymerase, helicase)	2 (DNA polymerase and recombinase)	1 (DNA polymerase)
Primers	2	2	2 or 4	2	2	2	4 or 6
Primer design	Simple	Simple	Complex	Simple	Simple	Simple	Complex
Temperature (°C)	3 different temperature: (95, 50 – 65, 72) °C	Isothermal ~41°C	Isothermal 37°C	Isothermal 60°C	Isothermal 37 – 65°C	Isothermal 37 – 42 °C	Isothermal 60 – 65°C
Reaction time (h)	2 - 3 h	1.5 – 2 h	2 h	1.5 h	0.5 – 2 h	0.5 – 1.5 h	<1 h
Target	DNA and RNA	RNA (DNA)	DNA	DNA (RNA)	DNA	DNA	DNA and RNA
Amplicon	dsDNA	RNA, DNA	dsDNA	Circular DNA	dsDNA	dsDNA	Concatenated DNA
Efficiency	2^{30} - fold in 2 to 3 hours	10^6–10^9	10^7	10^9	10^7	10^4 in 10 min	10^9
Product detection method	Gel electrophoresis, Real-time and ELISA	Gel electrophoresis, Real-time and ELISA, ECL	Gel electrophoresis, Real-time	Gel electrophoresis, Real-time	Gel electrophoresis, Real-time and ELISA	Gel electrophoresis, Real-time and ELISA	Gel electrophoresis, Real-time and turbidity
Tolerance to biological components	-	-	-	-	+		+
Need to template denaturation	+	+	+	-	-	-	-
Denaturing agents	Heat	RNase H	Restriction enzymes	Strand-displacement property of ϕ29 DNA polymerase	Helicase	Recombinase	Strand-displacement property of *Bst* polymerase

Table A2. LAMP-on-a-chip variants and their characteristics.

Technique	Target	Type of target	Nr of targets	Pre-treatment	Sample movement	Heating	Detection method	LOD	Ref
Microfluidic	Methicillin-resistant *Staphylococcus aureus*	DNA	1	On chip	Vacuum pump off chip	Heater on chip	Spectrophotometer	10 fg/μL	Wang *et al.*, 2011
	Foodborne pathogen	DNA	1	On chip	Centrifugal force on chip	Hot air gun off chip	Visual	5 fg/μL	Sayad *et al.*, 2016
	Three influenza A subtypes	DNA	3	Off chip	Capillary force on chip	Heater off chip	Optical sensor	10 copies/μL	Fang *et al.*, 2011
	invA gene from *S. Typhimurium*, toxR gene from *V. parahaemolyticus*	DNA	2	On chip	Centrifugal force on chip	Heater off chip	Lateral flow strip	50 CFUs	Park *et al.*, 2017
	Nervous necrosis virus	RNA	1	On chip	Pneumatic pump on chip	Micro heater on chip	Electrophoresis	Not defined	Wang *et al.*, 2011a
	Zika virus	RNA	1	On chip	Silica membrane on chip	Chemically exothermic reaction on chip	Visual	Not defined	Song *et al.*, 2016
Paper-based	**Target**	**Type of target**	**Gene**	**Pre-treatment**	**Material**	**Heating**	**Detection method**	**LOD**	**REF**
	HIV virus	RNA	1	On chip	FTA	Thin film heater on chip	Optical sensor	< 10 HIV particles	Liu *et al.*, 2011
	CYP2C19 gene from human blood samples	DNA	1	On chip	FTA	Oven off chip	Visual	Not defined	Zhang *et al.*, 2014
	malB gene of E. coli	DNA	1	On chip	FTA	Heater off chip	Grey value of image analysis	≈ 5 cells	Connelly *et al.*, 2015
	Hepatitis B virus in clinical blood samples	DNA	1	On chip	Glass fiber-PDMS-FTA	Heater off chip	LFA	≈ 5 pM	Choi *et al.*, 2016
	MS2 phage	RNA	1	Off chip	PDMS on Al-coated paper	Heater off chip	Fluorescence	Not defined	Hiltunen *et al.*, 2018

	Target	Type of target	Sample Volume	Reaction chambers	Number of chambers	Sample Loading		REF
Digital-LAMP	λ-phage	DNA	≈ 6 nL	Reaction wells	5,000	Air pressure		Gansen *et al.*, 2012
	β-actin gene of pMD 18-THA	DNA	≈ 6 nL	Reaction wells	384	Pressure difference		Zhu *et al.*, 2012
	16s rRNA gene for *Neisseria Gonorrhoeae*	DNA	≈ 10 pL	Droplet	100,000	Droplet generator		Rane *et al.*, 2015
	-	DNA	≈ 6 nL	Droplet/wells	1,280	Syringe and pipette		Du *et al.*, 2009
	E. coli W3110 Reference DNA	DNA	≈ 31 pL	Droplet	2,000	Droplet generator		Schuler *et al.*, 2016

GCTTTTATGAGCTGTAACACTCACCGCGAAGGTCCGCAGCTTCACTCCTGAAGCCAGCGAGACCACGAGC
CTACTGGGAGGAACGAACAACTCCCGACGCGCCGCCTTAAGAGCTGTAACACTCACCGCGAAGGTCTGCA
GCTTCACTCCTGAGCCAGCGAGACCACGAACCCACCAGAAGGAAAAAACTCCGAACACATCTGAACATCA
GAAGCAACAAACTCCGGACACGCCGCCTTTAAGAACTGTAACACTCACTGCGAGGGTCCGCGGCTTCATT
CTTGAAGTGAGTGAGACCAAGAACCCACCAGTTCTGGACACAATTTCAAGTCCTCAGGTGCCATCAATAT
TCTGAAAATGGCAGTGATTTTTATTCAACCTGTATAAGGCACTTTCACCATGTACCTGGAAGCAACATCT
ACATCTTTTTCAGCAATCTAGATGCTGGGGACACAAGGTCCACCTTCCAGGAATATGGCCATGACACCAG
AAATCACAAACATGATGAGAATGGAATGACTGGGGAAGAAGTGCCAGATGCTTCACTTGTAAATGAAGAC
CCAGCCTCTGGGGATGCAGATACCACCTCCCTGAAGAAGCTGAATATCTGCAGATAAGTGGAGTTCACCA
ATGATGAGGAGCGGGATGGAGAAAGGAGGTAGGGAGAGTCATCCAAGGAACATGAGCAACATGTTAAAAG
CCAAGTGGTTTAATTTCTGGAGATGGTGAACCCAAGAGGCTCTGCTGGGAGACAACAAAAATAATGAAGA
ATTGAACCAGAGTCCGGTGAATATCAGCACTGGGACCAGTTAGCAGAGGAAAAGGAAAGAATAAAAGCGA
AAAGAATGAAGAGTCATATGATTACCAACTTTTCCTTTTTCATATAAATTGAGTGTATATGGGTCTGGAA
CAACCTGAATTTCCATCAAGTCCTGGCTAACCTCATTATGTCCTATGAATATTTTTGACTAATCCCACTT
TACATTAATCTGTATTGTGAATGTGGATATTGAATTATATTTCTTTGTAATCCCATTATCCAAAATCCAG
TTCAGAGACTATTAGTTACCAATGTTCACTGTGAAGGAAAAAAAAAAAAAAAAAGCTCAGAGGATAAACA
TGTGATATGGTTTGGCTGTGTCCCCACCCAAATATCATCTTGAATTGTAGCTCCCATAATTCCCACGTGT
TGTGGGAGGGACCCGGTGGGAGATAATTGTATCATGGGGGTGGTTCCCCCATACTATTCTCATAGTAGTG
AATAAGTCTCACAAAATCTGATGGTTTTATGAGGGAAAACCCCTTTCACCTGGTTCTCATTCTCTTCTCT
GGTCTGTCGTCATGTAAGACATGCCTTTCACCTTCTCCACCATGACTGTGAGGCCTCCCCAGCCACGTGG
AACTGTGAGCCCATTAAACCTCTTTCACTTATAAAT

Figure A1. Primer alignment of *SChLAP1* gene. Sequence of isoform number 1of SChLAP1 gene (NCBI Reference Sequence NR_104319.1). Underline with (----) is the matching area with the other 6 isoforms of ScHLAP1. (----) represents the site recognized by the F3 primer; (----) represents the area recognized by B3 primer; (----) represents the area recognized by the F2 portion of FIP primers and (----) represents the area recognized by the B2 portion of BIP primer. The distance between F3 primer to B3 primer are 226 base pairs, corresponding to the SChLAP1 amplicon obtained via PCR.

CCCTTTAAATATCCACACACACAGGAAGCACAAAAGGAAGCACAGAGATCCCTGGGAGAAATGCCCG
GCCGCCATCTTGGGTCATCGATGAGCCTCGCCCTGTGCCTGGTCCCGCTTGTGAGGGAAGGACATTA
GAAAATGAATTGATGTGTTCCTTAAAGGATGGGCAGGAAAACAGATCCTGTTGTGGATATTTATTTG
AACGGGATTACAGATTTGAAATGAAGTCACAAAGTGAGCATTACCAATGAGAGGAAAACAGACGAGA
AAATCTTGATGGCTTCACAAGACATGCAACAAACAAAATGGAATACTGTGATGACATGAGGCAGCCA
AGCTGGGGAGGAGATAACCACGGGGCAGAGGGTCAGGATTCTGGCCCTGCTGCCTAAACTGTGCGTT
CATAACCAAATCATTTCATATTTCTAACCCTCAAAACAAAGCTGTTGTAATATCTGATCTCTACGGT
TCCTTCTGGGCCCAACATTCTCCATATATCCAGCCACACTCATTTTTAATATTTAGTTCCCAGATCT
GTACTGTGACCTTTCTACACTGTAGAATAACATTACTCATTTTGTTCAAAGACCCTTCGTGTTGCTG
CCTAATATGTAGCTGACTGTTTTTCCTAAGGAGTGTTCTGGCCCAGGGGATCTGTGAACAGGCTGGG
AAGCATCTCAAGATCTTTCCAGGGTTATACTTACTAGCACACAGCATGATCATTACGGAGTGAATTA
TCTAATCAACATCATCCTCAGTGTCTTTGCCCATACTGAAATTCATTTCCCACTTTTGTGCCCATTC
TCAAGACCTCAAAATGTCATTCCATTAATATCACAGGATTAACTTTTTTTTTTTAACCTGGAAGAATT
CAATGTTACATGCAGCTATGGGAATTTAATTACATATTTTGTTTTCCAGTGCAAAGATGACTAAGTC
CTTTATCCCTCCCCTTTGTTTGATTTTTTTTCCAGTATAAAGTTAAAATGCTTAGCCTTGTACTGAG
GCTGTATACAGCCACAGCCTCTCCCCATCCCTCCAGCCTTATCTGTCATCACCATCAACCCCTCCCA
TGCACCTAAACAAAATCTAACTTGTAATTCCTTGAACATGTCAGGCA

Figure A2. Primer alignment of *PCA3* gene. Part of the sequence exon 3 of *PCA3* gene (NCBI Reference Sequence NR_132312.1), which is present in the 3 isoforms of *PCA3* gene. Underline with (----)is represented the site recognized by the F3 primer; (----) represents the area recognized by B3 primer; (----) represents the area recognized by the F2 portion of FIP primers and (----) represents the area recognized by the B2 portion of BIP primer. The distance between F3 primer to B3 primer are 213 base pairs, corresponding to the *PCA3* amplicon obtained via PCR.

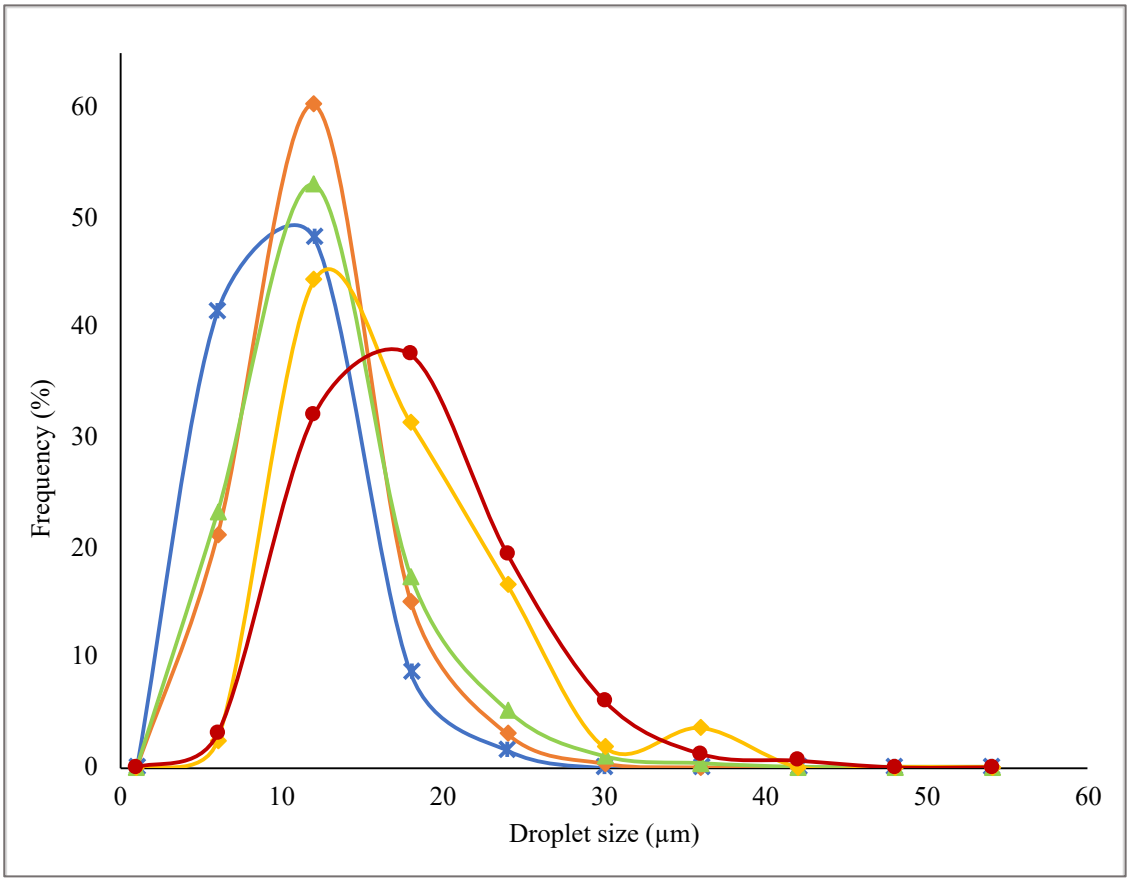

Figure A3. Representation of the droplet sizes in frequency for each incubation time at 65ºC. Legend: (×) Droplet size after 0 minutes at 65ºC. (◆) Droplet size after 15 minutes at 65ºC. (▲) Droplet size after 30 minutes at 65ºC. (◆) Droplet size after 45 minutes at 65ºC. (●) Droplet size after 60 minutes at 65ºC.

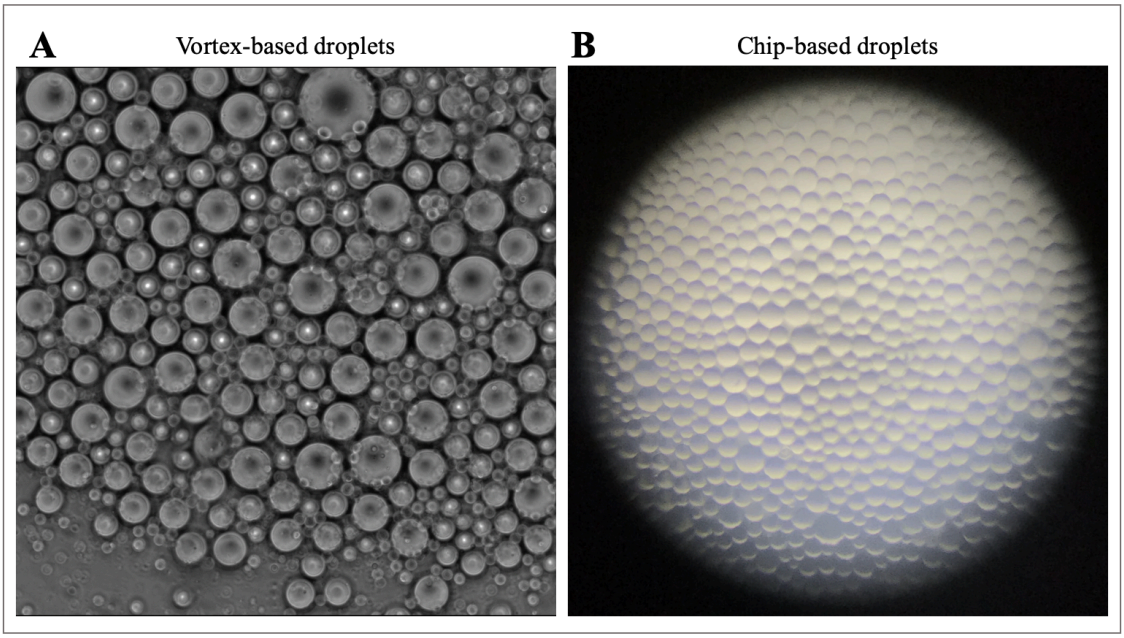

Figure A4. Comparison between vortex-based droplets with chip-based droplets. (A) Brightfield microscopy image of vortex-based droplets with a weighted average size of 18 µm and a CV of 11%. The image was obtained with an 20x objective. **(B)** Image of chip-based droplets with a weighted average size of 150 µm and a CV of 3%.

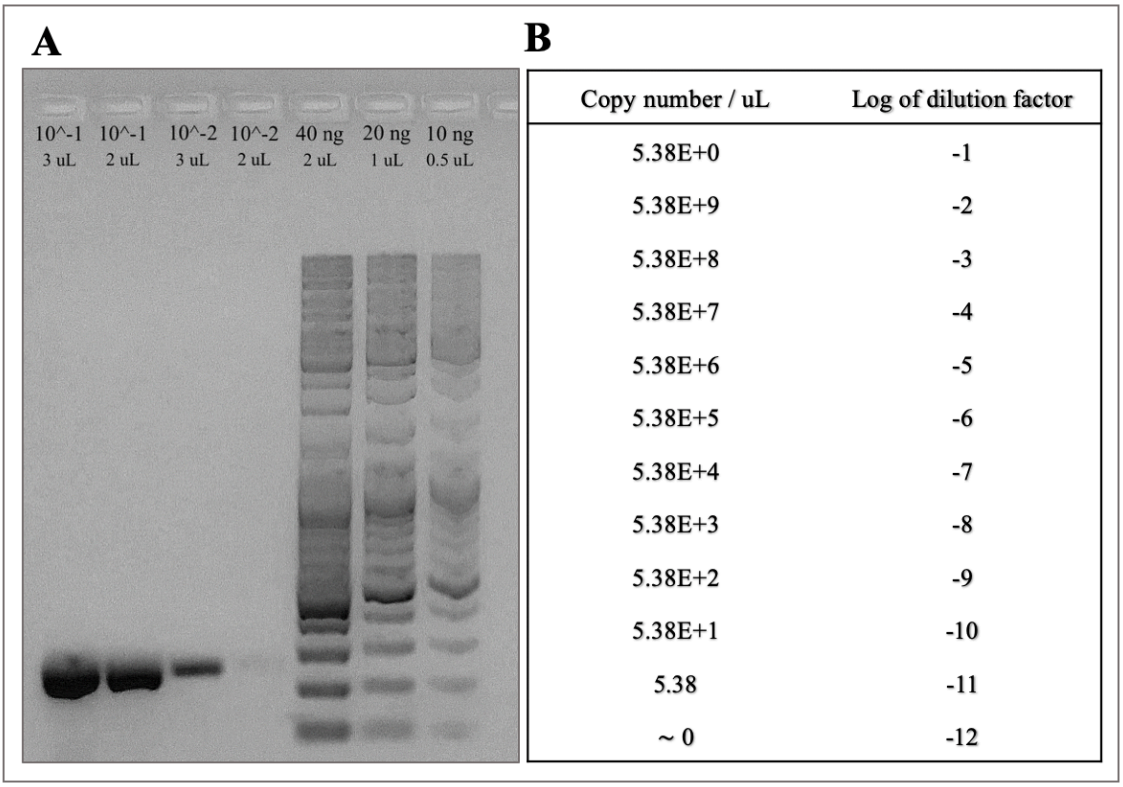

B

Copy number / uL	Log of dilution factor
5.38E+0	-1
5.38E+9	-2
5.38E+8	-3
5.38E+7	-4
5.38E+6	-5
5.38E+5	-6
5.38E+4	-7
5.38E+3	-8
5.38E+2	-9
5.38E+1	-10
5.38	-11
~ 0	-12

Figure A5. Copy number quantification based on gel electrophoreses. (A) Gel electrophoreses of the *c-Myc* PCR product with -1 and -2 logarithm of dilution factors, used for copy number calculations. **(B)** Copy number of c-Myc PCR products per µL with the several serial dilutions.

Table A3. 260nm/230nm and 260nm/280nm ratios obtain with Nanodrop for RNA extracted from PC-3 cell line with TRIsure protocol.

RATIO	VALUE
Abs 260nm /Abs 230nm	1.86
Abs 260nm /Abs 280nm	2.09

The purity of RNA was analyzed with Nanodrop, through the ratios of absorbance at 230nm and 280nm (**Table A3**). Since the absorbance ratio 260/280 is 2.09, the RNA sample can be considered free from contamination with proteins and/or other reagents that strongly absorb at 280nm. However, the absorbance ratio 260/230 is 1,86, which is slightly lower than the range that allows the assumption of a clean RNA, it is possible to infer that some components of trizol, like phenol that absorbs both at 230nm and 270nm, might be present.

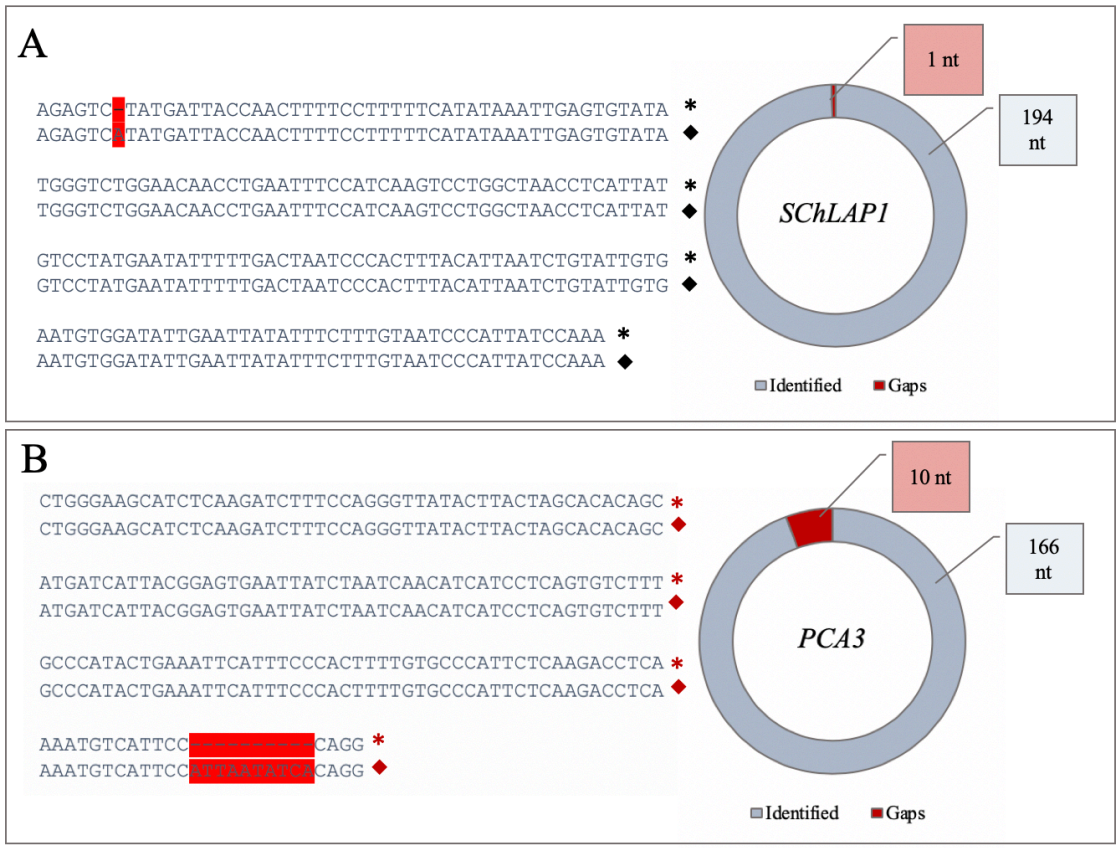

Figure A6. Results of the Sanger sequencing for *SChLAP1* and *PCA3* PCR products. (A) Results of Sanger sequencing with F3 (forward) primer the for the PCR product of *SChLAP1* gene. 1/195 nucleotides is a gap. (*) represent Sanger sequencing result and (◆) reference sequence for *SChLAP1* gene, sequence ID: NR_104319.1 **(B)** Results of Sanger sequencing with F3 (forward) primer the for the PCR product of *PCA3* gene. 10/166 nucleotides are gaps. (*) represent Sanger sequencing result and (◆) reference sequence for *PCA3* gene, sequence ID: NR_132312.1.

Table A4. Values of time threshold for each concentration of Evagreen dye with cDNA, PCR product as templates for the RT-LAMP reaction of SChLAP1 gene. The error present was calculated with the standard deviation for three experiments (n=3).

Evagreen concentration	cDNA	Error (cDNA)	PCR	Error (PCR prod)
0,2x	47	0,70	25	3,10
0,5x	49	2,50	41	7,02
1x	47	3,89	45	1,82
2x	61	0,40	59	2,73
Δ T_T (min)	**13**		**33**	

Table A5. Values of time threshold for each concentration of cDNA as templates for the RT-PCR and RT-LAMP reactions of *SChLAP1* and *PCA3* genes. The results presented are the average values of three experiments (n=3). The delta time threshold was calculated as the difference between the time threshold with 1000ng and the T_T for 1ng of cDNA.

	SChLAP1		***PCA3***	
Concentration (ng/µL)	PCR	LAMP	PCR	LAMP
1000	75	72	86	56
500	80	75	93	65
100	86	86	102	65
50	87	79	104	67
10	89	83	107	70
1	94	85	112	73
Delta T_T (min)	19	13	26	17

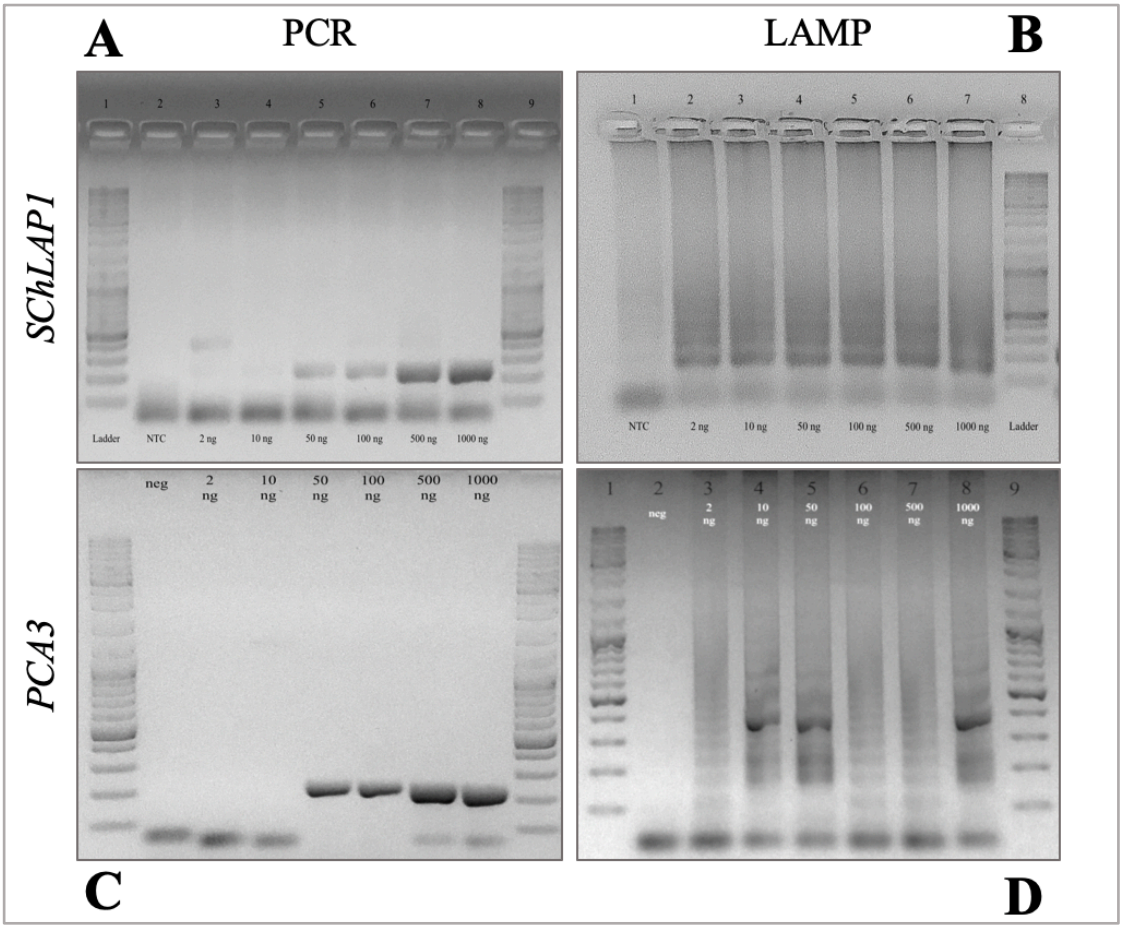

Figure A7. Results of real-time amplification PCR and LAMP reactions for *SChLAP1* and *PCA3* genes with different template concentrations. The electrophoresis was performed in a 1.5% agarose gel and run at 60V for 90 min. **(A)** RT-PCR results for *SChLAP1* gene. (1) Ladder (2) Non-template control (3) Amplification *SChLAP1*gene with 2ng of cDNA (4) Amplification of *SChLAP1*gene with 10ng of cDNA (5) Amplification of *SChLAP1*gene with 50ng of cDNA (6) Amplification of *SChLAP1*gene with 100ng of cDNA (7) Amplification of *SChLAP1*gene with 500ng of cDNA (8) Amplification of *SChLAP1*gene with 1000ng of cDNA (9) Ladder. **(B)** RT-LAMP results for *SChLAP1* gene. (1) Non-template control (2) Amplification *SChLAP1*gene with 2ng of cDNA (3) Amplification of *SChLAP1*gene with 10ng of cDNA (4) Amplification of *SChLAP1*gene with 50ng of cDNA (5) Amplification of *SChLAP1*gene with 100ng of cDNA (6) Amplification of *SChLAP1*gene with 500ng of cDNA (7) Amplification of *SChLAP1*gene with 1000ng of cDNA (8) Ladder. **(C)** Results of RT-PCR of *PCA3* gene. (1) Ladder (2) Non-template control (3) Amplification *PCA3* gene with 2ng of cDNA (4) Amplification of *PCA3* gene with 10ng of cDNA (5) Amplification of *PCA3* gene with 50ng of cDNA (6) Amplification of *PCA3* gene with 100ng of cDNA 7) Amplification of *PCA3* gene with 500ng of cDNA (8) Amplification of *PCA3* gene with 1000ng of cDNA (9) Ladder. **(D)** Results of RT-LAMP of *PCA3* gene. (1) Ladder (2) Non-template control (3) Amplification *PCA3* gene with 2ng of cDNA (4) Amplification of *PCA3* gene with 10ng of cDNA (5) Amplification of *PCA3* gene with 50ng of cDNA (6) Amplification of *PCA3* gene with 100ng of cDNA 7) Amplification of *PCA3* gene with 500ng of cDNA (8) Amplification of *PCA3* gene with 1000ng of cDNA (9) Ladder.